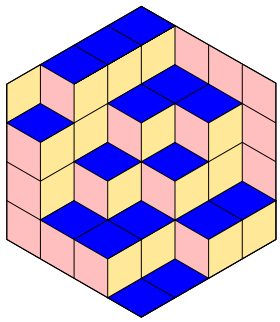

ALGEBRAIC COMBINATORICS

Daniel C. Douglas & Zhe Sun

Tropical Fock–Goncharov coordinates for SL_3-webs on surfaces II: naturality

Volume 8, issue 1 (2025), p. 101-156.
https://doi.org/10.5802/alco.408

Algebraic Combinatorics is published by The Combinatorics Consortium and is a member of the Centre Mersenne for Open Scientific Publishing
www.tccpublishing.org www.centre-mersenne.org
e-ISSN: 2589-5486

Algebraic Combinatorics
Volume 8, issue 1 (2025), p. 101–156
https://doi.org/10.5802/alco.408

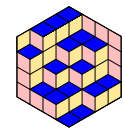

Tropical Fock–Goncharov coordinates for SL_3-webs on surfaces II: naturality

Daniel C. Douglas & Zhe Sun

Abstract In a companion article, we constructed nonnegative integer coordinates $\Phi_{\mathcal{T}}(\mathcal{W}_{3,\widehat{S}}) \subset \mathbb{Z}^N_{\geqslant 0}$ for the collection $\mathcal{W}_{3,\widehat{S}}$ of reduced SL_3-webs on a finite-type punctured surface $\widehat{S}$, depending on an ideal triangulation $\mathcal{T}$ of $\widehat{S}$. We show that these coordinates are natural with respect to the choice of triangulation, in the sense that if a different triangulation $\mathcal{T}'$ is chosen, then the coordinate change map relating $\Phi_{\mathcal{T}}(\mathcal{W}_{3,\widehat{S}})$ to $\Phi_{\mathcal{T}'}(\mathcal{W}_{3,\widehat{S}})$ is a tropical $\mathcal{A}$-coordinate cluster transformation. We can therefore view the webs $\mathcal{W}_{3,\widehat{S}}$ as a concrete topological model for the Fock–Goncharov–Shen positive integer tropical points $\mathcal{A}^+_{\mathrm{PGL}_3,\widehat{S}}(\mathbb{Z}^t)$.

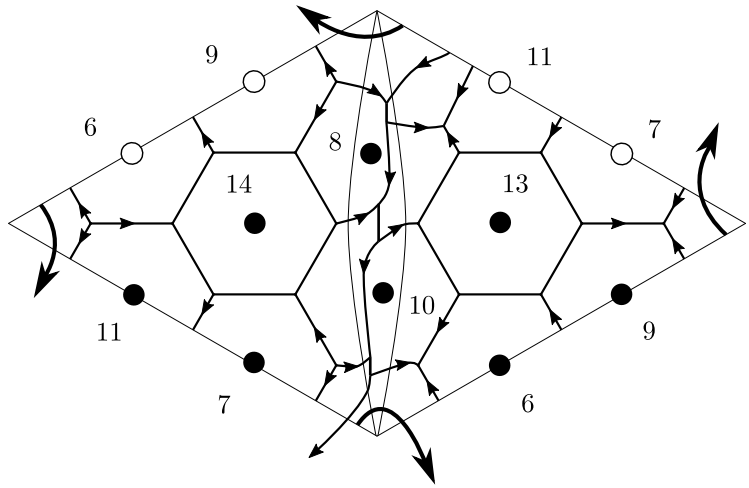

Figure 1. Positive tropical integer $\mathcal{A}$-coordinates for a reduced SL_3-web on the once punctured torus, with respect to an ideal triangulation $\mathcal{T}$.

Manuscript received 7th June 2023, revised 8th October 2024, accepted 14th November 2024.

Keywords. Webs, tropical coordinates, cluster transformations.

Acknowledgements. This work was partially supported by the U.S. National Science Foundation grants DMS-1107452, 1107263, 1107367 "RNMS: GEometric structures And Representation varieties" (the GEAR Network). The first author was also partially supported by the U.S. National Science Foundation grants DMS-1406559 and 1711297, and the second author by the China Postdoctoral Science Foundation grant 2018T110084, the FNR AFR Bilateral grant COALAS 11802479-2, and the Huawei Young Talents Program at IHES.

For a finitely generated group Γ and a suitable Lie group G, a primary object of study in higher Teichmüller theory [50] is the G-character variety

$$\mathcal{R}_{G,\Gamma} = \{\rho : \Gamma \to G\}/\!\!/G$$

consisting of group homomorphisms from the group Γ to the Lie group G, considered up to conjugation. Here, the double bar indicates that the quotient is being taken in the algebraic geometric sense of geometric invariant theory [38].

We are interested in studying the character variety $\mathcal{R}_{\mathrm{SL}_3,\pi_1(S)}$, which we simply denote by $\mathcal{R}_{\mathrm{SL}_3,S}$, in the case where the group $\Gamma = \pi_1(S)$ is the fundamental group of a finite-type punctured surface S with negative Euler characteristic, and where the Lie group $G = \mathrm{SL}_3$ is the special linear group.

Sikora [44] associated to any SL_3-web W in the surface S (Figure 1) a trace regular function $\mathrm{Tr}_W \in \mathcal{O}(\mathcal{R}_{\mathrm{SL}_3,S})$ on the SL_3-character variety. A theorem of Sikora–Westbury [46] implies that the preferred subset $\mathcal{W}_{3,S}$ of reduced SL_3-webs indexes, by taking trace functions, a linear basis for the algebra $\mathcal{O}(\mathcal{R}_{\mathrm{SL}_3,S})$ of regular functions on the SL_3-character variety.

In a companion paper [9], we constructed explicit nonnegative integer coordinates for this SL_3-web basis $\mathcal{W}_{3,S}$. In particular, we identified $\mathcal{W}_{3,S}$ with the set of solutions in $\mathbb{Z}^N_{\geqslant 0}$ of finitely many Knutson–Tao inequalities [29] and modulo 3 congruence conditions. These coordinates depend on a choice of an ideal triangulation $\mathcal{T}$ of the punctured surface S.

In the present article, we prove that these web coordinates satisfy a surprising naturality property with respect to this choice of ideal triangulation $\mathcal{T}$. Specifically, if another ideal triangulation $\mathcal{T}'$ is chosen, then the induced coordinate change map takes the form of a tropicalized $\mathcal{A}$-coordinate cluster transformation [10, 15].

Global aspects. More precisely, let $\widehat{S}$ be a marked surface, namely a compact oriented surface together with a finite subset $M \subset \partial\widehat{S}$ of preferred points, called marked points, lying on some of the boundary components of $\widehat{S}$. By a puncture we mean a boundary component of $\widehat{S}$ containing no marked points, which is thought of as shrunk down to a point. We say the surface $\widehat{S} = S$ is non-marked if $M = \varnothing$. We always assume that $\widehat{S}$ admits an ideal triangulation $\mathcal{T}$, namely a triangulation whose vertex set is equal to the set of punctures and marked points. See Section 1.1.

Fock–Goncharov duality. Fock–Goncharov [10] introduced a pair of mutually dual moduli spaces $\mathcal{X}_{\mathrm{PGL}_n,\widehat{S}}$ and $\mathcal{A}_{\mathrm{SL}_n,\widehat{S}}$ (as well as for more general Lie groups). In the case $\widehat{S} = S$ of non-marked surfaces, the spaces $\mathcal{X}_{\mathrm{PGL}_n,S}$ and $\mathcal{A}_{\mathrm{SL}_n,S}$ are variations of the PGL_n- and SL_n-character varieties; for $n = 2$, they generalize the enhanced Teichmüller space [11] and the decorated Teichmüller space [39], respectively. Fock–Goncharov duality is a canonical mapping

$$\mathbb{I} : \mathcal{A}_{\mathrm{SL}_n,S}(\mathbb{Z}^t) \to \mathcal{O}(\mathcal{X}_{\mathrm{PGL}_n,S})$$

from the discrete set $\mathcal{A}_{\mathrm{SL}_n,S}(\mathbb{Z}^t)$ of tropical integer points of the moduli space $\mathcal{A}_{\mathrm{SL}_n,S}$ to the algebra $\mathcal{O}(\mathcal{X}_{\mathrm{PGL}_n,S})$ of regular functions on the moduli space $\mathcal{X}_{\mathrm{PGL}_n,S}$, satisfying enjoyable properties; for instance, the image of $\mathbb{I}$ should form a linear basis for the algebra of functions $\mathcal{O}(\mathcal{X}_{\mathrm{PGL}_n,S})$. In the case $n = 2$, Fock–Goncharov gave a concrete topological construction of duality by identifying the tropical integer points with laminations on the surface.

There are various ways to formulate Fock–Goncharov duality. A closely related version is

$$\mathbb{I} : \mathcal{A}_{\mathrm{PGL}_n,S}(\mathbb{Z}^t) \to \mathcal{O}(\mathcal{X}_{\mathrm{SL}_n,S})$$

(compare [10, Theorem 12.3 and the following Remark] for $n = 2$). There are also formulations of duality in the setting of marked surfaces $\widehat{S}$, where the moduli spaces $\mathcal{X}_{\mathrm{PGL}_n,\widehat{S}}$ and $\mathcal{X}_{\mathrm{SL}_n,\widehat{S}}$ are replaced [19, 21] by slightly more general constructions $\mathcal{P}_{\mathrm{PGL}_n,\widehat{S}}$ and $\mathcal{P}_{\mathrm{SL}_n,\widehat{S}}$.

Investigating Fock–Goncharov duality has led to many exciting developments. By employing powerful conceptual methods (scattering diagrams, broken lines, theta functions, Donaldson–Thomas transformations), works such as [20, 21, 22] have established general formulations of duality. On the other hand, explicit higher rank constructions, in the spirit of Fock–Goncharov's topological approach in the case $n = 2$, are not as well understood.

Following [19] (see also [10, Proposition 12.2]), we focus on the positive points $\mathcal{A}^{+}_{\mathrm{PGL}_n,\widehat{S}}(\mathbb{Z}^t) \subset \mathcal{A}_{\mathrm{PGL}_n,\widehat{S}}(\mathbb{Z}^t)$, defined with respect to the tropicalized Goncharov–Shen potential $P^t : \mathcal{A}_{\mathrm{PGL}_n,\widehat{S}}(\mathbb{Z}^t) \to \mathbb{Z}$ by $\mathcal{A}^{+}_{\mathrm{PGL}_n,\widehat{S}}(\mathbb{Z}^t) = (P^t)^{-1}(\mathbb{Z}_{\geqslant 0})$. These positive tropical integer points play an important role in a variation of the previously mentioned duality,

$$\text{(a)} \qquad \mathbb{I} : \mathcal{A}^{+}_{\mathrm{PGL}_n,\widehat{S}}(\mathbb{Z}^t) \to \mathcal{O}(\mathcal{R}_{\mathrm{SL}_n,\widehat{S}})$$

(see [19, Conjecture 10.11 and Theorem 10.12, as well as Theorems 10.14, 10.15 for $G = \mathrm{PGL}_2$]). Here, the space $\mathcal{R}_{\mathrm{SL}_n,\widehat{S}}$, introduced in [19, Section 10.2] (they denote it by $\mathrm{Loc}_{\mathrm{SL}_n,\widehat{S}}$), is a generalized (twisted) version of the SL_n-character variety $\mathcal{R}_{\mathrm{SL}_n,S}$ valid for marked surfaces $\widehat{S}$.

As PGL_n is not simply connected, the moduli space $\mathcal{A}_{\mathrm{PGL}_n,\widehat{S}}$ does not have the standard Fock–Goncharov cluster structure, but it does have a positive structure. So the tropical spaces $\mathcal{A}_{\mathrm{PGL}_n,\widehat{S}}(\mathbb{Z}^t)$ and $\mathcal{A}^{+}_{\mathrm{PGL}_n,\widehat{S}}(\mathbb{Z}^t)$ are defined; moreover, they are contained in the real tropical space $\mathcal{A}_{\mathrm{SL}_n,\widehat{S}}(\mathbb{R}^t)$, which has a tropical cluster structure. Our goal is to construct, in the case $n = 3$, a concrete topological model for the space $\mathcal{A}^{+}_{\mathrm{PGL}_3,\widehat{S}}(\mathbb{Z}^t)$ of positive tropical integer points, which also exhibits this tropical cluster structure.

See Appendix A for a brief overview of the underlying Fock–Goncharov–Shen theory.

Topological indexing of linear bases. One of our guiding principles is that tropical integer points should correspond to topological objects generalizing laminations [48] on surfaces in the case $n = 2$. Such so-called higher laminations can be studied from many points of view, blending ideas from geometry, topology, and physics; see, for instance, [2, 16, 19, 32, 35, 52]. In the present article, we focus attention on one of the topological approaches to studying higher laminations, via webs [5, 31, 44]; see also [18]. Webs are certain n-valent graphs-with-boundary embedded in the marked surface $\widehat{S}$ (considered up to equivalence in $\widehat{S} - M$). Webs also appear naturally in the context of quantizations of character varieties via skein modules and algebras [26, 37, 40, 45, 49, 51].

We begin by reviewing the case $n = 2$. For a marked surface $\widehat{S}$, define the set $\mathcal{L}_{2,\widehat{S}}$ of (positive bounded) 2-laminations on $\widehat{S}$ so that $\ell \in \mathcal{L}_{2,\widehat{S}}$ is a finite collection of mutually-non-intersecting simple loops and arcs on $\widehat{S}$ such that: first, there are no contractible loops; and, second, arcs end only on boundary components of $\widehat{S}$ containing marked points, and there are no arcs contracting to a boundary interval without marked points.

In the case where the surface $\widehat{S} = S$ is non-marked, a 2-lamination $\ell \in \mathcal{L}_{2,S}$ corresponds to a trace function $\mathrm{Tr}_\ell \in \mathcal{O}(\mathcal{R}_{\mathrm{SL}_2,S})$, namely the regular function on the character variety $\mathcal{R}_{\mathrm{SL}_2,S}$ defined by sending $\rho : \pi_1(S) \to \mathrm{SL}_2$ to the product $\prod_\gamma \mathrm{Tr}(\rho(\gamma))$ of the traces along the components γ of ℓ. It is well-known [4, 41] that the trace functions Tr_ℓ, varying over the 2-laminations $\ell \in \mathcal{L}_{2,S}$, form a linear basis for the algebra $\mathcal{O}(\mathcal{R}_{\mathrm{SL}_2,S})$ of regular functions on the SL_2-character variety.

On the opposite topological extreme, consider the case where the surface $\widehat{S} = \widehat{D}$ is a disk with k marked points m_i on its boundary, cyclically ordered. For each i, assign a positive integer n_i to the i-th boundary interval located between the marked points m_i and m_{i+1}. This determines a subset $\mathcal{L}_{2,\widehat{D}}(n_1, \ldots, n_k) \subset \mathcal{L}_{2,\widehat{D}}$ consisting of the 2-laminations ℓ having geometric intersection number equal to n_i on the i-th boundary interval. It follows from the Clebsch–Gordan theorem (see, for instance, [31, Section 2.2, 2.3]) that the subset $\mathcal{L}_{2,\widehat{D}}(n_1, \ldots, n_k)$ of 2-laminations indexes a linear basis for the space of SL_2-invariant tensors $(V_{n_1} \otimes \cdots \otimes V_{n_k})^{\mathrm{SL}_2}$, where V_{n_i} is the unique n_i-dimensional irreducible representation of SL_2.

For a general marked surface $\widehat{S}$, Goncharov–Shen's moduli space $\mathcal{R}_{\mathrm{SL}_2,\widehat{S}}$ simultaneously generalizes both (a twisted version of) the character variety $\mathcal{R}_{\mathrm{SL}_2,S}$ for non-marked surfaces $\widehat{S} = S$, as well as the spaces of invariant tensors $(V_{n_1} \otimes V_{n_2} \otimes \cdots \otimes V_{n_k})^{\mathrm{SL}_2}$ for marked disks $\widehat{S} = \widehat{D}$. By [19, Theorem 10.14], the set of 2-laminations $\mathcal{L}_{2,\widehat{S}}$ canonically indexes a linear basis for the algebra of functions $\mathcal{O}(\mathcal{R}_{\mathrm{SL}_2,\widehat{S}})$ on the generalized character variety for the marked surface $\widehat{S}$, closely related to the linear bases in the specialized cases $\widehat{S} = S$ and $\widehat{S} = \widehat{D}$.

We now turn to the case $n = 3$. In the setting of the disk $\widehat{S} = \widehat{D}$ with k marked points on its boundary, the integers n_i are replaced with highest weights λ_i of irreducible SL_3-representations V_{λ_i}, and the object of interest is the space $(V_{\lambda_1} \otimes V_{\lambda_2} \otimes \cdots \otimes V_{\lambda_k})^{\mathrm{SL}_3}$ of SL_3-invariant tensors. Kuperberg [31] proved that the set $\mathcal{W}_{3,\widehat{D}}(\lambda_1, \ldots, \lambda_k)$ of non-convex non-elliptic 3-webs W on $\widehat{D}$, matching certain fixed topological boundary conditions corresponding to the weights λ_i, indexes a linear basis for the invariant space $(V_{\lambda_1} \otimes V_{\lambda_2} \otimes \cdots \otimes V_{\lambda_k})^{\mathrm{SL}_3}$ (so can be thought of as the SL_3-analogue of the subset $\mathcal{L}_{2,\widehat{D}}(n_1, \ldots, n_k) \subset \mathcal{L}_{2,\widehat{D}}$).

On the other hand, for non-marked surfaces $\widehat{S} = S$, Sikora [44] constructed, for any 3-web W on S, a trace function Tr_W on the character variety $\mathcal{R}_{\mathrm{SL}_3,S}$, generalizing the trace functions Tr_ℓ for 2-laminations $\ell \in \mathcal{L}_{2,S}$ (Sikora also constructed $\mathrm{Tr}_W \in \mathcal{O}(\mathcal{R}_{\mathrm{SL}_n,S})$ for any n-web W). A theorem of Sikora–Westbury [46] implies that the subset $\mathcal{W}_{3,S}$ of non-elliptic 3-webs W indexes, by taking trace functions Tr_W, a linear basis for the algebra of regular functions $\mathcal{O}(\mathcal{R}_{\mathrm{SL}_3,S})$ on the SL_3-character variety.

For a general marked surface $\widehat{S}$, Frohman–Sikora's work [17] suggests that a good definition for the (positive bounded) 3-laminations is the set $\mathcal{W}_{3,\widehat{S}}$ of reduced 3-webs W on $\widehat{S}$, which in particular are allowed to have boundary; see Section 1. Indeed, by [17, Proposition 4], this set $\mathcal{W}_{3,\widehat{S}}$ forms a linear basis for the reduced SL_3-skein algebra. As for non-marked surfaces S, where skein algebras quantize character varieties, we suspect that Frohman–Sikora's reduced SL_3-skein algebra is a quantization of Goncharov–Shen's generalized SL_3-character variety $\mathcal{R}_{\mathrm{SL}_3,\widehat{S}}$. In particular, we suspect that the set $\mathcal{W}_{3,\widehat{S}}$ indexes a canonical linear basis for the algebra of regular functions $\mathcal{O}(\mathcal{R}_{\mathrm{SL}_3,\widehat{S}})$, generalizing the case $n = 2$ [19, Theorem 10.14]; see [17, Conjecture 23].

Tropical coordinates for higher laminations. Let a positive integer cone mean a subset of $\mathbb{Z}^k_{\geqslant 0}$ closed under addition and containing zero.

As in [10, 11], in the case $n = 2$, given a choice of ideal triangulation $\mathcal{T}$, with N_2 edges, of the marked surface $\widehat{S}$, one assigns N_2 nonnegative integer coordinates to a given 2-lamination $\ell \in \mathcal{L}_{2,\widehat{S}}$ by taking the geometric intersection numbers of ℓ with the edges of the ideal triangulation $\mathcal{T}$. This assignment determines an injective coordinate mapping

$$\Phi^{(2)}_{\mathcal{T}} : \mathcal{L}_{2,\widehat{S}} \hookrightarrow \mathbb{Z}^{N_2}_{\geqslant 0}$$

on the set of 2-laminations $\mathcal{L}_{2,\widehat{S}}$. Moreover, the image of $\Phi^{(2)}_{\mathcal{T}}$ is a positive integer cone in $\mathbb{Z}^{N_2}_{\geqslant 0}$, which is characterized as the set of solutions of finitely many inequalities and parity conditions of the form

$$a + b - c \geqslant 0 \text{ and } a + b - c \in 2\mathbb{Z} \ (a, b, c \in \mathbb{Z}_{\geqslant 0}).$$

Moreover, these integer coordinates are natural with respect to the choice of $\mathcal{T}$, in the sense that if a different ideal triangulation $\mathcal{T}'$ is chosen, then the induced coordinate transformation is the SL_2 tropical $\mathcal{A}$-coordinate cluster transformation [11, Figure 8]. These natural coordinates provide an identification $\mathcal{L}_{2,\widehat{S}} \cong \mathcal{A}^{+}_{\mathrm{PGL}_2,\widehat{S}}(\mathbb{Z}^t)$ as in [19, Theorem 10.15]. Taken together, [19, Theorems 10.14, 10.15] constitute a compelling topological version of the duality (a) in the case $n = 2$; see [19, the two paragraphs after Theorem 10.15].

Our main result generalizes these natural coordinates to the setting $n = 3$.

More precisely, given an ideal triangulation $\mathcal{T}$ of a marked surface $\widehat{S}$, put N_3 to be twice the number of edges (including boundary edges) of $\mathcal{T}$ plus the number of triangles of $\mathcal{T}$. Recall the set $\mathcal{W}_{3,\widehat{S}}$ of (equivalence classes of) reduced 3-webs on $\widehat{S}$, discussed above.

THEOREM 0.1. *Given an ideal triangulation $\mathcal{T}$ of the marked surface $\widehat{S}$, there is an injection*

$$\Phi_{\mathcal{T}} : \mathcal{W}_{3,\widehat{S}} \hookrightarrow \mathbb{Z}^{N_3}_{\geqslant 0}$$

satisfying the property that the image of $\Phi_{\mathcal{T}}$ is a positive integer cone in $\mathbb{Z}^{N_3}_{\geqslant 0}$, which is characterized as the set of solutions of finitely many Knutson–Tao rhombus inequalities [29] *and modulo* 3 *congruence conditions of the form*

$$a + b - c - d \geqslant 0 \text{ and } a + b - c - d \in 3\mathbb{Z} \ (a, b, c, d \in \mathbb{Z}_{\geqslant 0}).$$

Moreover, these coordinates are natural with respect to the action of the mapping class group of the marked surface $\widehat{S}$. More precisely, if a different ideal triangulation $\mathcal{T}'$ is chosen, then the coordinate change map relating $\Phi_{\mathcal{T}}$ and $\Phi_{\mathcal{T}'}$ is given by the SL_3 *tropical $\mathcal{A}$-coordinate cluster transformation* [10, 15]*, expressed locally as in* (b)-(f)*; see Figure* 2*.*

See Theorems 1.14, 2.4 and Corollary 2.13. The construction of $\Phi_{\mathcal{T}}$ (Theorem 1.14) was done in [9].

This construction was motivated by earlier work of Xie [52] and Goncharov–Shen [19].

In particular, Goncharov–Shen used the Knutson–Tao rhombus inequalities associated to an ideal triangulation $\mathcal{T}$ of $\widehat{S}$ to index the set of positive $\mathcal{A}$ tropical integer points, which they showed parametrizes a linear basis for the algebra of regular functions $\mathcal{O}(\mathcal{R}_{\mathrm{SL}_3,\widehat{S}})$; see [19, Section 3.1 and Theorem 10.12 (stated for more general Lie groups)]. Their parametrization is not mapping class group equivariant; see the remark in [19, page 614] immediately after the aforementioned theorem. In [21] they construct equivariant bases using the abstract machinery of [22]. Theorem 0.1 provides a concrete model indexing the set $\mathcal{A}^{+}_{\mathrm{PGL}_3,\widehat{S}}(\mathbb{Z}^t)$ of positive tropical integer points, also

based on the Knutson–Tao inequalities, which in addition is equivariant with respect to the action of the mapping class group. This natural indexing $\mathcal{W}_{3,\widehat{S}} \cong \mathcal{A}^+_{\mathrm{PGL}_3,\widehat{S}}(\mathbb{Z}^t)$ provided by Theorem 0.1 generalizes the $n = 2$ case [19, Theorem 10.15].

We think of the web coordinates of Theorem 0.1 as positive tropical integer $\mathcal{A}$-coordinates. We call the positive integer cone $\Phi_{\mathcal{T}}(\mathcal{W}_{3,\widehat{S}}) \subset \mathbb{Z}^{N_3}_{\geqslant 0}$ the SL_3 Knutson–Tao–Goncharov–Shen (KTGS) cone with respect to the ideal triangulation $\mathcal{T}$ of $\widehat{S}$.

These tropical web coordinates were constructed for some simple examples, such as the triangle webs shown in Figure 9, in [52]. They also appeared implicitly in [47, Theorem 8.22], in the geometric context of eruption flows on the $\mathrm{PGL}_n(\mathbb{R})$-Hitchin component ($n = 3$). Xie [52] checked the mapping class group equivariance, in the above sense, of these coordinates on a handful of examples.

Frohman–Sikora [17] independently constructed nonnegative integer coordinates for the set $\mathcal{W}_{3,\widehat{S}}$ of reduced 3-webs. Their coordinates are related to, but different than, the coordinates of Theorem 0.1.

As an application, Kim [27] constructed an explicit SL_3-version of Fock–Goncharov duality using the tropical web coordinates of Theorem 0.1. We expect that Kim's approach, together with the SL_3-quantum trace map [6, 7, 27], will lead to an explicit SL_3-version of quantum Fock–Goncharov duality [13]; see [3] for the $n = 2$ case.

As another application, Ishibashi–Kano [25] generalized the coordinates of Theorem 0.1 to an SL_3-version of shearing coordinates for (unbounded) 3-laminations (with pinnings).

To end this section, we briefly recall from [9] the construction of the coordinate map $\Phi_{\mathcal{T}}$ from Theorem 0.1; see Section 1. Given the ideal triangulation $\mathcal{T}$, form the split ideal triangulation $\widehat{\mathcal{T}}$ by replacing each edge E of $\mathcal{T}$ with two parallel edges E' and E''; in other words, fatten each edge E into a bigon. One then puts a given reduced 3-web $W \in \mathcal{W}_{3,\widehat{S}}$ into good position with respect to the split ideal triangulation $\widehat{\mathcal{T}}$. The result is that most of the complexity of the 3-web W is pushed into the bigons (Figure 6), whereas over each triangle there is only a single (possibly empty) honeycomb together with finitely many arcs lying on the corners (Figure 7). Once the 3-web W is in good position, its coordinates $\Phi_{\mathcal{T}}(W) \in \mathbb{Z}^{N_3}_{\geqslant 0}$ are readily computed. For an example in the once punctured torus, see Figure 1.

As has already been partly discussed, in principle the model presented in this paper should be translatable into the language of [2, 21, 33, 34]. In particular, compare Theorem 2.4 to the main result of [2].

Local aspects. The first new contribution of the present work is a proof of the naturality statement appearing in Theorem 0.1; see Section 2. This is a completely local statement, since any two ideal triangulations $\mathcal{T}$ and $\mathcal{T}'$ are related by a sequence of diagonal flips inside ideal squares. It therefore suffices to check the desired tropical coordinate change formulas for a single square:

$$x_i = x'_i \ (i = 1, 2, \ldots, 8), \tag{b}$$

$$\max\{x_2 + y_3, y_1 + x_3\} - y_2 = z_2, \tag{c}$$

$$\max\{y_1 + x_6, x_7 + y_3\} - y_4 = z_4, \tag{d}$$

$$\max\{x'_1 + z_4, x'_8 + z_2\} - y_1 = z_1, \tag{e}$$

$$\max\{z_2 + x'_5, z_4 + x'_4\} - y_3 = z_3. \tag{f}$$

See Figure 2 for the notation.

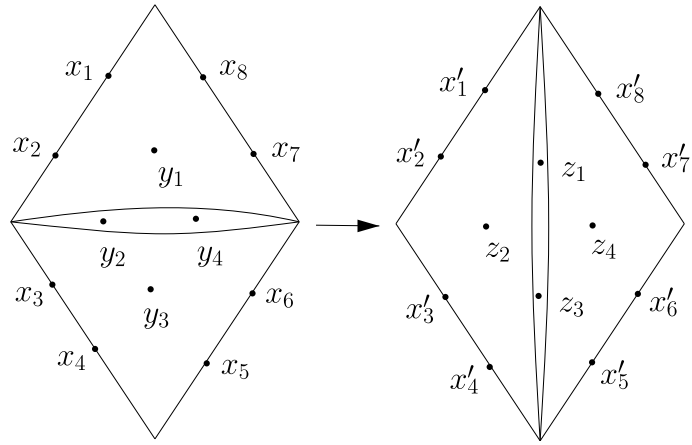

FIGURE 2. Local SL_3 tropical $\mathcal{A}$-coordinate cluster transformation, corresponding to a diagonal flip $\mathcal{T} \to \mathcal{T}'$ in the square. See (b)-(f).

Given a 3-web $W \in \mathcal{W}_{3,\widehat{S}}$ in good position with respect to $\mathcal{T}$, the restriction $W|_\square$ of W to a triangulated ideal square $(\square, \mathcal{T}|_\square) \subset (\widehat{S}, \mathcal{T})$ falls into one of 42 families $\mathcal{W}^k_{\mathcal{T}|_\square} \subset \mathcal{W}_{3,\square}$ for $k = 1, 2, \ldots, 42$; see Section 4.1. Depending on which family $\mathcal{W}^k_{\mathcal{T}|_\square}$ the restricted web $W|_\square$ belongs to, there is an explicit topological description of how $W|_\square$ rearranges itself into good position after the flip; see Appendix C. These local 42 families of 3-webs in the square have a geometric interpretation, leading to our second main result.

Let $\widehat{S} = \square$ be a disk with four marked points, namely an ideal square, and let $\mathcal{T}$ be a choice of diagonal of $\square$. Theorem 0.1 says that the set $\mathcal{W}_{3,\square}$ of reduced 3-webs in $\square$ embeds via $\Phi_\mathcal{T}$ as a positive integer cone inside $\mathbb{Z}^{12}_{\geqslant 0}$. This cone possesses a finite subset of irreducible elements spanning it over $\mathbb{Z}_{\geqslant 0}$, called its Hilbert basis [23, 42]; see Section 3.

THEOREM 0.2. *The Knutson–Tao–Goncharov–Shen cone* $\Phi_\mathcal{T}(\mathcal{W}_{3,\square}) \subset \mathbb{Z}^{12}_{\geqslant 0}$ *associated to the triangulated ideal square* $(\square, \mathcal{T})$ *has a Hilbert basis consisting of* 22 *elements, corresponding via* $\Phi_\mathcal{T}$ *to* 22 *reduced* 3*-webs* $W^i_\mathcal{T} \in \mathcal{W}_{3,\square}$ *for* $i = 1, 2, \ldots, 22$.

Moreover, this positive integer cone

$$\Phi_\mathcal{T}(\mathcal{W}_{3,\square}) = \bigcup_{k=1}^{42} \mathcal{C}^k_\mathcal{T} \subset \mathbb{Z}^{12}_{\geqslant 0}$$

can be decomposed into 42 *sectors* $\mathcal{C}^k_\mathcal{T}$ *such that:*

(I) *each sector is generated over* $\mathbb{Z}_{\geqslant 0}$ *by* 12 *of the* 22 *Hilbert basis elements;*
(II) *adjacent sectors are separated by a codimension* 1 *wall, and these* 42 *sectors* $\mathcal{C}^k_\mathcal{T}$ *are in one-to-one correspondence with the* 42 *families* $\mathcal{W}^k_\mathcal{T} \subset \mathcal{W}_{3,\square}$ *of* 3*-webs in the square, discussed just above.*

Lastly, each family $\mathcal{W}^k_\mathcal{T} \subset \mathcal{W}_{3,\square}$ *contains* 12 *distinguished* 3*-webs* $W^{i(k,j)}_\mathcal{T} \in \{W^i_\mathcal{T}\}_{i=1,2,\ldots,22}$ *for* $j = 1, 2, \ldots, 12$*, corresponding via* $\Phi_\mathcal{T}$ *to the* 12 *Hilbert basis elements generating the sector* $\mathcal{C}^k_\mathcal{T}$*. We refer to the set* $\{W^{i(k,j)}_\mathcal{T}\}_{j=1,2,\ldots,12}$ *of these* 12 *distinguished* 3*-webs as the topological type of the sector* $\mathcal{C}^k_\mathcal{T}$*. Then, two sectors* $\mathcal{C}^k_\mathcal{T}$ *and* $\mathcal{C}^{k'}_\mathcal{T}$ *are adjacent if and only if their topological types differ by exactly one distinguished* 3*-web; see Figure* 3.

See Theorems 3.3 and 4.8 (as well as Remark 4.11).

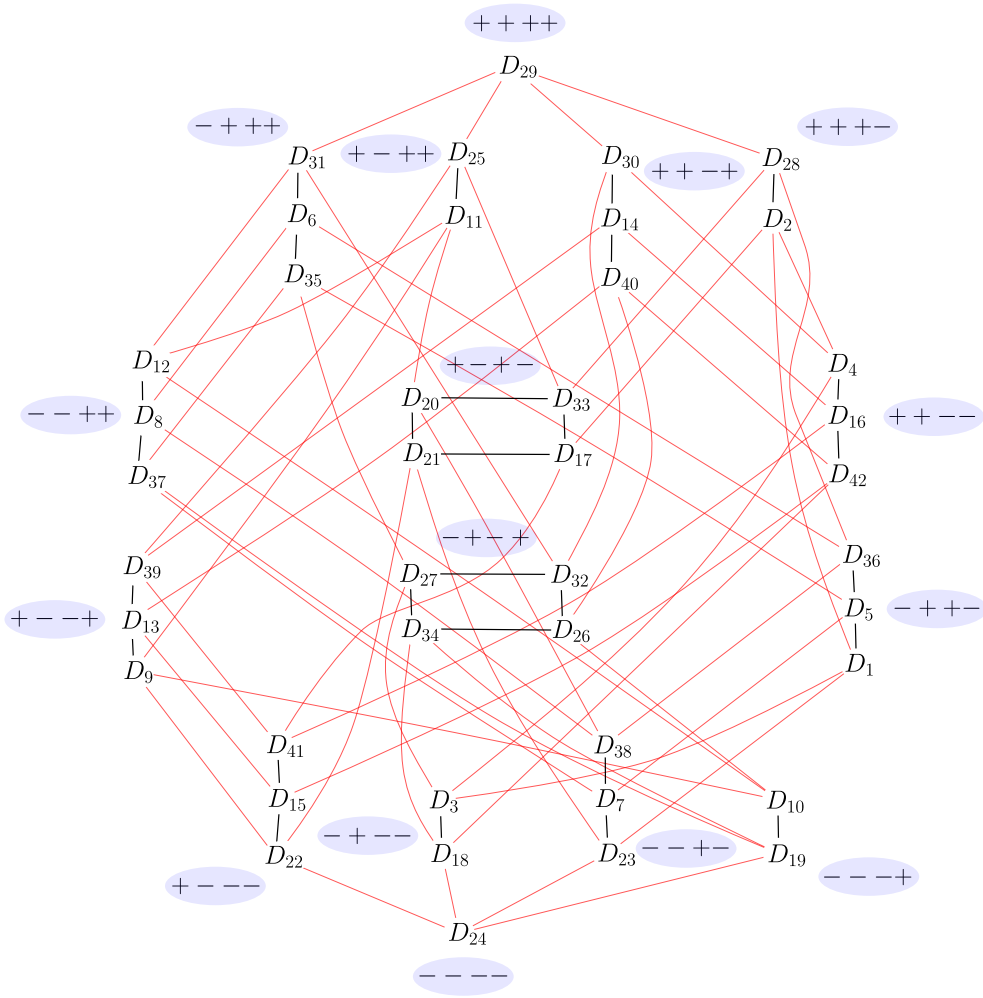

FIGURE 3. Sectors and walls in the Knutson–Tao–Goncharov–Shen (KTGS) cone $\Phi_{\mathcal{T}}(\mathcal{W}_{3,\square}) \subset \mathbb{Z}^{12}_{\geqslant 0}$ for a triangulated ideal square $(\square, \mathcal{T})$. More precisely, displayed is a corresponding sector decomposition $\{D_i\}_{i=1,2,\ldots,42}$ of (a projection to $\mathbb{R}^4$ of a real version of) an isomorphic cone in $\mathbb{Z}^8_+ \times \mathbb{Z}^4$, obtained from the KTGS cone via a transformation defined using the 4 tropical integer $\mathcal{X}$-coordinates. The sectors D_i are grouped depending on which orthant of $\mathbb{R}^4$ they belong to. These sectors are the vertices of a 4-valent graph, where two sectors are connected by an edge if and only if they share a wall; equivalently, their topological types differ by a single web. See Theorem 0.2.

For a related appearance of Hilbert bases, in the $n = 2$ setting, see [1].

The proof of Theorem 0.2 is geometric in nature and might be of independent interest. Recall [10] there are two dual sets of coordinates for the two dual moduli spaces of interest, respectively, the $\mathcal{A}$-coordinates and the $\mathcal{X}$-coordinates, as well as their tropical counterparts. For a triangulated ideal square $(\square, \mathcal{T})$, via the mapping $\Phi_{\mathcal{T}}$ each 3-web $W \in \mathcal{W}_{3,\square}$ is assigned 12 positive tropical integer $\mathcal{A}$-coordinates $\Phi_{\mathcal{T}}(W) \in \mathbb{Z}^{12}_{\geqslant 0}$. We show that there are also assigned to W four internal tropical

integer $\mathcal{X}$-coordinates valued in $\mathbb{Z}$, two associated to the unique internal edge of $\mathcal{T}$ and one for each triangle of $\mathcal{T}$; see Figure 16. We find that the decomposition of the $\mathcal{A}$-cone $\Phi_{\mathcal{T}}(\mathcal{W}_{3,\square}) \subset \mathbb{Z}^{12}_{\geqslant 0}$ into 42 sectors is mirrored by a corresponding decomposition of the $\mathcal{X}$-lattice $\mathbb{Z}^4$ into 42 sectors; see Figure 3. We think of this as a manifestation of Fock–Goncharov's tropicalized canonical map:

$$p^t : \mathcal{W}_{3,\square} \cong \Phi_{\mathcal{T}}(\mathcal{W}_{3,\square}) \cong \mathcal{A}^+_{\mathrm{PGL}_3,\square}(\mathbb{Z}^t)_{\mathcal{T}} \subset \mathcal{A}_{\mathrm{SL}_3,\square}(\mathbb{R}^t)_{\mathcal{T}} \overset{\text{canonical}}{\to} \mathcal{X}_{\mathrm{PGL}_3,\square}(\mathbb{R}^t)_{\mathcal{T}}.$$

The image of the map p^t is $\mathcal{X}_{\mathrm{PGL}_3,\square}(\mathbb{Z}^t)_{\mathcal{T}} \cong \mathbb{Z}^4$, and p^t maps sectors of the positive integer cone $\Phi_{\mathcal{T}}(\mathcal{W}_{3,\square}) \cong \mathcal{A}^+_{\mathrm{PGL}_3,\square}(\mathbb{Z}^t)_{\mathcal{T}}$ to sectors of the integer lattice $\mathcal{X}_{\mathrm{PGL}_3,\square}(\mathbb{Z}^t)_{\mathcal{T}} \cong \mathbb{Z}^4$. See Section 4.

1. Tropical points and webs

We introduce the main object of study, the Knutson–Tao–Goncharov–Shen cone $\mathcal{C}_{\mathcal{T}} \subset \mathbb{Z}^N_+$ associated to an ideal triangulation $\mathcal{T}$ of a marked surface $\widehat{S}$, and we summarize the work of [9] relating tropical points to topological objects called webs.

1.1. Marked surfaces, ideal triangulations, and rhombi.

Definition 1.1. A ***marked surface*** $\widehat{S}$ is a pair (S, m_b) where S is a compact oriented finite-type surface with at least one boundary component, and $m_b \subset \partial S$ is a finite set of ***marked points*** on ∂S. Let $m_p \subset \{\text{components of } \partial S\}$ be the set of ***punctures***, defined as the subset of boundary components without marked points; as is common in the literature, for the remainder of the article we identify such unmarked boundary components in m_p with the (actual) punctures obtained by removing them and shrinking the resulting hole down to a point.

We assume the Euler characteristic condition $\chi(S) < d/2$, where d is the number of components of $\partial S - m_b$ limiting to a marked point. (For example, $d = 3$ for a once punctured disk with three marked points on its boundary.) This topological condition is equivalent to the existence of an ***ideal triangulation*** $\mathcal{T}$ of $\widehat{S}$, namely a triangulation of the compactified surface whose set of vertices is equal to $m_b \cup m_p$; the vertices of $\mathcal{T}$ are called ***ideal vertices***.

For simplicity, we always assume that $\mathcal{T}$ does not contain any ***self-folded triangles***. That is, we assume each triangle of $\mathcal{T}$ has three distinct sides. (Our results should generalize, essentially without change, to allow for self-folded triangles.)

Given an ideal triangulation $\mathcal{T}$ of $\widehat{S}$, we define the ***ideal 3-triangulation*** $\mathcal{T}_3$ of $\mathcal{T}$ to be the triangulation of $\widehat{S}$ obtained by subdividing each ideal triangle Δ of $\mathcal{T}$ into 9 triangles; see Figure 17. The 3-triangulation $\mathcal{T}_3$ has as many ideal vertices as $\mathcal{T}$, and has N ***non-ideal vertices***, where N is defined in Notation 1.2.

A ***pointed ideal triangle*** is a triangle Δ in an ideal triangulation $\mathcal{T}$ together with a preferred ideal vertex; Δ is called a ***pointed ideal 3-triangle*** when subdivided as part of the associated 3-triangulation $\mathcal{T}_3$.

Given a pointed ideal 3-triangle, we may talk about the three associated ***rhombi***; see Figure 18. In the figure, the red rhombus is called the ***corner rhombus***, and the yellow and green rhombi are called the ***interior rhombi***. Each rhombus has two ***acute vertices*** and two ***obtuse vertices***. Note that exactly one of these eight vertices, the ***corner vertex***, is an ideal vertex of $\mathcal{T}_3$; specifically, the top (acute) vertex of the corner rhombus. (We will see that the other vertices correspond to Fock–Goncharov $\mathcal{A}$-coordinates.)

Notation 1.2.

(I) The natural number N is defined as twice the total number of edges (including boundary edges) of $\mathcal{T}$ plus the number of triangles of $\mathcal{T}$. (Note that N is what we called N_3 in the introduction.)

(II) It will be convenient to denote the nonnegative real numbers by $\mathbb{R}_+ = \mathbb{R}_{\geqslant 0}$ and the nonnegative integers by $\mathbb{Z}_+ = \mathbb{Z}_{\geqslant 0}$. Similarly, put $\mathbb{R}_- = \mathbb{R}_{\leqslant 0}$ and $\mathbb{Z}_- = \mathbb{Z}_{\leqslant 0}$.

1.2. The Knutson–Tao–Goncharov–Shen cone and reduced webs. Let $\widehat{S}$ be a marked surface. (In this subsection, we will use some of the terminology of Appendix B.)

1.2.1. *KTGS cone.*

Definition 1.3. Given a pointed ideal triangle Δ in an ideal triangulation $\mathcal{T}$ of $\widehat{S}$ (Section 1.1), assume integers (see also Remark A.4((I))) $a, b, c, d \in \mathbb{Z}$ (resp. $a, b, c \in \mathbb{Z}$) are assigned to some interior (resp. corner) rhombus, where the numbers a, b are assigned to the two obtuse vertices, and the numbers c, d are assigned to the two acute vertices. To such an assigned rhombus, we associate a ***Knutson-Tao rhombus inequality*** $a + b - c - d \geqslant 0$ and a ***modulo 3 congruence condition*** $(a + b - c - d)/3 \in \mathbb{Z}$. Here, we set $d = 0$ if the rhombus is a corner rhombus, where then d corresponds to the corner vertex.

Recall the definition (Notation 1.2) of the natural number N. This is the same as the number of non-ideal points of the 3-triangulation $\mathcal{T}_3$. We order these N non-ideal points arbitrarily in the following definition, so that to each such non-ideal point of $\mathcal{T}_3$ we associate a coordinate of $\mathbb{Z}^N$. In this way, a point of $\mathbb{Z}^N$ assigns to each rhombus in a pointed ideal triangle Δ four numbers $a, b, c, d \in \mathbb{Z}$ as above.

Definition 1.4. Given an ideal triangulation $\mathcal{T}$ of $\widehat{S}$, let the ***Knutson–Tao–Goncharov–Shen cone*** $\mathcal{C}_{\mathcal{T}} \subset \mathbb{Z}^N$, or just the ***KTGS cone*** for short, be the submonoid (Definition B.2) defined by the property that its points satisfy all of the Knutson-Tao rhombus inequalities and modulo 3 congruence conditions, varying over all rhombi of all pointed ideal triangles Δ of $\mathcal{T}$.

Proposition 1.5. *The KTGS cone $\mathcal{C}_{\mathcal{T}} \subset \mathbb{Z}_+^N \subset \mathbb{Z}^N$ is a positive integer cone* (*Definition* B.4).

Proof. This is by [9, Corollary 6.7 and Definition 6.10]; see also Remark A.4((I)). □

Conceptual Remark 1.6 (throughout the paper, conceptual remarks make reference to the theory reviewed in Appendix A). We think of the KTGS cone $\mathcal{C}_{\mathcal{T}} \subset \mathbb{Z}_+^N$, defined above, as the isomorphic coordinate chart

$$\mathcal{C}_{\mathcal{T}} \cong -3\mathcal{A}^+_{\mathrm{PGL}_3,\widehat{S}}(\mathbb{Z}^t)_{\mathcal{T}}$$

where $\mathcal{A}_{\mathrm{PGL}_3,\widehat{S}}(\mathbb{Z}^t)_{\mathcal{T}} \subset ((1/3)\mathbb{Z})^N \cong \mathcal{A}_{\mathrm{SL}_3,\widehat{S}}((1/3)\mathbb{Z}^t)_{\mathcal{T}}$ and $\mathcal{A}^+_{\mathrm{PGL}_3,\widehat{S}}(\mathbb{Z}^t)_{\mathcal{T}} \subset \mathcal{A}_{\mathrm{PGL}_3,\widehat{S}}(\mathbb{Z}^t)_{\mathcal{T}} \cap (-(1/3)\mathbb{Z}_+)^N$ as in Remark A.4((I)).

1.2.2. *Reduced webs.*

Definition 1.7. A ***web (possibly with boundary)*** W in $\widehat{S}$ [9, Section 9.1] is an oriented trivalent graph embedded in $\widehat{S}$ such that:

(I) the boundary $\partial W = W \cap (\partial\widehat{S} - m_b)$ of the web lies on the boundary of the surface (minus the marked points) and may be nonempty, in which case its boundary points are required to be monovalent vertices;

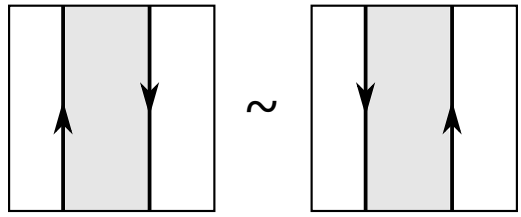

FIGURE 4. Boundary parallel move in the ideal square.

(II) the three edges of W at an internal vertex are either all oriented in or all oriented out;
(III) we allow W to have components homeomorphic to the circle, called ***loops***, which do not contain any vertices;
(IV) we allow W to have components homeomorphic to the closed interval, called ***arcs***, which have exactly two vertices on $\partial\widehat{S}-m_b$ and do not have any internal vertices.

Webs are considered up to ***parallel equivalence***, meaning related either by an ambient isotopy of $\widehat{S}-m_b$ or a homotopy in $\widehat{S}-m_b$ exchanging two 'parallel' loop (resp. arc) components of W bounding an embedded annulus (resp. rectangle, two of whose sides are contained in $\partial\widehat{S}-m_b$, as in Figure 4).

A ***face*** of a web W [9, Section 9.1] is a contractible component of the complement $W^c \subset \widehat{S}$. ***Internal*** (resp. ***external***) faces are those not intersecting (resp. intersecting) the boundary $\partial\widehat{S}-m_b$. A face with n sides (counted with multiplicity, and including sides on the boundary $\partial\widehat{S}-m_b$) is called a n***-face***. Internal faces always have an even number of sides. An ***external H-4-face*** is an external 4-face limiting to a single component of W (there is only one type of external 2- or 3-face).

A web W is ***reduced*** if each internal face has at least six sides, and there are no external 2-, 3-, or H-4-faces. (Reduced webs were called 'rung-less essential webs' in [9, Section 9.2]; see also [17].) Denote by $\mathcal{W}_{\widehat{S}}$ the set of reduced webs up to parallel equivalence. (Note that $\mathcal{W}_{\widehat{S}}$ is what we called $\mathcal{W}_{3,\widehat{S}}$ in the introduction.)

REMARK 1.8. As a caution, throughout we tend to be sloppy about distinguishing between web equivalence classes and their representatives, for example writing $W \in \mathcal{W}_{\widehat{S}}$ to indicate a representative web W, as this distinction will generally be immaterial for our purposes.

1.3. WEB TROPICAL COORDINATE MAP. In [9, Section 9.2], for any marked surface $\widehat{S}$ and for each ideal triangulation $\mathcal{T}$ of $\widehat{S}$, we defined a bijection of sets

$$\Phi_{\mathcal{T}} : \mathcal{W}_{\widehat{S}} \xrightarrow{\sim} \mathcal{C}_{\mathcal{T}}$$

from the set $\mathcal{W}_{\widehat{S}}$ of parallel equivalence classes of reduced webs to the KTGS cone $\mathcal{C}_{\mathcal{T}} \subset \mathbb{Z}_+^N$, called the 'web tropical coordinate map'. We now recall the definition of this map.

1.3.1. *Split ideal triangulations, good positions, and web schematics.*

DEFINITION 1.9. The ***split ideal triangulation*** associated to $\mathcal{T}$, which by abuse of notation we also denote by $\mathcal{T}$, is defined by splitting each ideal edge of $\mathcal{T}$ (including boundary edges) into two disjoint ideal edges. In particular, the surface $\widehat{S}$ is cut into ideal triangles and ***bigons***, as shown in Figure 5. Note that although bigons do not

admit ideal triangulations (in particular, they do not satisfy the hypothesis $\chi < d/2$ of Section 1.1 since $d = 2$), we can still consider them as marked surfaces, where all the definitions for webs make sense.

As proved in [17] and [9, Section 9.2], by isotopy we can put any reduced web $W \in \mathcal{W}_{\widehat{S}}$ into ***good position*** with respect to the split ideal triangulation $\mathcal{T}$, meaning (see just below for more details):

(I) the restriction of the web W to any bigon of $\mathcal{T}$ is a ***ladder web*** (see the left hand side of Figure 6);
(II) the restriction of the web W to any triangle of $\mathcal{T}$ is a ***honeycomb web***, namely an oriented honeycomb together with oriented corner arcs (see the left hand side of Figure 7).

More precisely, the triangle condition (called 'rung-less essential' in [9, Section 4.4]) is equivalent to saying that the restriction of W to the triangle is reduced. The bigon condition (called 'essential' in [9, Section 4.4]) is equivalent to asking that (1) all internal faces have at least six sides; and (2) for each edge E of the bigon, and for every compact embedded arc α in the bigon such that $\partial\alpha = \alpha \cap E$ and such that α intersects W generically, we have that the number of intersection points $W \cap \overline{E}$ does not exceed the number of intersection points $W \cap \alpha$; here, $\overline{E} \subset E$ is the segment in E between the two endpoints of α. Note this is a weaker condition than $W|_{\text{bigon}}$ being reduced, since, although it does not allow for external 2- or 3-faces, it does allow for external H-4-faces (also called 'rungs' of the ladder web).

In particular, W has minimal geometric intersection with the split ideal triangulation $\mathcal{T}$.

Note that for a web W in good position: there are two types of honeycombs in triangles, 'out-' and 'in-honeycombs' (see Figure 7); there may or may not be a honeycomb in a given triangle; and, no conditions on the orientations of the corner arcs in a triangle are assumed.

Remark 1.10. For an earlier appearance of these honeycomb webs in ideal triangles, see [31, pp. 140-141].

In the right hand side of Figure 6 we show the 'bigon schematic diagram' for a ladder web in a bigon, where each 'H' is replaced by a crossing.

In the right hand side of Figure 7 we show the 'triangle schematic diagram' for a honeycomb web in a triangle. Here, the honeycomb component is completely determined by two pieces of information: its orientation (either all in or all out) and a nonnegative integer $x \in \mathbb{Z}_+$. Note that the schematic for corner arcs is not a 'faithful' diagrammatic representation, in general, because it forgets the ordering of the oriented arcs on each corner; see Remark 1.11. However, as we will see, this schematic is sufficient to recover the web tropical coordinates.

Remark 1.11. Note that the schematic is indeed faithful at the level of parallel equivalence classes of reduced webs in the ideal triangle. This is because permuting corner arcs preserves the equivalence class of the web; see Section 1.2. (Recall also Figure 4, showing a boundary parallel move in the ideal square.)

Definition 1.12. Given the split ideal triangulation as in Figure 8, suppose we are given two oriented arcs intersecting in the bigon along the ideal edge between the two triangles. The intersection is called a:

(I) ***non-admissible crossing*** if the arcs go toward a common ideal triangle (left hand side of Figure 8);
(II) ***admissible crossing*** if the arcs go toward different ideal triangles (right hand side of Figure 8).

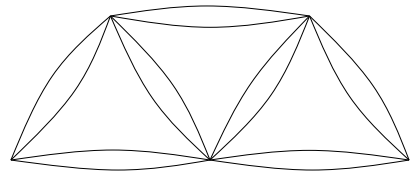

FIGURE 5. Split ideal triangulation.

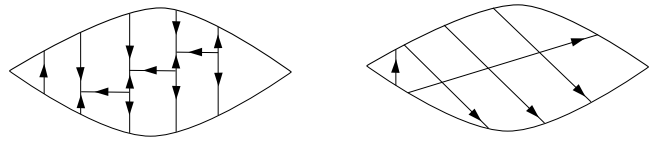

FIGURE 6. Ladder web in a bigon.

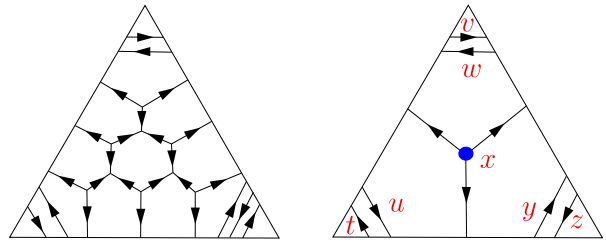

FIGURE 7. Honeycomb web in a triangle: $x = 3$, $y = 2$, and $z = t = u = v = w = 1$. Here the honeycomb is oriented outward (there may also be inward oriented honeycombs).

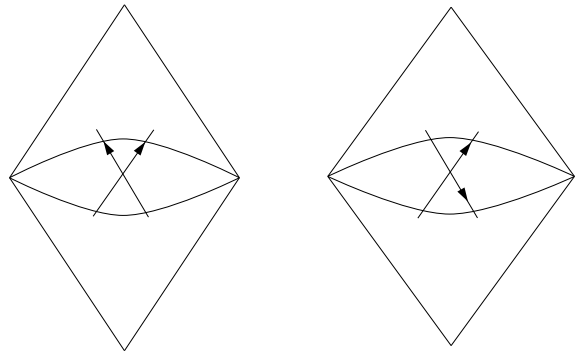

FIGURE 8. Left: Non-admissible crossing. Right: Admissible crossing.

The following fact is essentially by definition.

OBSERVATION 1.13. *For any reduced web* W *in good position with respect to the split ideal triangulation* $\mathcal{T}$*, the schematic diagram (right hand side of Figure* 6*) of any ladder web obtained by restricting* W *to a bigon has only admissible crossings.* □

1.3.2. *Definition of the web tropical coordinates.* Another way to think of an ideal triangle Δ is as an ideal polygon with three marked points (a, b, c) on its boundary, labeled counterclockwise say. (An ideal square is an ideal polygon with four marked points on its boundary, and so on.)

Let a reduced web W be in good position with respect to a split ideal triangulation $\mathcal{T}$ of $\widehat{S}$. We start by defining the web tropical coordinates $\Phi(W|_\Delta) \in \mathcal{C}_\Delta$ 'locally' for each restriction $W|_\Delta$ of W to an ideal triangle Δ of $\mathcal{T}$, as in the left hand side of Figure 7.

First, the images in $\mathcal{C}_\Delta \subset \mathbb{Z}_+^7$ under Φ of the eight 'irreducible' (see Section 3) local reduced webs $R_a, L_a, R_b, L_b, R_c, L_c, T_{in}, T_{out}$ displayed in Figure 9 are defined as in that figure. One checks directly that these images satisfy the Knutson-Tao rhombus inequalities and the modulo 3 congruence conditions (Section 1.2).

Then, the image under Φ of the restriction $W|_\Delta$ is defined as follows. Let $T \in \{T_{in}, T_{out}\}$ be the oriented honeycomb appearing in $W|_\Delta$. Let the nonnegative integers $(x, w, v, u, t, y, z) \in \mathbb{Z}_+^7$ be defined by the schematic for $W|_\Delta$, as in the right hand side of Figure 7. Put

$$\Phi(W|_\Delta) \coloneqq x\Phi(T) + v\Phi(L_a) + w\Phi(R_a) + t\Phi(L_b) + u\Phi(R_b) + z\Phi(L_c) + y\Phi(R_c) \in \mathcal{C}_\Delta \subset \mathbb{Z}_+^7.$$

Lastly, the web tropical coordinates $\Phi_\mathcal{T}(W) \in \mathcal{C}_\mathcal{T} \subset \mathbb{Z}_+^N$ for W are defined by 'gluing together' the local coordinates $\Phi(W|_\Delta)$ for the triangles Δ across the edges of $\mathcal{T}$. Note that the pair of coordinates of $\Phi(W|_\Delta)$ along an edge E at the bigon interface between two triangles Δ and Δ' matches the corresponding pair of coordinates of $\Phi(W|_{\Delta'})$ along the other bigon edge E', since these coordinates depend only on the number of oriented in- and out-strands crossing the bigon at either boundary edge E or E'. Thus, this gluing procedure is well-defined. In particular, in this way coordinates are assigned to the un-split ideal triangulation $\mathcal{T}$; this is why, in practice, one can go back and forth between the split and un-split triangulation.

See Figure 10 for an example where $\widehat{S}$ is the once punctured torus. As another example, the face coordinate (namely, the coordinate that is 3 for T_{in} and T_{out}) for the honeycomb web W shown in the left hand side of Figure 7 is $3\times3+4\times1+3\times2 = 19$. There are plenty of examples of computing web coordinates throughout the paper; for instance, see Appendix C.

In [9, Section 9.2] we showed $\Phi_\mathcal{T}(W) \in \mathcal{C}_\mathcal{T}$ is independent of the choice of good position of W with respect to the split ideal triangulation $\mathcal{T}$. Moreover, we proved the result mentioned at the beginning of this subsection:

Theorem 1.14 ([9, Theorem 9.1]). *For each ideal triangulation $\mathcal{T}$ of the marked surface $\widehat{S}$, the web tropical coordinate map*

$$\Phi_\mathcal{T} : \mathcal{W}_{\widehat{S}} \xrightarrow{\sim} \mathcal{C}_\mathcal{T}$$

from the set $\mathcal{W}_{\widehat{S}}$ of parallel equivalence classes of reduced webs in $\widehat{S}$ to the Knutson–Tao–Goncharov–Shen cone $\mathcal{C}_\mathcal{T} \subset \mathbb{Z}_+^N$ is a bijection of sets.

We will need the following fact, which is immediate from the definitions.

Observation 1.15. *For any disjoint reduced webs $W, W' \in \mathcal{W}_{\widehat{S}}$, we have $W \cup W' \in \mathcal{W}_{\widehat{S}}$ and*

$$\Phi_\mathcal{T}(W \cup W') = \Phi_\mathcal{T}(W) + \Phi_\mathcal{T}(W') \in \mathcal{C}_\mathcal{T}.$$

□

2. Naturality of the web tropical coordinates

In Section 1, we recalled the construction [9] of the web tropical coordinate map $\Phi_\mathcal{T} : \mathcal{W}_{\widehat{S}} \to \mathcal{C}_\mathcal{T} \subset \mathbb{Z}_+^N$, depending on a choice of ideal triangulation $\mathcal{T}$ of the marked surface $\widehat{S}$. By Theorem 1.14, $\Phi_\mathcal{T}$ is a bijection.

In this section, we show that these coordinates are 'natural' with respect to changing the triangulation $\mathcal{T} \to \mathcal{T}'$. That is, the induced coordinate change map

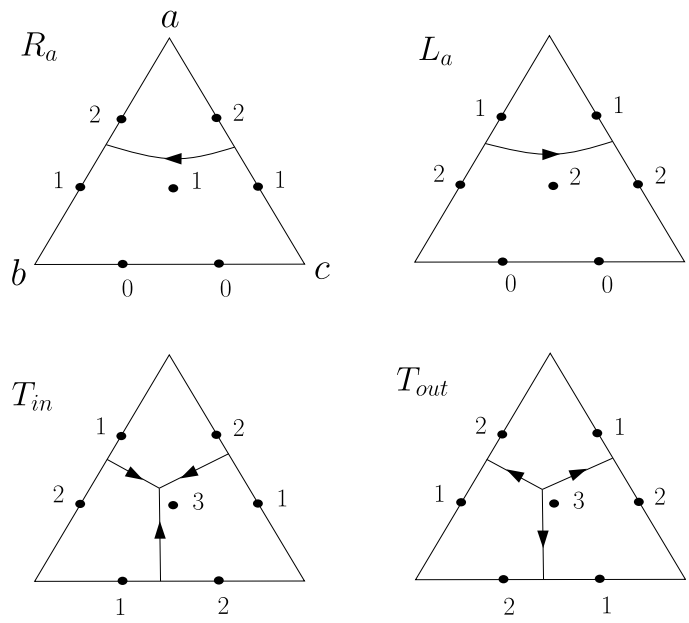

FIGURE 9. Tropical web coordinates for the eight 'irreducible' reduced webs in the triangle. (The coordinates for the other four arcs R_b, L_b, R_c, L_c are obtained by triangular symmetry.)

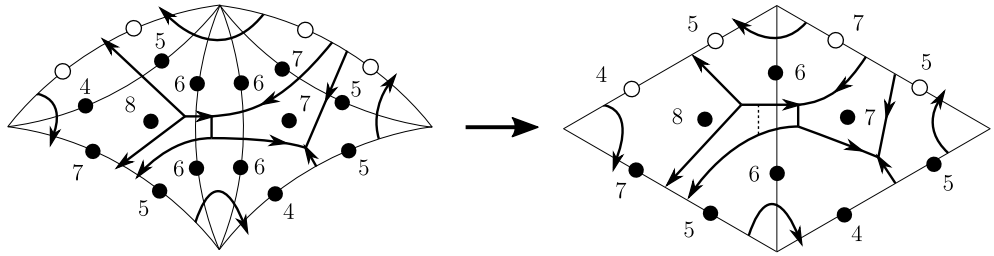

FIGURE 10. Gluing construction for the tropical coordinates for a reduced web in the once punctured torus.

$\mathcal{C}_{\mathcal{T}} \to \mathcal{C}_{\mathcal{T}'}$ is a tropical $\mathcal{A}$-coordinate cluster transformation, in the language of Fock–Goncharov [10].

REMARK 2.1. See [43] for a more conceptual proof of the main result of this section, and paper, Theorem 2.4. Moreover, in [43] the tropical web coordinates are further realized in a new and more topological way, via an algebraic intersection number between the webs and the dual web laminations. The work of [43] more satisfactorily explains the generalization to the rank 2 setting of Fock–Goncharov's theory of rank 1 laminations.

The first version of the arXiv version [8] of this article proved Theorem 2.4 via a case-by-case analysis consisting of 42 cases, 9 of which were demonstrated and the remaining 33 of which were variants of these 9 cases and so were omitted; compare Section 4.1. In the subsequent arXiv versions and present version of this article, we have replaced this case-by-case analysis with a more uniform and complete proof. (In Appendix C, as a concrete demonstration we still provide 3 of the cases from our original proof of Theorem 2.4.)

2.1. Naturality for the square.

Definition 2.2. Recall that an ***ideal square*** $\square$ is a disk with four marked points on its boundary. An ideal triangulation of $\square$ is a choice of diagonal of the square; there are two such triangulations, related by a ***diagonal flip***.

Definition 2.3. Let $\mathcal{T}$ and $\mathcal{T}'$ be the two ideal triangulations of the square $\square$, as in Figure 2 ($\mathcal{T}$ on the left, $\mathcal{T}'$ on the right). The ***tropical $\mathcal{A}$-coordinate cluster transformation for the square*** is the piecewise-linear function

$$\mu_{\mathcal{T}',\mathcal{T}} : \mathbb{Z}^{12} \to \mathbb{Z}^{12}$$

defined by

$$\mu_{\mathcal{T}',\mathcal{T}}(x_1, x_2, x_3, x_4, x_5, x_6, x_7, x_8, y_1, y_2, y_3, y_4) = (x_1', x_2', x_3', x_4', x_5', x_6', x_7', x_8', z_1, z_2, z_3, z_4),$$

where the right hand side of the equation is given by (b), (c), (d), (e), (f) from the introduction. See also Figure 2. (Here, we think of the domain of $\mu_{\mathcal{T}',\mathcal{T}}$ as associated to $\mathcal{T}$, and the codomain to $\mathcal{T}'$.)

Note that (e), (f) use (b), (c), (d).

The main result of this paper is:

Theorem 2.4. *Let $\mathcal{T}$ and $\mathcal{T}'$ be the two ideal triangulations of the square $\square$, and let $\Phi_{\mathcal{T}} : \mathcal{W}_{\square} \to \mathcal{C}_{\mathcal{T}} \subset \mathbb{Z}_+^{12}$ and $\Phi_{\mathcal{T}'} : \mathcal{W}_{\square} \to \mathcal{C}_{\mathcal{T}'} \subset \mathbb{Z}_+^{12}$ be the associated web tropical coordinate maps. Then,*

$$\mu_{\mathcal{T}',\mathcal{T}}(c) = \Phi_{\mathcal{T}'} \circ \Phi_{\mathcal{T}}^{-1}(c) \in \mathcal{C}_{\mathcal{T}'} \ (c \in \mathcal{C}_{\mathcal{T}}).$$

Remark 2.5. Note it is not even clear, a priori, from the definitions that $\mu_{\mathcal{T}',\mathcal{T}}(c) \geqslant 0$ for $c \in \mathcal{C}_{\mathcal{T}}$.

2.2. Proof of Theorem 2.4. By definition of the tropical coordinates, and of good position of a reduced web W in $\mathcal{W}_{\square}$ with respect to the triangulations $\mathcal{T}$ and $\mathcal{T}'$, we immediately get:

Observation 2.6. *For all $W \in \mathcal{W}_{\square}$, the images $c = \Phi_{\mathcal{T}}(W) \in \mathcal{C}_{\mathcal{T}}$ and $\Phi_{\mathcal{T}'} \circ \Phi_{\mathcal{T}}^{-1}(c) \in \mathcal{C}_{\mathcal{T}'}$ satisfy* (b). $\square$

Definition 2.7. Let the punctures of the square $\square$ be labeled a, b, c, d as in Figure 13. Also as in the figure, define the 8 oriented ***corner arcs*** $L_a, R_a, L_b, R_b, L_c, R_c, L_d, R_d$ in $\mathcal{W}_{\square}$. Their 12 coordinates are provided in the figure as well.

One checks by direct computation that:

Observation 2.8. *The images $c = \Phi_{\mathcal{T}}(W) \in \mathcal{C}_{\mathcal{T}}$, for $W = L_a$, R_a, L_b, R_b, L_c, R_c, L_d, R_d any of the* 8 *corner arcs, satisfy Theorem* 2.4. $\square$

Definition 2.9. A given reduced web W in $\mathcal{W}_{\square}$ is the disjoint union of, first, all its corner arc components, together called the ***corner part*** and denoted W_r; and, second, their complement $W_c = W - W_r$, which we call the ***cornerless part*** of the web W.

A reduced web W is ***cornerless*** if $W = W_c$. That is, W has no corner arcs.

Let $\mathcal{R} \subset \mathcal{W}_{\square}$ be the set of ***corner webs***, that is, webs whose cornerless parts are empty: $W = W_r$. That is, an element of $\mathcal{R}$ is a disjoint union of corner arcs.

Lemma 2.10. *For any disjoint reduced webs $W \in \mathcal{R}$ and $W' \in \mathcal{W}_{\square}$, we have $W \cup W' \in \mathcal{W}_{\square}$ and*

$$\mu_{\mathcal{T}',\mathcal{T}}(\Phi_{\mathcal{T}}(W)) + \mu_{\mathcal{T}',\mathcal{T}}(\Phi_{\mathcal{T}}(W')) = \mu_{\mathcal{T}',\mathcal{T}}(\Phi_{\mathcal{T}}(W \cup W')) \in \mathbb{Z}^{12}.$$

Proof. By Observation 1.15, we get

$$\Phi_{\mathcal{T}}(W) + \Phi_{\mathcal{T}}(W') = \Phi_{\mathcal{T}}(W \cup W') \in \mathcal{C}_{\mathcal{T}}.$$

For any corner arc (Figure 13) thus for any $W \in \mathcal{R}$ (again by Observation 1.15), the left hand sides of (c), (d), (e), (f) are always of the form $\max\{u, u\} - v$. Since

$$(\max\{u, u\} - v) + (\max\{x, y\} - z) = \max\{u + x, u + y\} - (v + z) \in \mathbb{Z}$$

we obtain the desired equality. □

Proof of Theorem 2.4. Recall by Theorem 1.14 that any $c \in \mathcal{C}_{\mathcal{T}}$ is of the form $c = \Phi_{\mathcal{T}}(W)$ for some $W \in \mathcal{W}_{\square}$. For any reduced web $W \in \mathcal{W}_{\square}$, suppose that its coordinates via $\Phi_{\mathcal{T}}$ are labeled as in the left hand side of Figure 2, and via $\Phi_{\mathcal{T}'}$ as in the right hand side of Figure 2. By Observation 2.6, (b) is satisfied for any web W in $\mathcal{W}_{\square}$. In addition, by Observation 2.8, the (c), (d), (e), (f) are satisfied for any web W in $\mathcal{R}$, that is, W consisting only of corner arcs. By Lemma 2.10 together with another application of Observation 1.15 to $\mathcal{T}'$, we have thus reduced the problem to establishing (c), (d), (e), (f) for any cornerless web $W = W_c$.

The main difficulty is that, for a given cornerless web $W = W_c$ in good position with respect to the ideal triangulation $\mathcal{T}$, after flipping the diagonal $\mathcal{T} \to \mathcal{T}'$ it is not obvious how W 'rearranges itself' back into good position with respect to the new triangulation $\mathcal{T}'$. (See, however, Appendix C for examples of this rearrangement into good position after the flip.)

We circumvent this difficulty by solving the problem 'uniformly', that is, without knowing how the new good position looks after the flip. The hypothesis that the web $W = W_c$ does not have any corner arcs will be important here.

To start, observe that it suffices to establish just (c). Indeed, (d), (e), (f) then immediately follow by 90 degree rotational symmetry. (Solve for y_1 and y_3, respectively, in the last two equations.)

With this goal in mind, we argue

$$z_2 = x_2' + x_3' = x_2 + x_3 = \max(x_2 + y_3, x_3 + y_1) - y_2 \in \mathbb{Z}_+. \tag{g}$$

Throughout, consider Figure 11, recalling the notion of a web schematic; see Section 1.3.1 and Remark 1.11.

The second equation of (g) has already been justified, by Observation 2.6.

Let us justify the first equation of (g). There are two cases, namely when m' represents an out- or an in-honeycomb.

When m' is 'out', we compute:

$$x_2' = b' + 2z' + m',\ x_3' = c' + 2y' + 2m',\ z_2 = b' + c' + 2y' + 2z' + 3m'.$$

When m' is 'in', we compute:

$$x_2' = b' + 2z' + 2m',\ x_3' = c' + 2y' + m',\ z_2 = b' + c' + 2y' + 2z' + 3m'.$$

In both cases, the desired formula $z_2 = x_2' + x_3'$ holds.

The justification of the third equation of (g) is more involved. We begin with a topological consequence.

Claim 2.11. *Let $W = W_c$ be a cornerless reduced web in the square. Up to* 180 *degree rotational symmetry of the square, there are three cases.*

(I) *When the n and m honeycombs are both 'out': Then,*

$$a + n + x = b + y \text{ and } w + d = z + m + c.$$

Moreover, if $y \geqslant n + x$, then $b = 0$; and, if $y \leqslant n + x$, then $a = 0$.
(*Note this is the case displayed in the left hand side of Figure* 11.)

(II) *When the n honeycomb is 'out', and the m honeycomb is 'in': Then,*

$$a + n + x = b + y + m \text{ and } w + d = z + c.$$

Moreover, if $y + m \geqslant n + x$, then $b = 0$; and, if $y + m \leqslant n + x$, then $a = 0$.

(III) *When the n and m honeycombs are both 'in': Then,*

$$a + x = b + y + m \text{ and } w + d + n = z + c.$$

Moreover, if $y + m \geqslant x$, then $b = 0$; and, if $y + m \leqslant x$, then $a = 0$.

The key topological property used to prove all three statements of the claim is the following: The number of 'out' strands (resp. 'in' strands) along one boundary edge of the bigon, as displayed on the left hand side of Figure 11, is equal to the number of 'in' strands (resp. 'out' strands) along the other boundary edge of the bigon.

We prove the first statement, (I), of the claim; the proofs of the second and third statements are similar. So assume the n and m honeycombs are both 'out'.

By the above topological property, we have the desired two identities of the statement.

For the second part of the statement: When $y \geqslant n + x$, if b were nonzero, then a would have to be nonzero, since $b + y = a + n + x$. Then b would be attaching to a; see the schematic shown in the left hand side of Figure 12 (see also the caption of Figure 11). But this contradicts the hypothesis that W has no corner arcs. Similarly, $a = 0$ when $y \leqslant n + x$; see the right hand side of Figure 12. This establishes the claim.

Claim 2.12. *Let $W = W_c$ be a cornerless reduced web in the square. Up to* 180 *degree rotational symmetry of the square, there are three cases.*

(I) *When the n and m honeycombs are both 'out': Then, $x_2 + y_3 \nabla x_3 + y_1$ if and only if $y \nabla n + x$, for $\nabla \in \{>, =, <\}$.*
(*Note this is the case displayed in the left hand side of Figure* 11.)

(II) *When the n honeycomb is 'out', and the m honeycomb is 'in': Then, $x_2 + y_3 \nabla x_3 + y_1$ if and only if $y + m \nabla n + x$, for $\nabla \in \{>, =, <\}$.*

(III) *When the n and m honeycombs are both 'in': Then, $x_2 + y_3 \nabla x_3 + y_1$ if and only if $y + m \nabla x$, for $\nabla \in \{>, =, <\}$.*

We prove the first statement; the proofs of the second and third statements are similar. So assume the n and m honeycombs are both 'out'. By Figure 11, we compute:

$$x_2 = w + 2a + n, \; y_3 = b + c + 2y + 2z + 3m,$$
$$x_3 = z + 2b + 2m, \; y_1 = a + d + 2x + 2w + 3n.$$

Thus,

$$(x_2 + y_3) - (x_3 + y_1) = -w + a - 2n - b + c + 2y + z + m - d - 2x \nabla 0$$
$$\Leftrightarrow a + c + 2y + z + m \nabla w + 2n + b + d + 2x.$$

By applying the two identities of the first part of Claim 2.11, the above inequality is equivalent to $3y \nabla 3n + 3x$ as desired. This establishes the claim.

We are now prepared to justify the third equation of (g), which we recall is

(h) $$x_2 + x_3 = \max(x_2 + y_3, x_3 + y_1) - y_2.$$

First, let us assume the n and m honeycombs are both 'out', as in the left hand side of Figure 11. The values of x_2, y_3, x_3, y_1 were computed above, and we gather

$$x_2 + x_3 = w + 2a + n + z + 2b + 2m,$$
$$x_2 + y_3 = w + 2a + n + b + c + 2y + 2z + 3m,$$
$$x_3 + y_1 = z + 2b + 2m + a + d + 2x + 2w + 3n.$$

By Figure 11, there are two ways to express y_2:

$$y_2 = w + d + 2a + 2n + 2x = z + m + c + 2b + 2y.$$

There are two cases to establish (h). In the case $x_2 + y_3 \geqslant x_3 + y_1$, we compute, using the second form of y_2 above:

$$\max(x_2 + y_3, x_3 + y_1) - y_2 = (x_2 + y_3) - y_2$$
$$= w + 2a + n - b + z + 2m \stackrel{?}{=} x_2 + x_3 \Leftrightarrow b \stackrel{?}{=} 0.$$

For this case, by the first part of Claim 2.12, we have $y \geqslant n + x$. Thus, $b = 0$ by the first part of Claim 2.11, as desired.

In the case $x_2 + y_3 \leqslant x_3 + y_1$, we compute, using the first form of y_2 above:

$$\max(x_2 + y_3, x_3 + y_1) - y_2 = (x_3 + y_1) - y_2$$
$$= z + 2b + 2m - a + w + n \stackrel{?}{=} x_2 + x_3 \Leftrightarrow a \stackrel{?}{=} 0.$$

For this case, by the first part of Claim 2.12, we have $y \leqslant n + x$. Thus, $a = 0$ by the first part of Claim 2.11, as desired.

This establishes (h) when both the honeycombs are 'out'. When the n honeycomb is 'out', and the m honeycomb is 'in'; or, when the n and m honeycombs are both 'in': By essentially the same calculation, one computes again that, in the case $x_2+y_3 \geqslant x_3+y_1$, then (h) is equivalent to $b = 0$, and in the case $x_2+y_3 \leqslant x_3+y_1$, then (h) is equivalent to $a = 0$. These are justified by parts (II) and (III), respectively, of Claims 2.12 and 2.11.

This completes the proof of the main result. □

2.3. Naturality for a marked surface. We briefly summarize the natural generalization of Theorem 2.4 to any marked surface $\widehat{S}$, according to the standard cluster theory [10, 15]. See the arXiv version [8] of this article for more details.

Let $\mathcal{T}$ be an ideal triangulation of $\widehat{S}$, and let N denote the number of global tropical coordinates; see Section 1.1. In Section 1, we introduced the web tropical coordinate map $\Phi_{\mathcal{T}} : \mathcal{W}_{\widehat{S}} \to \mathcal{C}_{\mathcal{T}}$, where we implicitly chose an inclusion $\mathcal{C}_{\mathcal{T}} \subset \mathbb{Z}_+^N$ of the KTGS cone of $\mathcal{T}$ (permutations of the coordinates of $\mathbb{Z}^N$ determine different inclusions). This choice played essentially no role there, since we were only considering a single triangulation. As we are now changing the triangulation, it becomes necessary to keep track of this choice.

Corollary 2.13. *Let $\mathcal{T}$ and $\mathcal{T}'$ be ideal triangulations of $\widehat{S}$, and let $\mu_{\mathcal{T}',\mathcal{T}} \colon \mathbb{Z}^N \to \mathbb{Z}^N$ be the corresponding tropical $\mathcal{A}$-coordinate cluster transformation* [10, 15]*, which is only defined up to permutation of the coordinates of the codomain $\mathbb{Z}^N$. For the associated web tropical coordinate maps $\Phi_{\mathcal{T}} \colon \mathcal{W}_{\widehat{S}} \to \mathcal{C}_{\mathcal{T}} \subset \mathbb{Z}_+^N$ and $\Phi_{\mathcal{T}'} \colon \mathcal{W}_{\widehat{S}} \to \mathcal{C}_{\mathcal{T}'} \subset \mathbb{Z}_+^N$, we have*

$$\mu_{\mathcal{T}',\mathcal{T}}(c) = \Phi_{\mathcal{T}'} \circ \Phi_{\mathcal{T}}^{-1}(c) \in \mathcal{C}_{\mathcal{T}'} \ (c \in \mathcal{C}_{\mathcal{T}}). \quad \square$$

Conceptual Remark 2.14. Another way to express Corollary 2.13 is to say that the web tropical coordinates, determined by the maps $\{\Phi_{\mathcal{T}}\}_{\mathcal{T}}$, are equivariant with respect to the action of the mapping class group of the marked surface $\widehat{S}$. Said another way, they form natural coordinates for the positive tropical integer PGL_3-points $\mathcal{A}^+_{\mathrm{PGL}_3,\widehat{S}}(\mathbb{Z}^t)$, where a point in $\mathcal{A}^+_{\mathrm{PGL}_3,\widehat{S}}(\mathbb{Z}^t)$ is thought of concretely as a reduced web W in $\mathcal{W}_{\widehat{S}}$.

Application 2.15. Generalizing Fock–Goncharov's (bounded) SL_2-laminations [10, Section 12], Kim [27] considers the space $\widetilde{\mathcal{W}}_{\widehat{S}}$ of '(bounded) SL_3-laminations' (he

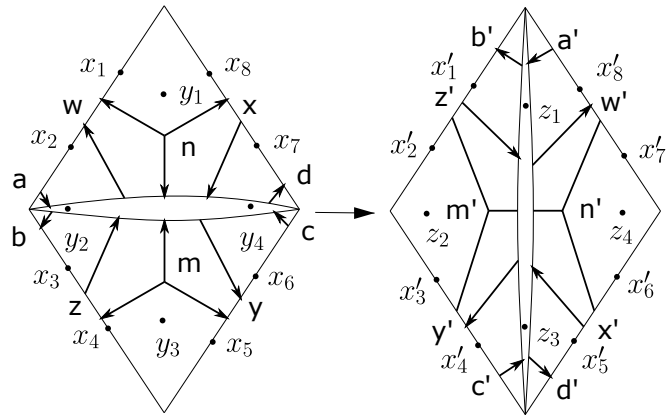

FIGURE 11. Schematic for the cornerless web $W = W_c$ in the square, before and after the flip. The variables $a, b, c, d, x, y, z, w, n, m$ are known, and can be read off from the good position of W with respect to $\mathcal{T}$. The primed variables $a', b', \ldots, m'$ are not assumed to be known. Because W has no corner arcs, there are no arcs at the top and bottom vertices before the flip, nor at the left and right vertices after the flip; it follows by Observation 1.13 that we cannot have a and b (or c and d) simultaneously nonzero. To be concrete, we have shown the case where the honeycombs labeled n and m are out-honeycombs; we will justify the other cases as well. Note that the orientations of the n' and m' honeycombs are not assumed to be known (and do not follow from the orientations of the n and m honeycombs).

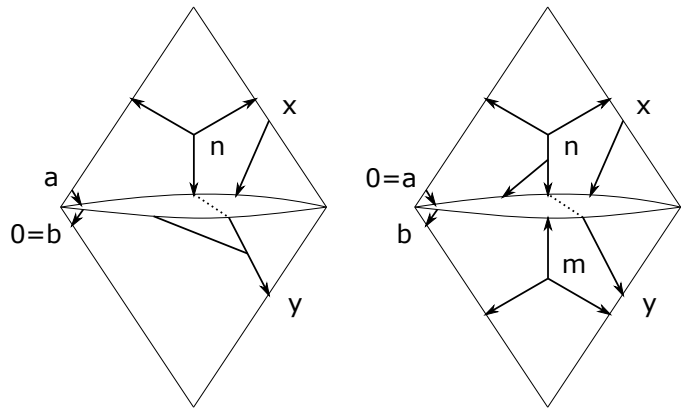

FIGURE 12. Proof of Claim 2.11. The web is assumed not to have any corner arcs. Shown is the case when the n and m honeycombs are both 'out'. Left: $y \geqslant n + x$. Right: $y \leqslant n + x$.

denotes this space by $\mathcal{A}_L(\widehat{S}, \mathbb{Z})$), which extends the space $\mathcal{W}_{\widehat{S}}$ of reduced webs by allowing for negative integer weights around the peripheral loops and arcs. He also extends the web tropical coordinate map $\Phi_{\mathcal{T}} : \mathcal{W}_{\widehat{S}} \to \mathcal{C}_{\mathcal{T}} \subset \mathbb{Z}_+^N$ of Theorem 1.14 to an injective map $\widetilde{\Phi}_{\mathcal{T}} : \widetilde{\mathcal{W}}_{\widehat{S}} \to \mathbb{Z}^N$, and characterizes the image as an integer lattice defined by certain 'balancedness' conditions; it turns out that these conditions are equivalent to the modulo 3 congruence conditions of Definition 1.4. That is, whereas

the reduced webs $\mathcal{W}_{\widehat{S}}$ correspond to solutions of both the modulo 3 congruence conditions and the Knutson-Tao inequalities, the SL_3-laminations $\widetilde{\mathcal{W}}_{\widehat{S}} \supset \mathcal{W}_{\widehat{S}}$ correspond to solutions of only the modulo 3 congruence conditions. By [27, Proposition 3.35], which generalizes Corollary 2.13, the lamination tropical coordinates $\{\widetilde{\Phi}_{\mathcal{T}}\}_{\mathcal{T}}$ are also natural, thereby constituting an explicit model for the tropical integer PGL_3-points $\mathcal{A}_{\mathrm{PGL}_3,\widehat{S}}(\mathbb{Z}^t)$; compare Remark 2.14 and see also Remark A.4((II)).

Kim's proof of [27, Proposition 3.35] uses Corollary 2.13. One way to think about upgrading the naturality statement from webs to laminations is in terms of the proof strategy of Theorem 2.4; see Section 2.2. Indeed, since Lemma 2.10 works as well for corner arcs with integer coefficients, the proof of Theorem 2.4 works more generally for the laminations $\widetilde{\mathcal{W}}_{\widehat{S}}$. (See also [28].)

3. KTGS cone for the square: Hilbert basis

In the remaining two sections, we study the structure of the Knutson–Tao–Goncharov–Shen cone $\mathcal{C}_{\mathcal{T}} \subset \mathbb{Z}_+^N$ associated to an ideal triangulation $\mathcal{T}$ of a marked surface $\widehat{S}$ (Definition 1.4 and Proposition 1.5) when $\widehat{S} = \square$ is an ideal square. In this case, an ideal triangulation $\mathcal{T}$ is simply a choice of a diagonal of $\square$. (In this section, we will use some of the terminology and results of Appendix B.)

3.1. Hilbert basis of the KTGS cone for the triangle and the square.

3.1.1. *Hilbert basis for the triangle.* We begin by recalling from [9, Section 6] the case of a single ideal triangle $\widehat{S} = \mathcal{T} = \Delta$. Let $\mathcal{C}_\Delta \subset \mathbb{Z}_+^7$ be the corresponding KTGS positive integer cone.

Recall the eight 'irreducible' webs $L_a, R_a, L_b, R_b, L_c, R_c, T_{in}, T_{out}$ in $\mathcal{W}_\Delta$ defined in Section 1.3.2. For each such web W^H, its 7 tropical coordinates $\Phi_\Delta(W^H) \in \mathcal{C}_\Delta \subset \mathbb{Z}_+^7$ are provided in Figure 9.

Proposition 3.1. *The* 8*-element subset*

$$\mathcal{H}_\Delta = \{\Phi_\Delta(W^H); W^H = L_a, R_a, L_b, R_b, L_c, R_c, T_{in}, T_{out}\} \subset \mathcal{C}_\Delta$$

is the Hilbert basis (*Definition* B.7) *of the KTGS cone* $\mathcal{C}_\Delta \subset \mathbb{Z}_+^7$ *for the triangle.*

Proof. This is a consequence of [9, Proposition 6.6] and its proof. A detailed proof is provided in the arXiv version [8] of this article. □

Remark 3.2. As a caution, it is not implied that an element of $\mathcal{C}_\Delta$ has a unique decomposition as a sum of Hilbert basis elements. Indeed, in $\mathcal{C}_\Delta$, we have the relation $\Phi_\Delta(T_{in}) + \Phi_\Delta(T_{out}) = \Phi_\Delta(L_a) + \Phi_\Delta(L_b) + \Phi_\Delta(L_c)$. See also Section 3.2.

It is also not true that if $\Phi_\Delta(W') \leqslant \Phi_\Delta(W) \in \mathcal{C}_\Delta \subset \mathbb{Z}_+^7$, in the sense that the inequality holds for each coordinate, then W' is topologically 'contained in' W. Indeed, in the above example, we have $\Phi_\Delta(T_{in})$ or $\Phi_\Delta(T_{out}) \leqslant \Phi_\Delta(L_a) + \Phi_\Delta(L_b) + \Phi_\Delta(L_c)$ in $\mathcal{C}_\Delta$. An even simpler example is $\Phi_\Delta(L_a) \leqslant \Phi_\Delta(R_b) + \Phi_\Delta(R_c)$.

3.1.2. *Hilbert basis for the square.* We turn to the square $\square$, which for the rest of this section is equipped with an ideal triangulation $\mathcal{T}$, namely a choice of diagonal of $\square$.

Recall the 8 oriented corner arcs in the square $\square$ (Definition 2.7); these are the 'irreducible' webs (1)-(8) in $\mathcal{W}_\square$ depicted in Figure 13. The triangulation $\mathcal{T}$ determines 14 more 'irreducible' webs in $\square$, namely the webs (9)-(22) in $\mathcal{W}_\square$ depicted in Figure 14. The bracket notation used in Figure 14 is explained in the caption of the figure. In sum, let us denote these 22 'irreducible' webs by $W_i^H \in \mathcal{W}_\square$ for $i = 1, 2, \ldots, 22$.

Let $\Phi_{\mathcal{T}} : \mathcal{W}_\square \to \mathcal{C}_{\mathcal{T}}$ be the associated web tropical coordinate map. For each web W_i^H, its 12 tropical coordinates $\Phi_{\mathcal{T}}(W_i^H) \in \mathcal{C}_{\mathcal{T}} \subset \mathbb{Z}_+^{12}$ are also provided in Figure 14.

Theorem 3.3. *For the webs* $\{W_i^H\}_{i=1,2,\ldots,22}$ *in* $\mathcal{W}_\square$ *displayed in Figures* 13 *and* 14*, the subset*

$$\mathcal{H}_{(\square,\mathcal{T})} = \{\Phi_\mathcal{T}(W_i^H); i = 1, 2, \ldots, 22\} \subset \mathcal{C}_\mathcal{T}$$

is the Hilbert basis of the KTGS cone $\mathcal{C}_\mathcal{T} \subset \mathbb{Z}_+^{12}$ *for the triangulated square* $(\square, \mathcal{T})$*.*

Remark 3.4. Note that if the other triangulation $\mathcal{T}'$ of $\square$ had been chosen, then only the webs $W_1^H, \ldots, W_{16}^H$ and $W_{19}^H, \ldots, W_{22}^H$ would appear among the 22 'irreducible' webs $W_i'^H$ corresponding to $\mathcal{T}'$. In other words, the set of webs corresponding to the Hilbert basis $\mathcal{H}_{(\square,\mathcal{T})}$ of $\mathcal{C}_\mathcal{T}$ depends on which triangulation $\mathcal{T}$ of the square is chosen.

We will need a little bit of preparation before proving the theorem.

Let Δ and Δ' be the two triangles appearing in the split triangulation $\mathcal{T}$ of $\square$ (Section 1.3.1). Say, Δ is the top triangle on the left hand side of Figure 2, and Δ' is the bottom triangle. In particular, neither Δ nor Δ' include the intermediate bigon. If W is a reduced web in $\square$ in good position with respect to the split ideal triangulation $\mathcal{T}$, then the restrictions $W|_\Delta$ and $W|_{\Delta'}$ are in good position in their respective triangles (by definition of good position of W with respect to $\mathcal{T}$). At the level of coordinates, this induces two projections $\pi_\Delta \colon \mathcal{C}_\mathcal{T} \to \mathcal{C}_\Delta$ and $\pi_{\Delta'} \colon \mathcal{C}_\mathcal{T} \to \mathcal{C}_{\Delta'}$ defined by $\pi_\Delta(\Phi_\mathcal{T}(W)) = \Phi_\Delta(W|_\Delta)$ and $\pi_{\Delta'}(\Phi_\mathcal{T}(W)) = \Phi_{\Delta'}(W|_{\Delta'})$. Compare Figure 10.

Lemma 3.5. *For a reduced web* W *in* $\mathcal{W}_\square$*, suppose its image* $\Phi_\mathcal{T}(W)$ *is an irreducible element of* $\mathcal{C}_\mathcal{T}$*. Then, the projections* $\pi_\Delta(\Phi_\mathcal{T}(W))$ *and* $\pi_{\Delta'}(\Phi_\mathcal{T}(W))$ *are, respectively, in the Hilbert bases* $\mathcal{H}_\Delta$ *and* $\mathcal{H}_{\Delta'}$ *of the cones* $\mathcal{C}_\Delta$ *and* $\mathcal{C}_{\Delta'}$*.*

Consequently, the set of irreducible elements of $\mathcal{C}_\mathcal{T}$ *is finite* (*thus forming a Hilbert basis*) *and is a subset of* $\mathcal{H}_{(\square,\mathcal{T})}$*, as defined in Theorem* 3.3. (*This is because* $\mathcal{H}_{(\square,\mathcal{T})}$ *is formed by taking all possible gluings across the bigon of irreducible elements in the two triangles.*)

Proof. Assuming the first statement, the second statement immediately follows by Definition B.7, Proposition 3.1, and the construction of the 22 element set $\mathcal{H}_{(\square,\mathcal{T})} \subset \mathcal{C}_\mathcal{T}$.

To establish the first statement, assume W is in good position with respect to $\mathcal{T}$. It suffices to show that if $\pi_\Delta(\Phi_\mathcal{T}(W)) = \Phi_\Delta(W|_\Delta) \in \mathcal{C}_\Delta$ is reducible, then $\Phi_\mathcal{T}(W) \in \mathcal{C}_\mathcal{T}$ is reducible. So assume that there are nonempty reduced webs A_1 and A_2 in $\mathcal{W}_\Delta$ such that $\Phi_\Delta(W|_\Delta) = \Phi_\Delta(A_1) + \Phi_\Delta(A_2)$ in $\mathcal{C}_\Delta$. (At this point, one should be mindful of Remark 3.2.) We explicitly construct nonempty reduced webs W_1 and W_2 in $\mathcal{W}_\square$ such that

$$\text{(i)} \qquad \Phi_\mathcal{T}(W) = \Phi_\mathcal{T}(W_1) + \Phi_\mathcal{T}(W_2) \in \mathcal{C}_\mathcal{T}.$$

Let E (resp. E') denote the bigon edge intersecting Δ (resp. Δ'). Let n and m (resp. n_i and m_i for $i = 1, 2$) be, respectively, the number of out- and in-strand-ends of $W|_\Delta$ (resp. A_i) on E; similarly, let n' and m' be, respectively, the number of out- and in-strand-ends of $W|_{\Delta'}$ on E'. Note $n' = m$ and $m' = n$.

By [9, Definition 5.1, property 2], which says that the two edge coordinates on E uniquely determine the number of out- and in-strand-ends on E (this is a simple linear algebra calculation), we must have $n = n_1 + n_2$ and $m = m_1 + m_2$. We gather $n' = m_1 + m_2$ and $m' = n_1 + n_2$.

Now, recall from Section 1.3.1 that a reduced web in a triangle consists of a honeycomb (possibly empty) together with corner arcs (possibly none). For each $i = 1, 2$, arbitrarily choose m_i out-strand-ends and n_i in-strand-ends of $W|_{\Delta'}$ on E', which we call 'i-strand-ends' of $W|_{\Delta'}$. Let us say that a component C' of $W|_{\Delta'}$ is 'A_i-connecting' if at least one of its strand-ends on E' is an i-strand-end; note that (1) a corner arc C' is A_i-connecting for at most one i (possibly none, when C' is on the

corner opposite E'), and (2) a honeycomb C' is A_i-connecting for at least one i, and may be both A_1- and A_2-connecting.

Let $h' \in \mathbb{Z}_+$ be the size of the honeycomb H' of $W|_{\Delta'}$, and let $h'^{(i)}$ be the number of i-strand-ends of H'; note that $h' = h'^{(1)} + h'^{(2)}$. For each $i = 1, 2$, define A'_i to be the reduced web in $\mathcal{W}_{\Delta'}$ consisting of the A_i-connecting corner arc components C' of $W|_{\Delta'}$ together with a honeycomb of size $h'^{(i)}$ oriented as H' (and we can include the non-A_i-connecting components C' into A'_1, say); note in particular that $\Phi_{\Delta'}(W|_{\Delta'}) = \Phi_{\Delta'}(A'_1) + \Phi_{\Delta'}(A'_2) \in \mathcal{C}_{\Delta'}$.

Lastly, for each $i = 1, 2$, define W_i in $\mathcal{W}_\square$ to be the unique nonempty reduced web in the square obtained from the triangle webs $A_i \in \mathcal{W}_\Delta$ and $A'_i \in \mathcal{W}_{\Delta'}$ by gluing across the bigon in the usual way (as in Figure 6). (Technically, it is the class of W_i in $\mathcal{W}_\square$ that is unique, and W_i is determined up to corner arc permutations). By construction, (i) holds. □

Proof of Theorem 3.3. By the last paragraph of Lemma 3.5, it remains to show that each element of $\mathcal{H}_{(\square,\mathcal{T})}$ is irreducible in $\mathcal{C}_\mathcal{T}$. This property can be checked by hand. (The irreducibility becomes clearer in light of the linear map $\theta_\mathcal{T} : \mathbb{R}^{12} \to \mathbb{R}^{18}$ of Section 3.1.3, where the image $\theta_\mathcal{T}(\mathcal{H}_{(\square,\mathcal{T})}) \subset \mathbb{Z}_+^{18}$ is written explicitly). □

Remark 3.6. It follows by Proposition B.5 that the Hilbert basis of the KTGS cone $\mathcal{C}_\mathcal{T} \subset \mathbb{Z}_+^{12}$ for the triangulated square $(\square, \mathcal{T})$ appearing in Theorem 3.3 spans $\mathcal{C}_\mathcal{T}$ over $\mathbb{Z}_+$. Actually, we will prove this finite generation of $\mathcal{C}_\mathcal{T}$ directly in Section 4 as a consequence of Theorem 1.14; see the proof of Theorem 4.8 in Section 4.3.3. Strictly speaking then, Theorem 3.3 is not required at the technical level in what follows; the computations throughout this section will be used, however.

Note, in particular, that for these reasons the positivity of the KTGS cone $\mathcal{C}_\mathcal{T} \subset \mathbb{Z}_+^{12}$, while possibly conceptually interesting, plays a complementary role; see also Remark B.6.

3.1.3. *Two linear isomorphisms: first isomorphism $\theta_\mathcal{T}$ by rhombus numbers.* Recall (Definition 1.4) that the KTGS cone $\mathcal{C}_\mathcal{T}$ for any triangulated marked surface $(\widehat{S}, \mathcal{T})$ is defined as the points in $\mathbb{Z}^N$ satisfying two conditions per rhombus, where there are three rhombi per pointed ideal triangle Δ of $\mathcal{T}$ (Section 1.1). Both conditions involve the quantity $3\beta = a + b - c - d$ associated to the rhombus; the first being that $3\beta = a + b - c - d \geqslant 0$, and the second that $\beta = (a + b - c - d)/3 \in \mathbb{Z}$ is an integer. (Recall $d = 0$ if the rhombus is a corner rhombus; Section 1.1.) Let $\{\beta_i\}_i$ denote these 'rhombus numbers', varying over all the rhombi of $\mathcal{T}$.

It will be convenient in the remainder of the paper to talk about real vector spaces $\mathbb{R}^N$, which we think of as containing $\mathbb{Z}^N$, in particular the KTGS cone $\mathcal{C}_\mathcal{T}$, as a subset.

In this sub-subsection, for the triangulated ideal square $(\square, \mathcal{T})$ we define a linear isomorphism $\theta_\mathcal{T}$ of real 12-dimensional vector spaces, which is mentioned in the proof of Theorem 3.3 and used in Section 4. Here, 12 is the number of tropical coordinates for the square. Note that the triangulated square has 18 rhombi $\{\beta_i\}_{i=1,2,\ldots,18}$, as displayed in Figure 16 in Section 4.

Definition 3.7. Let $(\square, \mathcal{T})$ be the triangulated square, whose coordinates are labeled as in the left hand side of Figure 2. Define a linear map

$$\theta_\mathcal{T} : \mathbb{R}^{12} \to \mathbb{R}^{18}$$

by the formula

$$\theta_\mathcal{T}(x_1, x_2, \ldots, x_8, y_1, \ldots, y_4)$$
$$= (\beta_1, \beta_2, \beta_3, \beta_4, \beta_5, \beta_6, \beta_7, \beta_8, \beta_9, \beta_{10}, \beta_{11}, \beta_{12}, \beta_{13}, \beta_{14}, \beta_{15}, \beta_{16}, \beta_{17}, \beta_{18})$$

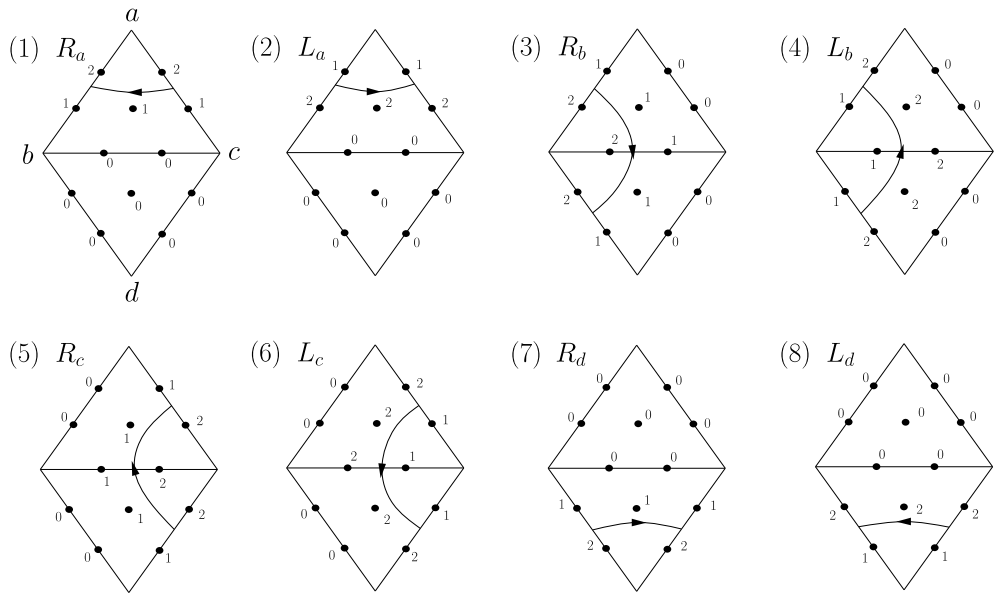

FIGURE 13. (See also Figure 14.) The first 8 elements of the 22 element Hilbert basis for the KTGS cone $\mathcal{C}_{\mathcal{T}}$ of the triangulated square $(\square, \mathcal{T})$, pictured via the corresponding 'irreducible' reduced webs $\{W_i^H\}_{i=1,2,\ldots,22}$.

where the $\{\beta_i\}_{i=1,2,\ldots,18}$ are the 18 rhombus numbers defined above.

For example, the images under $\theta_{\mathcal{T}}$ of the 22-element Hilbert basis $\mathcal{H}_{(\square,\mathcal{T})} \subset \mathcal{C}_{\mathcal{T}}$ of Theorem 3.3 are calculated from Figures 13, 14, and 16 to be:

(1) $\theta_{\mathcal{T}}(\Phi_{\mathcal{T}}([R_a])) = (1,0,0,0,0,0,0,0,0,0,0,0,0,0,0,0,0,0)$;
(2) $\theta_{\mathcal{T}}(\Phi_{\mathcal{T}}([L_a])) = (0,1,1,0,0,0,0,0,0,0,0,0,0,0,0,0,0,0)$;
(3) $\theta_{\mathcal{T}}(\Phi_{\mathcal{T}}([R_b])) = (0,0,0,1,0,0,0,0,0,0,0,0,0,1,0,0,0,0,0,0)$;
(4) $\theta_{\mathcal{T}}(\Phi_{\mathcal{T}}([L_b])) = (0,0,0,0,1,1,0,0,0,0,0,0,0,0,1,1,0,0,0,0)$;
(5) $\theta_{\mathcal{T}}(\Phi_{\mathcal{T}}([R_c])) = (0,0,0,0,0,0,1,0,0,0,0,0,0,0,0,0,1,0,0,0)$;
(6) $\theta_{\mathcal{T}}(\Phi_{\mathcal{T}}([L_c])) = (0,0,0,0,0,0,0,1,1,0,0,0,0,0,0,0,1,1)$;
(7) $\theta_{\mathcal{T}}(\Phi_{\mathcal{T}}([R_d])) = (0,0,0,0,0,0,0,0,0,1,0,0,0,0,0,0,0,0,0,0)$;
(8) $\theta_{\mathcal{T}}(\Phi_{\mathcal{T}}([L_d])) = (0,0,0,0,0,0,0,0,0,0,1,1,0,0,0,0,0,0,0,0)$;
(9) $\theta_{\mathcal{T}}(\Phi_{\mathcal{T}}([T_{out},R_b])) = (0,0,1,0,0,1,0,0,1,0,0,0,1,0,0,0,0,0,0,0)$;
(10) $\theta_{\mathcal{T}}(\Phi_{\mathcal{T}}([T_{out},L_c])) = (0,0,1,0,0,1,0,0,1,0,0,0,0,0,0,0,0,1,1)$;
(11) $\theta_{\mathcal{T}}(\Phi_{\mathcal{T}}([T_{in},L_b])) = (0,1,0,0,1,0,0,1,0,0,0,0,0,0,1,1,0,0,0,0)$;
(12) $\theta_{\mathcal{T}}(\Phi_{\mathcal{T}}([T_{in},R_c])) = (0,1,0,0,1,0,0,1,0,0,0,0,0,0,0,0,1,0,0,0)$;
(13) $\theta_{\mathcal{T}}(\Phi_{\mathcal{T}}([L_b,T_{out}])) = (0,0,0,0,1,1,0,0,0,0,0,0,1,0,0,1,0,0,0,1)$;
(14) $\theta_{\mathcal{T}}(\Phi_{\mathcal{T}}([L_c,T_{in}])) = (0,0,0,0,0,0,0,0,1,1,0,1,0,0,1,0,0,1,0)$;
(15) $\theta_{\mathcal{T}}(\Phi_{\mathcal{T}}([R_b,T_{in}])) = (0,0,0,1,0,0,0,0,0,0,0,1,0,0,1,0,0,1,0)$;
(16) $\theta_{\mathcal{T}}(\Phi_{\mathcal{T}}([R_c,T_{out}])) = (0,0,0,0,0,0,1,0,0,0,0,0,1,0,0,1,0,0,1)$;
(17) $\theta_{\mathcal{T}}(\Phi_{\mathcal{T}}([T_{out},T_{in}])) = (0,0,1,0,0,1,0,0,1,0,1,0,0,1,0,0,1,0)$;
(18) $\theta_{\mathcal{T}}(\Phi_{\mathcal{T}}([T_{in},T_{out}])) = (0,1,0,0,1,0,0,1,0,0,0,1,0,0,1,0,0,1)$;
(19) $\theta_{\mathcal{T}}(\Phi_{\mathcal{T}}([L_b,R_c])) = (0,0,0,0,1,1,0,0,0,0,0,0,0,0,0,1,0,0)$;
(20) $\theta_{\mathcal{T}}(\Phi_{\mathcal{T}}([R_b,L_c])) = (0,0,0,1,0,0,0,0,0,0,0,0,0,0,0,0,1,1)$;
(21) $\theta_{\mathcal{T}}(\Phi_{\mathcal{T}}([R_c,L_b])) = (0,0,0,0,0,0,1,0,0,0,0,0,0,1,1,0,0,0)$;
(22) $\theta_{\mathcal{T}}(\Phi_{\mathcal{T}}([L_c,R_b])) = (0,0,0,0,0,0,0,1,1,0,0,0,1,0,0,0,0,0)$.

When there is no confusion, we also let β_i denote the general i-th coordinate of $\mathbb{R}^{18}$.

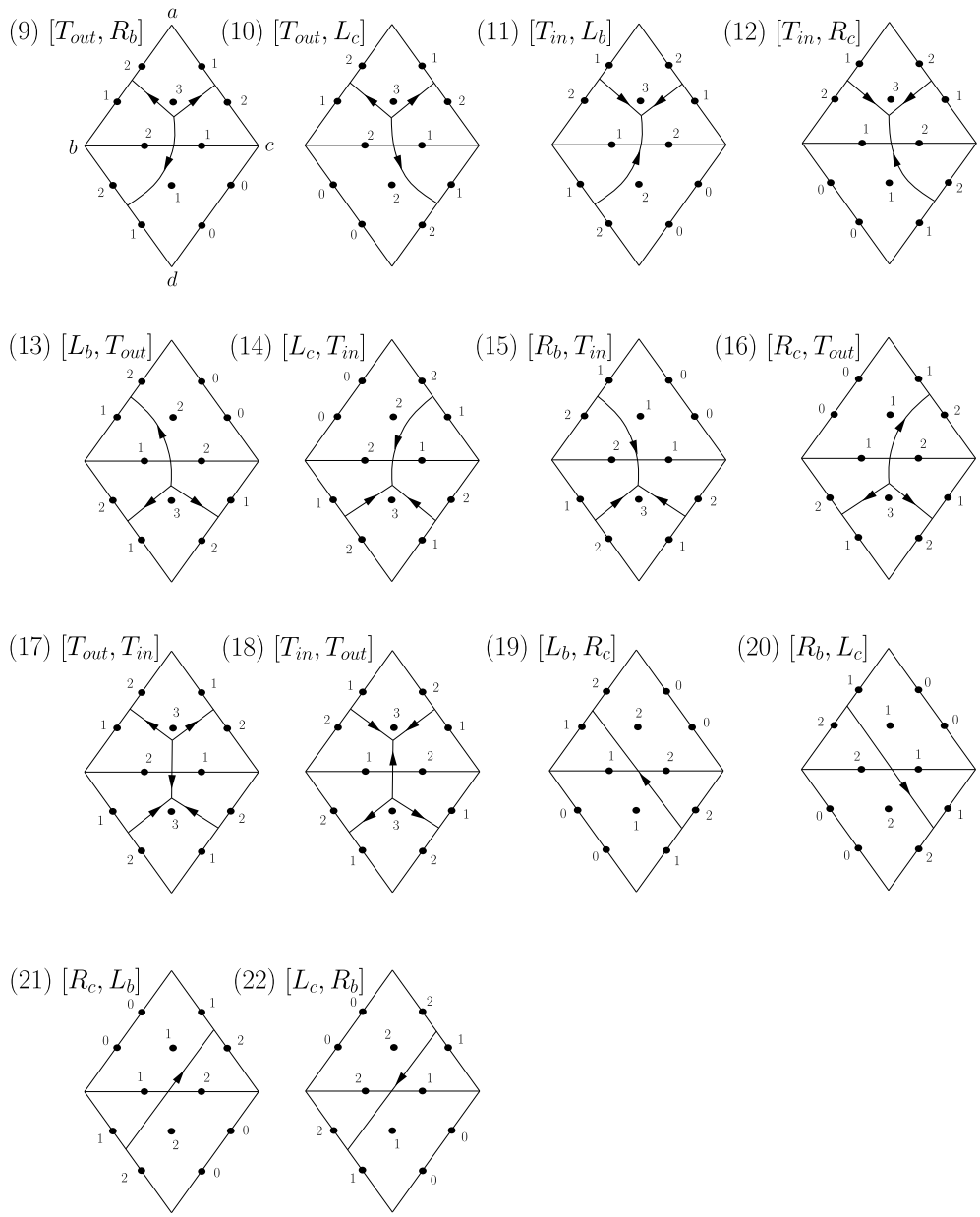

FIGURE 14. (See also Figure 13.) The last 14 elements of the 22 element Hilbert basis for the KTGS cone $\mathcal{C}_{\mathcal{T}}$ of the triangulated square $(\square, \mathcal{T})$, pictured via the corresponding 'irreducible' reduced webs $\{W_i^H\}_{i=1,2,\ldots,22}$. The square bracket is a purely notational device for webs (9)-(22); the first entry of $[\cdot, \cdot]$ corresponds to the top triangle, and the second entry to the bottom triangle.

Consider the subspace $V_{\mathcal{T}} \subset \mathbb{R}^{18}$ defined by

(j)
$$V_{\mathcal{T}} = \{(\beta_i)_i \in \mathbb{R}_{18}; X_1 \coloneqq \beta_3 - \beta_2 = \beta_6 - \beta_5 = \beta_9 - \beta_8, X_2 \coloneqq \beta_4 - \beta_{13} = \beta_{17} - \beta_9,$$
$$X_3 \coloneqq \beta_{12} - \beta_{11} = \beta_{15} - \beta_{14} = \beta_{18} - \beta_{17}, X_4 \coloneqq \beta_{16} - \beta_7 = \beta_5 - \beta_{15}\}.$$

See Section 4.3.1 for a discussion of the geometric meaning of the subspace $V_{\mathcal{T}}$ and the quantities X_i.

Proposition 3.8. *The linear map $\theta_{\mathcal{T}} : \mathbb{R}^{12} \to \mathbb{R}^{18}$ is an isomorphism of $\mathbb{R}^{12}$ onto $V_{\mathcal{T}}$. That is, $\theta_{\mathcal{T}}$ is injective, and the image of $\theta_{\mathcal{T}}$ is equal to $V_{\mathcal{T}}$. In particular, $V_{\mathcal{T}}$ is 12-dimensional.*

Proof. That $\theta_{\mathcal{T}}(\mathbb{R}^{12}) \subset V_{\mathcal{T}}$ follows from the definition of the rhombus numbers $\{\beta_i\}_{i=1,2,\dots,18}$; compare Figure 16. The remainder of the proof is elementary. □

Conceptual Remark 3.9. Recall from Remark 1.6 that we view the positive integer cone $\mathcal{C}_{\mathcal{T}} \cong -3\mathcal{A}^+_{\mathrm{PGL}_3,\square}(\mathbb{Z}^t)_{\mathcal{T}}$ as a $\mathcal{T}$-chart for the positive tropical integer points $\mathcal{A}^+_{\mathrm{PGL}_3,\square}(\mathbb{Z}^t) \subset \mathcal{A}_{\mathrm{PGL}_3,\square}(\mathbb{R}^t) = \mathcal{A}_{\mathrm{SL}_3,\square}(\mathbb{R}^t)$, with one tropical $\mathcal{A}$-coordinate $-3(A^{i,j,k}_{a,b,c})^t$ per dot of $\mathcal{T}$.

We think of $\mathbb{R}^{12} \cong \mathcal{A}_{\mathrm{SL}_3,\square}(\mathbb{R}^t)_{\mathcal{T}}$ as the coordinate chart of $\mathcal{A}_{\mathrm{SL}_3,\square}(\mathbb{R}^t)$ associated to the ideal triangulation $\mathcal{T}$.

We view the rhombus numbers β_i for $i = 1, 2, \dots, 18$ as the tropicalizations $(\alpha^{i,j,k}_{a;b,c})^t$ of the rhombus functions $\alpha^{i,j,k}_{a;b,c}$ on the moduli space $\mathcal{A}_{\mathrm{PGL}_3,\square}$. By Proposition 3.8, we can also think of the rhombus numbers $(\beta_i)_i \in V_{\mathcal{T}} \subset \mathbb{R}^{18}$ as providing an alternative coordinate chart for $\mathcal{A}_{\mathrm{PGL}_3,\square}(\mathbb{R}^t)$ via the isomorphism $\theta_{\mathcal{T}}$, that is,

$$\mathcal{A}_{\mathrm{PGL}_3,\square}(\mathbb{R}^t)_{\mathcal{T}} \cong V_{\mathcal{T}} \overset{\theta_{\mathcal{T}}}{\cong} \mathbb{R}^{12} \cong \mathcal{A}_{\mathrm{SL}_3,\square}(\mathbb{R}^t)_{\mathcal{T}}.$$

3.2. Tropical skein relations in the KTGS cone for the square. We end this section with a noteworthy observation, which will not be needed later.

We saw in Remark 3.2 that there are interesting relations in the KTGS cone $\mathcal{C}_\Delta \subset \mathbb{Z}^7_+$ for the triangle. In fact, there is essentially only one relation (in the sense analogous to Proposition 3.10). The intuitive reason there is only 1 relation for the triangle is because the Hilbert basis for $\mathcal{C}_\Delta$ has 8 elements, whereas there are only 7 Fock–Goncharov coordinates.

We now describe all of the relations in the KTGS cone $\mathcal{C}_{\mathcal{T}} \subset \mathbb{Z}^{12}_+$ for the square. Intuitively, there are 10 relations because the Hilbert basis for $\mathcal{C}_{\mathcal{T}}$ has 22 elements, whereas there are only 12 Fock–Goncharov coordinates.

Proposition 3.10. *The following 10 linear relations are independent and complete among the 22 elements of the Hilbert basis $\mathcal{H}_{(\square,\mathcal{T})} \subset \mathcal{C}_{\mathcal{T}}$ for the KTGS cone for the square:*

(1) $\Phi_{\mathcal{T}}([T_{in}, L_b]) + \Phi_{\mathcal{T}}([T_{out}, L_c]) = \Phi_{\mathcal{T}}([L_a]) + \Phi_{\mathcal{T}}([L_b]) + \Phi_{\mathcal{T}}([L_c])$;
(2) $\Phi_{\mathcal{T}}([T_{out}, L_c]) + \Phi_{\mathcal{T}}([T_{in}, R_c]) = \Phi_{\mathcal{T}}([L_a]) + \Phi_{\mathcal{T}}([L_c]) + \Phi_{\mathcal{T}}([L_b, R_c])$;
(3) $\Phi_{\mathcal{T}}([L_c, T_{in}]) + \Phi_{\mathcal{T}}([L_b, T_{out}]) = \Phi_{\mathcal{T}}([L_b]) + \Phi_{\mathcal{T}}([L_c]) + \Phi_{\mathcal{T}}([L_d])$;
(4) $\Phi_{\mathcal{T}}([L_b, T_{out}]) + \Phi_{\mathcal{T}}([R_b, T_{in}]) + \Phi_{\mathcal{T}}([T_{out}, R_b]) = \Phi_{\mathcal{T}}([L_b]) + \Phi_{\mathcal{T}}([R_b]) + \Phi_{\mathcal{T}}([L_d]) + \Phi_{\mathcal{T}}([T_{out}, L_c])$;
(5) $\Phi_{\mathcal{T}}([R_c, T_{out}]) + \Phi_{\mathcal{T}}([L_b, R_c]) = \Phi_{\mathcal{T}}([L_b, T_{out}]) + \Phi_{\mathcal{T}}([R_c])$;
(6) $\Phi_{\mathcal{T}}([T_{out}, T_{in}]) + \Phi_{\mathcal{T}}([L_b, T_{out}]) = \Phi_{\mathcal{T}}([L_b]) + \Phi_{\mathcal{T}}([L_d]) + \Phi_{\mathcal{T}}([T_{out}, L_c])$;
(7) $\Phi_{\mathcal{T}}([T_{in}, T_{out}]) + \Phi_{\mathcal{T}}([T_{out}, L_c]) = \Phi_{\mathcal{T}}([L_a]) + \Phi_{\mathcal{T}}([L_c]) + \Phi_{\mathcal{T}}([L_b, T_{out}])$;
(8) $\Phi_{\mathcal{T}}([T_{out}, R_b]) + \Phi_{\mathcal{T}}([R_b, L_c]) = \Phi_{\mathcal{T}}([R_b]) + \Phi_{\mathcal{T}}([T_{out}, L_c])$;
(9) $\Phi_{\mathcal{T}}([L_b, R_c]) + \Phi_{\mathcal{T}}([R_c, L_b]) = \Phi_{\mathcal{T}}([L_b]) + \Phi_{\mathcal{T}}([R_c])$;
(10) $\Phi_{\mathcal{T}}([T_{out}, L_c]) + \Phi_{\mathcal{T}}([L_c, R_b]) = \Phi_{\mathcal{T}}([T_{out}, R_b]) + \Phi_{\mathcal{T}}([L_c])$.

Proof. More precisely, what is meant by the statement of the proposition is the following. Let $f : \mathbb{R}^{22} \to \mathbb{R}^{12}$ be the linear map $f(\lambda_1, \lambda_2, \dots, \lambda_{22}) = \sum_{i=1}^{22} \lambda_i \Phi_{\mathcal{T}}(W_i^H) \in \mathbb{R}^{12}$, where the webs W_i^H are as in Theorem 3.3. Each of the 10 relations above determines an element r_j of $\mathbb{R}^{22}$. Let $V \subset \mathbb{R}^{22}$ be the kernel of f. The claim is that the elements $\{r_j\}_{j=1,2,\dots,10}$ form a basis of V. The remainder of the proof is elementary. □

Remark 3.11. The relations of Proposition 3.10 can be viewed as 'tropical SL_3 skein relations'. Indeed, they can be 'predicted' as the result of resolving the overlapping webs in the square (corresponding to a side of a given relation in the cone) by the Kuperberg SL_3 skein relation [31, Section 4, $q = 1$] (one resolution per crossing in the picture). See also [52].

4. KTGS cone for the square: sector decomposition

In Section 3, we saw that the Knutson–Tao–Goncharov–Shen cone $\mathcal{C}_{\mathcal{T}} \subset \mathbb{Z}_+^{12}$ for the triangulated square $(\square, \mathcal{T})$ has a Hilbert basis $\mathcal{H}_{(\square,\mathcal{T})} \subset \mathcal{C}_{\mathcal{T}}$ consisting of 22 elements (Figures 13 and 14). There are many linear dependence relations in $\mathbb{R}^{12}$ among these Hilbert basis elements; see Proposition 3.10. In this last section, we study certain linearly independent subsets of the Hilbert basis $\mathcal{H}_{(\square,\mathcal{T})}$ that have topological interpretations in terms of webs.

More specifically, we show that each of the 42 web families $\mathcal{W}_i \subset \mathcal{W}_\square$ (Section 4.1 and Figure 15) corresponds to a 12-dimensional subcone $\mathcal{C}_{\mathcal{T}}^i \subset \mathcal{C}_{\mathcal{T}}$ (called a sector) generated by 12 Hilbert basis elements. Moreover, every point in the KTGS cone $\mathcal{C}_{\mathcal{T}}$ lies in such a sector $\mathcal{C}_{\mathcal{T}}^i$. These sectors have a geometric description in terms of tropical integer $\mathcal{X}$-coordinates (Figure 16) for reduced webs $W \in \mathcal{W}_\square$, which are functions of the corresponding positive tropical integer $\mathcal{A}$-coordinates (Figure 10); we already encountered some of these ideas in Section 3.1.3.

In summary, this analysis gives us a deeper understanding of the combinatorial, geometric, and topological properties of the KTGS cone $\mathcal{C}_{\mathcal{T}} \subset \mathbb{Z}_+^{12}$ for the square; see Figure 3. (In this section, we will use some of the terminology and results of Appendix B.)

4.1. Web families in the square.

Recall the notion of a web schematic; see Section 1.3.1 and Remark 1.11. Recall also Definitions 2.7 and 2.9, for the notions of corner webs $W = W_r \in \mathcal{R}$ and cornerless webs $W = W_c$.

Proposition 4.1. *We can write the reduced webs in the triangulated square as a union*

$$\mathcal{W}_\square = \cup_{i=1}^{42} \mathcal{W}_i$$

of 42 *families* $\mathcal{W}_i \subset \mathcal{W}_\square$ *of reduced webs, where by definition* $W \in \mathcal{W}_i$ *if its cornerless part* W_c *can be represented by the 'i-th cornerless schematic',* 9 *of which are shown in Figure* 15*; in fact, up to rotation, reflection, and orientation-reversing symmetry (see the caption of Figure* 15*), every family* $\mathcal{W}_i$ *falls into one of these* 9 *cases.*

Proof. This is a direct combinatorial count, done by hand. We note that the number of possibilities is restricted by the topology of web good positions; see Observation 1.13. □

Notation 4.2. Completely arbitrarily, the index i_j for the family $\mathcal{W}_{i_j}$ whose cornerless schematic is labeled (j) in Figure 15 $(j = 1, 2, \ldots, 9)$ is

$$i_1 = 29,\ i_2 = 30,\ i_3 = 42,\ i_4 = 17,\ i_5 = 5,\ i_6 = 6,\ i_7 = 2,\ i_8 = 1,\ i_9 = 33.$$

See also Remark 4.3 just below.

As we will see later in this section, the family $\mathcal{W}_i$ corresponds to the i-th sector shown in Figure 3.

Remark 4.3. If we define an equivalence relation on the 42 families $\mathcal{W}_i$ by rotation, reflection, and orientation-reversing symmetry, then (using Notation 4.2) the symmetry class of:

(1) $\mathcal{W}_{i_1}$ has four members, $\mathcal{W}_{i_1} = \mathcal{W}_{29}$, $\mathcal{W}_{21}, \mathcal{W}_{24}, \mathcal{W}_{32}$;
(2) $\mathcal{W}_{i_2}$ has four members, $\mathcal{W}_{i_2} = \mathcal{W}_{30}$, $\mathcal{W}_{23}, \mathcal{W}_{22}, \mathcal{W}_{31}$;

(3) $\mathcal{W}_{i_3}$ has eight members, $\mathcal{W}_{i_3} = \mathcal{W}_{42}$, $\mathcal{W}_{36}, \mathcal{W}_{37}, \mathcal{W}_{38}, \mathcal{W}_{39}, \mathcal{W}_{40}, \mathcal{W}_{41}, \mathcal{W}_{35}$;
(4) $\mathcal{W}_{i_4}$ has eight members, $\mathcal{W}_{i_4} = \mathcal{W}_{17}$, $\mathcal{W}_{18}, \mathcal{W}_{19}, \mathcal{W}_{20}, \mathcal{W}_{25}, \mathcal{W}_{26}, \mathcal{W}_{27}, \mathcal{W}_{28}$;
(5) $\mathcal{W}_{i_5}$ has four members, $\mathcal{W}_{i_5} = \mathcal{W}_5$, $\mathcal{W}_8, \mathcal{W}_{13}, \mathcal{W}_{16}$;
(6) $\mathcal{W}_{i_6}$ has four members, $\mathcal{W}_{i_6} = \mathcal{W}_6$, $\mathcal{W}_7, \mathcal{W}_{14}, \mathcal{W}_{15}$;
(7) $\mathcal{W}_{i_7}$ has four members, $\mathcal{W}_{i_7} = \mathcal{W}_2$, $\mathcal{W}_3, \mathcal{W}_{10}, \mathcal{W}_{11}$;
(8) $\mathcal{W}_{i_8}$ has four members, $\mathcal{W}_{i_8} = \mathcal{W}_1$, $\mathcal{W}_4, \mathcal{W}_9, \mathcal{W}_{12}$;
(9) $\mathcal{W}_{i_9}$ has two members, $\mathcal{W}_{i_9} = \mathcal{W}_{33}$, $\mathcal{W}_{34}$.

We emphasize that each schematic in Figure 15 represents a subset $\mathcal{W}_i \subset \mathcal{W}_\square$ of reduced webs in the square. Note these subsets are not disjoint. Indeed, each intersection $\mathcal{W}_i \cap \mathcal{W}_j$ is at least '8-dimensional', in an appropriate sense (see later in this section), since the set of corner webs $\mathcal{R}$ is contained in each family $\mathcal{W}_i$. This intersection can contain more than just the corner webs. For instance, the intersection $\mathcal{W}_{29} \cap \mathcal{W}_{30}$, corresponding to schematics (1) and (2) in Figure 15, is '11-dimensional' (thus, in Figure 3, sectors 29 and 30 are separated by a wall); the last, 12-th, dimension comes from the source or sink labeled with the weight $x \in \mathbb{Z}_+$ in schematics (1) and (2). As another example, $\mathcal{W}_{29} \cap \mathcal{W}_{33}$, corresponding to schematics (1) and (9) in Figure 15, is '10-dimensional' (thus, in Figure 3, sectors 29 and 33 are not separated by a wall). In fact, each family $\mathcal{W}_i$ is '12-dimensional' (intuitively, this is because the square has 12 Fock–Goncharov coordinates): 8 dimensions come from the corner part W_r, and 4 dimensions come from the cornerless part W_c. Correspondingly, each cornerless schematic in Figure 15 has four weights $x, y, z, t \in \mathbb{Z}_+$.

We remind (Remark 1.11) that, in schematics (1) and (2) in Figure 15, we could have reversed the orientations of the two arc components, without changing the class of the web in $\mathcal{W}_\square$. On the other hand, the orientation of the weight x component distinguishes schematic (1) from (2); note the caption of Figure 15. Also, the t and z strands in schematic (3), for example, do not cross in the upper triangle, for otherwise the web would have an external H-4-face (Section 1.3.1) on the boundary, violating the reduced property.

Lastly, we remark that the web families $\mathcal{W}_i$ depend on the choice of triangulation $\mathcal{T}$ of the square $\square$; compare Example (family (7)) in Appendix C, in particular the difference between the cases $z \geqslant t$ and $z \leqslant t$, the former case which is demonstrated in Figures 22-25.

4.2. Sector decomposition of the KTGS cone for the triangle and the square. Recall the notion of a sector decomposition $\{C_i\}_i$ of a full cone $C \subset \mathbb{R}^k$, and of a wall between two full cones; see Definitions B.9 and B.10.

Definition 4.4. Let $\widehat{S}$ be a marked surface, either the ideal triangle or the ideal square, and let $\mathcal{T}$ be an ideal triangulation of $\widehat{S}$. The ***completed Knutson–Tao–Goncharov–Shen (KTGS) cone*** $C_\mathcal{T}$ is the completion $C_\mathcal{T} = \overline{\mathcal{C}}_\mathcal{T} \subset \mathbb{R}^N_+$ of the KTGS cone $\mathcal{C}_\mathcal{T} \subset \mathbb{Z}^N_+$; see Definitions 1.4, B.15, Propositions 1.5, 3.1, and Theorem 3.3 (note however Remark 3.6).

4.2.1. *Sector decomposition for the triangle.* Let $S = \Delta$ be the ideal triangle. We will use the notation of Section 3.1.1.

Proposition 4.5. *The completed KTGS cone $C_\Delta \subset \mathbb{R}^7_+$ is 7-dimensional. Putting*

$$\mathcal{C}^{out}_\Delta = \mathrm{span}_{\mathbb{Z}_+}(\{\Phi_\Delta(W^H); W^H = L_a, R_a, L_b, R_b, L_c, R_c, T_{out}\}) \subset \mathcal{C}_\Delta \subset \mathbb{Z}^7_+,$$
$$\mathcal{C}^{in}_\Delta = \mathrm{span}_{\mathbb{Z}_+}(\{\Phi_\Delta(W^H); W^H = L_a, R_a, L_b, R_b, L_c, R_c, T_{in}\}) \subset \mathcal{C}_\Delta \subset \mathbb{Z}^7_+,$$
$$C^{out}_\Delta = \overline{\mathcal{C}}^{out}_\Delta,\ C^{in}_\Delta = \overline{\mathcal{C}}^{in}_\Delta \subset C_\Delta \subset \mathbb{R}^7_+$$

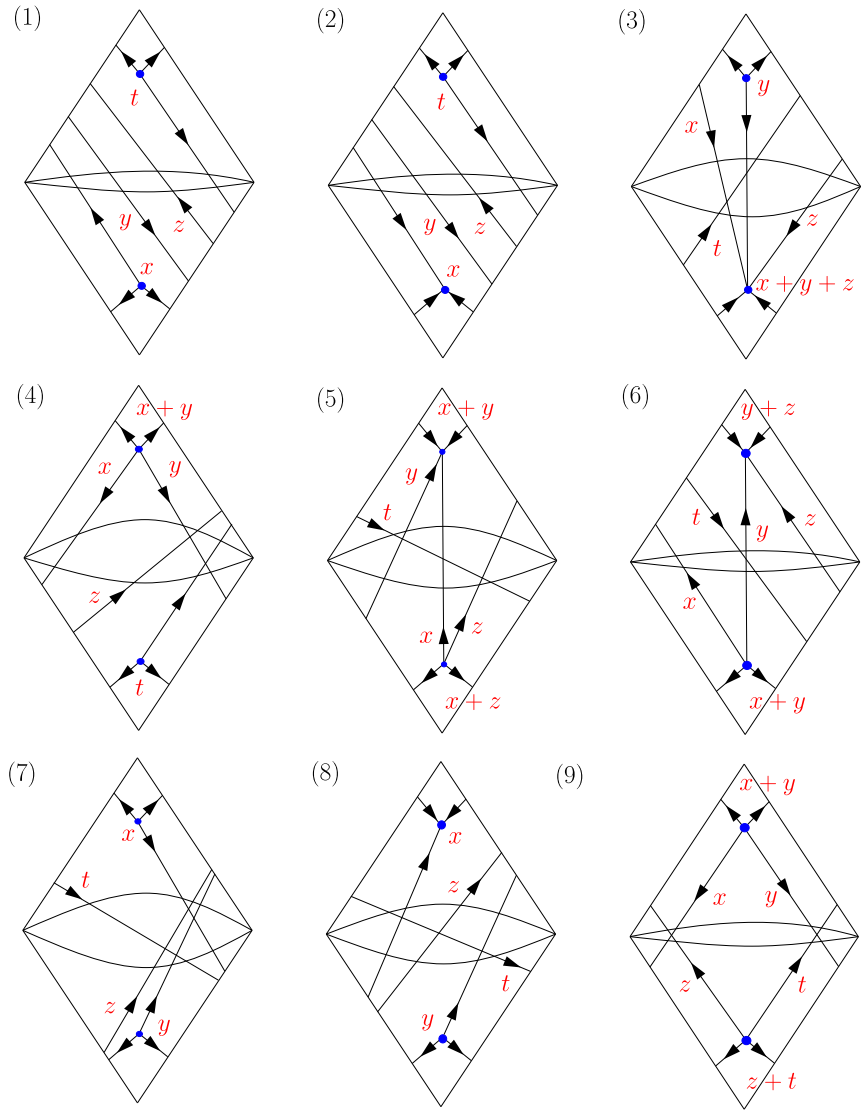

FIGURE 15. Families (1)-(9). Schematics for cornerless webs $W = W_c$. There are 9 reduced web families up to rotation, reflection, and orientation-reversing symmetry. (Note that orientation-reversing symmetry means simultaneously reversing the orientations of all components of the web.)

yields a sector decomposition $\{C_\Delta^{out}, C_\Delta^{in}\}$ *of* C_Δ*. Moreover,* $C_\Delta^{out} \cap C_\Delta^{in}$ *is a* 6*-dimensional wall, generated by the cone points* $\Phi_\Delta(W^H)$ *corresponding to the* 6 *corner arcs in* $\mathcal{W}_\Delta$*.*

Moreover, the rank (*Definition* B.9) *of the completed KTGS cone* $C_\Delta \subset \mathbb{R}_+^7$ *is* 8*.*

Proof. This is a consequence of [9, Proposition 6.6] and its proof. A detailed proof is provided in the arXiv version [8] of this article. □

4.2.2. *Sector decomposition for the square.* Let $S = \square$ be the ideal square, equipped with an ideal triangulation $\mathcal{T}$, namely a choice of diagonal. We will use the notation

of Section 3.1.2. In particular, recall the 22 Hilbert basis webs W_j^H in $\mathcal{W}_\square$ ($j = 1, 2, \ldots, 22$) associated to $\mathcal{T}$; see Figures 13 and 14.

We define 42 subcones $C_{\mathcal{T}}^i \subset C_{\mathcal{T}}$ ($i = 1, 2, \ldots, 42$) of the completed KTGS cone $C_{\mathcal{T}} \subset \mathbb{R}_+^{12}$ as follows. First, define 42 web subsets $\mathcal{Q}_i \subset \mathcal{W}_\square$ ($i = 1, 2, \ldots, 42$), each consisting of four Hilbert basis webs W^H, by:

(1) $\mathcal{Q}_1 = \{[T_{in}, L_b], [R_c, T_{out}], [R_c, L_b], [R_b, L_c]\}$;
(2) $\mathcal{Q}_2 = \{[T_{out}, L_c], [R_c, T_{out}], [R_c, L_b], [R_b, L_c]\}$;
(3) $\mathcal{Q}_3 = \{[T_{in}, L_b], [R_b, L_c], [R_b, T_{in}], [R_c, L_b]\}$;
(4) $\mathcal{Q}_4 = \{[T_{out}, L_c], [R_b, L_c], [R_b, T_{in}], [R_c, L_b]\}$;
(5) $\mathcal{Q}_5 = \{[T_{in}, T_{out}], [T_{in}, L_b], [R_c, T_{out}], [R_b, L_c]\}$;
(6) $\mathcal{Q}_6 = \{[L_b, T_{out}], [T_{in}, T_{out}], [T_{in}, R_c], [R_b, L_c]\}$;
(7) $\mathcal{Q}_7 = \{[T_{in}, L_b], [L_c, R_b], [T_{in}, T_{out}], [R_c, T_{out}]\}$;
(8) $\mathcal{Q}_8 = \{[T_{in}, T_{out}], [L_c, R_b], [L_b, T_{out}], [T_{in}, R_c]\}$;
(9) $\mathcal{Q}_9 = \{[T_{out}, R_b], [L_c, R_b], [L_c, T_{in}], [L_b, R_c]\}$;
(10) $\mathcal{Q}_{10} = \{[T_{in}, R_c], [L_c, R_b], [L_c, T_{in}], [L_b, R_c]\}$;
(11) $\mathcal{Q}_{11} = \{[T_{out}, R_b], [L_c, R_b], [L_b, T_{out}], [L_b, R_c]\}$;
(12) $\mathcal{Q}_{12} = \{[T_{in}, R_c], [L_c, R_b], [L_b, T_{out}], [L_b, R_c]\}$;
(13) $\mathcal{Q}_{13} = \{[T_{out}, T_{in}], [T_{out}, R_b], [L_c, T_{in}], [L_b, R_c]\}$;
(14) $\mathcal{Q}_{14} = \{[T_{out}, L_c], [R_b, T_{in}], [T_{out}, T_{in}], [L_b, R_c]\}$;
(15) $\mathcal{Q}_{15} = \{[T_{out}, T_{in}], [T_{out}, R_b], [L_c, T_{in}], [R_c, L_b]\}$;
(16) $\mathcal{Q}_{16} = \{[T_{out}, L_c], [R_b, T_{in}], [T_{out}, T_{in}], [R_c, L_b]\}$;
(17) $\mathcal{Q}_{17} = \{[T_{out}, R_b], [T_{out}, L_c], [R_c, L_b], [R_c, T_{out}]\}$;
(18) $\mathcal{Q}_{18} = \{[T_{in}, L_b], [R_b, T_{in}], [L_c, T_{in}], [R_c, L_b]\}$;
(19) $\mathcal{Q}_{19} = \{[T_{in}, L_b], [L_c, R_b], [L_c, T_{in}], [T_{in}, R_c]\}$;
(20) $\mathcal{Q}_{20} = \{[T_{out}, R_b], [L_c, R_b], [L_b, T_{out}], [R_c, T_{out}]\}$;
(21) $\mathcal{Q}_{21} = \{[T_{out}, R_b], [L_c, R_b], [R_c, T_{out}], [R_c, L_b]\}$;
(22) $\mathcal{Q}_{22} = \{[T_{out}, R_b], [L_c, R_b], [L_c, T_{in}], [R_c, L_b]\}$;
(23) $\mathcal{Q}_{23} = \{[T_{in}, L_b], [L_c, R_b], [R_c, T_{out}], [R_c, L_b]\}$;
(24) $\mathcal{Q}_{24} = \{[T_{in}, L_b], [L_c, R_b], [L_c, T_{in}], [R_c, L_b]\}$;
(25) $\mathcal{Q}_{25} = \{[T_{out}, L_c], [T_{out}, R_b], [L_b, T_{out}], [L_b, R_c]\}$;
(26) $\mathcal{Q}_{26} = \{[T_{in}, R_c], [R_b, T_{in}], [L_c, T_{in}], [L_b, R_c]\}$;
(27) $\mathcal{Q}_{27} = \{[T_{in}, L_b], [R_b, L_c], [R_b, T_{in}], [T_{in}, R_c]\}$;
(28) $\mathcal{Q}_{28} = \{[T_{out}, L_c], [R_b, L_c], [L_b, T_{out}], [R_c, T_{out}]\}$;
(29) $\mathcal{Q}_{29} = \{[L_b, T_{out}], [R_b, L_c], [L_b, R_c], [T_{out}, L_c]\}$;
(30) $\mathcal{Q}_{30} = \{[R_b, T_{in}], [R_b, L_c], [L_b, R_c], [T_{out}, L_c]\}$;
(31) $\mathcal{Q}_{31} = \{[T_{in}, R_c], [R_b, L_c], [L_b, T_{out}], [L_b, R_c]\}$;
(32) $\mathcal{Q}_{32} = \{[T_{in}, R_c], [R_b, L_c], [R_b, T_{in}], [L_b, R_c]\}$;
(33) $\mathcal{Q}_{33} = \{[T_{out}, R_b], [T_{out}, L_c], [L_b, T_{out}], [R_c, T_{out}]\}$;
(34) $\mathcal{Q}_{34} = \{[T_{in}, L_b], [R_b, T_{in}], [L_c, T_{in}], [T_{in}, R_c]\}$;
(35) $\mathcal{Q}_{35} = \{[T_{in}, T_{out}], [T_{in}, L_b], [T_{in}, R_c], [R_b, L_c]\}$;
(36) $\mathcal{Q}_{36} = \{[T_{in}, T_{out}], [R_b, L_c], [L_b, T_{out}], [R_c, T_{out}]\}$;
(37) $\mathcal{Q}_{37} = \{[T_{in}, L_b], [L_c, R_b], [T_{in}, T_{out}], [T_{in}, R_c]\}$;
(38) $\mathcal{Q}_{38} = \{[T_{in}, T_{out}], [L_c, R_b], [L_b, T_{out}], [R_c, T_{out}]\}$;
(39) $\mathcal{Q}_{39} = \{[T_{out}, L_c], [T_{out}, R_b], [T_{out}, T_{in}], [L_b, R_c]\}$;
(40) $\mathcal{Q}_{40} = \{[T_{out}, T_{in}], [R_b, T_{in}], [L_c, T_{in}], [L_b, R_c]\}$;
(41) $\mathcal{Q}_{41} = \{[T_{out}, L_c], [T_{out}, R_b], [T_{out}, T_{in}], [R_c, L_b]\}$;
(42) $\mathcal{Q}_{42} = \{[R_b, T_{in}], [T_{out}, T_{in}], [L_c, T_{in}], [R_c, L_b]\}$.

The i-th web subset $\mathcal{Q}_i \subset \mathcal{W}_i \subset \mathcal{W}_\square$ is moreover a subset of the i-th web family $\mathcal{W}_i$ (Section 4.1). More precisely, each of the four Hilbert basis webs $W^H \in \mathcal{Q}_i$ is determined by the schematic picture for the web family $\mathcal{W}_i$ (as in Figure 15) by putting all but one of the variables x, y, z, t to 0 and the remaining variable to 1.

Recall that the 9 specific web families denoted (j) in Figure 15 are the families $\mathcal{W}_{i_j}$ as explained in Notation 4.2.

DEFINITION 4.6. For $i = 1, 2, \ldots, 42$, let $\mathcal{Q}_i \subset \mathcal{W}_i \subset \mathcal{W}_\square$ be the set of four webs defined just above, and recall that W_j^H for $j = 1, 2, \ldots, 8$ are the 8 corner arcs in the square.

Define the ***i-th completed KTGS subcone*** $C_{\mathcal{T}}^i \subset C_{\mathcal{T}} \subset \mathbb{R}_+^{12}$ as the completion

$$C_{\mathcal{T}}^i = \overline{\mathcal{C}}_{\mathcal{T}}^i$$

of the ***i-th KTGS submonoid*** $\mathcal{C}_{\mathcal{T}}^i \subset \mathcal{C}_{\mathcal{T}} \subset \mathbb{Z}_+^{12}$, defined by

$$\mathcal{C}_{\mathcal{T}}^i = \mathrm{span}_{\mathbb{Z}_+}(\{\Phi_{\mathcal{T}}(W_1^H), \Phi_{\mathcal{T}}(W_2^H), \ldots, \Phi_{\mathcal{T}}(W_8^H)\} \cup \{\Phi_{\mathcal{T}}(W^H); W^H \in \mathcal{Q}_i\})$$

where $\Phi_{\mathcal{T}}(W^H) \in \mathcal{C}_{\mathcal{T}} \subset \mathbb{Z}_+^{12}$ is the point in the KTGS positive integer cone $\mathcal{C}_{\mathcal{T}}$ assigned to W^H by the web tropical coordinate map $\Phi_{\mathcal{T}} : \mathcal{W}_\square \to \mathcal{C}_{\mathcal{T}}$.

The set $\mathcal{Q}_i$ of four webs is called the ***topological type*** of the completed KTGS subcone $C_{\mathcal{T}}^i$.

By construction of the web tropical coordinate map $\Phi_{\mathcal{T}}$, we can immediately say:

OBSERVATION 4.7. *For $i = 1, 2, \ldots, 42$, we have the image $\Phi_{\mathcal{T}}(\mathcal{W}_i) = \mathcal{C}_{\mathcal{T}}^i \subset \mathbb{Z}_+^{12}$.* □

The main result of the second half of the paper is:

THEOREM 4.8. *Consider the completed KTGS cone $C_{\mathcal{T}} \subset \mathbb{R}_+^{12}$ for the triangulated square $(\square, \mathcal{T})$; see Definition* 4.4. *Then the following properties hold.*

(I) *$C_{\mathcal{T}}$ is 12-dimensional. Namely, $C_{\mathcal{T}}$ is a full cone; see Definition* B.9.

(II) *The completed KTGS subcones $C_{\mathcal{T}}^i \subset C_{\mathcal{T}}$ are full sectors forming a sector decomposition $\{C_{\mathcal{T}}^i\}_{i=1,2,\ldots,42}$ of $C_{\mathcal{T}}$; see Definition* B.10.

(III) *The intersection $C_{\mathcal{T}}^i \cap C_{\mathcal{T}}^\ell$ is a wall if and only if $\mathcal{Q}_i \cap \mathcal{Q}_\ell$ has 3 elements; that is, if and only if the topological types of $C_{\mathcal{T}}^i$ and $C_{\mathcal{T}}^\ell$ differ by a single web. In this case,*

(k)
$$C_{\mathcal{T}}^i \cap C_{\mathcal{T}}^\ell = \mathrm{span}_{\mathbb{R}_+}(\{\Phi_{\mathcal{T}}(W_1^H), \Phi_{\mathcal{T}}(W_2^H), \ldots, \Phi_{\mathcal{T}}(W_8^H)\} \cup \{\Phi_{\mathcal{T}}(W^H); W^H \in \mathcal{Q}_i \cap \mathcal{Q}_\ell\}) \subset \mathbb{R}_+^{12}.$$

Moreover, for each web $W^H \in \mathcal{Q}_i$, there exists a unique index $i^*(i, W^H) \in \{1, 2, \ldots, 42\}$ such that

$$\mathcal{Q}_i \cap \mathcal{Q}_{i^*(i,W^H)} = \mathcal{Q}_i - \{W^H\};$$

that is, such that there is a web $W^*(i, W^H) \in \mathcal{Q}_{i^*(i,W^H)}$ distinct from W^H satisfying the property that the topological type $\mathcal{Q}_{i^*(i,W^H)}$ of $C_{\mathcal{T}}^{i^*(i,W^H)}$ is obtained from the topological type $\mathcal{Q}_i$ of $C_{\mathcal{T}}^i$ by swapping W^H with $W^*(i, W^H)$.

In particular, each sector $C_{\mathcal{T}}^i$ has 4 walls. See Figure 3.

EXAMPLE 4.9. As an example of the second paragraph of the third item of Theorem 4.8, consider $i = i_1 = 29$, corresponding to family (1) in Figure 15. If $W^H = [L_b, T_{out}] \in \mathcal{Q}_{29}$, then $i^*(29, W^H) = i_2 = 30$ corresponding to family (2) in Figure 15, and $W^*(29, W^H) = [R_b, T_{in}] \in \mathcal{Q}_{30}$. One similarly checks that $i^*(29, [L_b, R_c]) = 28$ and $W^*(29, [L_b, R_c]) = [R_c, T_{out}] \in \mathcal{Q}_{28}$; that $i^*(29, [R_b, L_c]) = 25$ and $W^*(29, [R_b, L_c]) = [T_{out}, R_b] \in \mathcal{Q}_{25}$; and, that $i^*(29, [T_{out}, L_c]) = 31$ and $W^*(29, [T_{out}, L_c]) = [T_{in}, R_c] \in \mathcal{Q}_{31}$.

Note that Figure 3 provides some, but not all, of this topological information; the full information is contained in the definition of the subsets $\mathcal{Q}_i$ above.

Question 4.10. By Theorem 3.3, the Hilbert basis $\mathcal{H}_{(\square,\mathcal{T})}$ of the positive integer cone $\mathcal{C}_{\mathcal{T}} \subset \mathbb{Z}_+^{12}$ has 22 elements. It follows by Observation B.16 that $\operatorname{rank}(C_{\mathcal{T}}) \leqslant 22$. By Theorem 4.8, $\operatorname{rank}(C_{\mathcal{T}}) \geqslant 12$. What is the rank of $C_{\mathcal{T}}$? (Compare the last paragraph of Proposition 4.5.)

Remark 4.11. The authors enjoy imagining Theorem 4.8 as expressing a kind of 'topological wall-crossing phenomenon', where we interpret the swapping of topological types upon crossing a wall as a kind of 'web mutation'. Investigating how this phenomenon relates to other wall-crossing phenomena appearing in cluster geometry [30] could be of potential interest. In particular, there should be a relationship with the so-called D_4 cluster complex (see, for example, [14]). This is also related to Remark 3.4 and the last paragraph of Section 4.1.

4.3. Proof of Theorem 4.8. We make some preparations before proving the theorem.

4.3.1. *Two linear isomorphisms: second isomorphism $\phi_{\mathcal{T}}$ by tropical $\mathcal{X}$-coordinates.* In Section 3.1.3, to each ideal triangulation $\mathcal{T}$ of the square $\square$ we constructed a linear isomorphism $\theta_{\mathcal{T}} : \mathbb{R}^{12} \to V_{\mathcal{T}} \subset \mathbb{R}^{18}$. This map sends 12 real numbers $A_1, A_2, \ldots, A_{12}$, called the '(real) tropical $\mathcal{A}$-coordinates', to their 18 rhombus numbers $\beta_1, \beta_2, \ldots, \beta_{18}$. There are 6 relations (see (j) in Section 3.1.3) defining the 12-dimensional subspace $V_{\mathcal{T}} \subset \mathbb{R}^{18}$, which determine four real numbers X_1, X_2, X_3, X_4, called the '(real) tropical $\mathcal{X}$-coordinates': they are four numbers assigned to any 18-tuple in $V_{\mathcal{T}}$ of rhombus numbers. See Figure 16. See also [52].

Remark 4.12. The tropical $\mathcal{X}$-coordinates originate in Fock–Goncharov theory as tropicalized double and triple ratios [10, 12], and can be thought of in the following geometric way. For X_1, say, consider the hexagon in the top triangle in the top left square of Figure 16. There are six tropical $\mathcal{A}$-coordinates assigned to the vertices of this hexagon. Then X_1 is the signed sum of these coordinates, as indicated in the figure. Similarly for X_2, X_3, X_4.

Definition 4.13. Let $V_{\mathcal{T}} \subset \mathbb{R}^{18}$ be the 12-dimensional subspace just discussed. Define a linear map

$$\phi_{\mathcal{T}} : V_{\mathcal{T}} \to \mathbb{R}^8 \times \mathbb{R}^4$$

by

$$\phi_{\mathcal{T}}(\beta_1, \beta_2, \beta_3, \ldots, \beta_{18}) = (\beta_1, \beta_2, \beta_4, \beta_5, \beta_7, \beta_8, \beta_{10}, \beta_{11}; X_1, X_2, X_3, X_4).$$

See Figure 16, where the eight rhombi appearing in the first eight coordinates of the image of $\phi_{\mathcal{T}}$ are colored green.

For example, the images under $\phi_{\mathcal{T}}$ of $\theta_{\mathcal{T}}$ applied to the 22 Hilbert basis elements, $\theta_{\mathcal{T}}(\Phi_{\mathcal{T}}(W_j^H)) \in V_{\mathcal{T}}$, can be computed from Figures 13 and 14, or from the computations in Section 3.1.3, to be:

(1) $\phi_{\mathcal{T}}(\theta_{\mathcal{T}}(\Phi_{\mathcal{T}}([R_a]))) = (1,0,0,0,0,0,0,0;0,0,0,0)$;
(2) $\phi_{\mathcal{T}}(\theta_{\mathcal{T}}(\Phi_{\mathcal{T}}([L_a]))) = (0,1,0,0,0,0,0,0;0,0,0,0)$;
(3) $\phi_{\mathcal{T}}(\theta_{\mathcal{T}}(\Phi_{\mathcal{T}}([R_b]))) = (0,0,1,0,0,0,0,0;0,0,0,0)$;
(4) $\phi_{\mathcal{T}}(\theta_{\mathcal{T}}(\Phi_{\mathcal{T}}([L_b]))) = (0,0,0,1,0,0,0,0;0,0,0,0)$;
(5) $\phi_{\mathcal{T}}(\theta_{\mathcal{T}}(\Phi_{\mathcal{T}}([R_c]))) = (0,0,0,0,1,0,0,0;0,0,0,0)$;
(6) $\phi_{\mathcal{T}}(\theta_{\mathcal{T}}(\Phi_{\mathcal{T}}([L_c]))) = (0,0,0,0,0,1,0,0;0,0,0,0)$;
(7) $\phi_{\mathcal{T}}(\theta_{\mathcal{T}}(\Phi_{\mathcal{T}}([R_d]))) = (0,0,0,0,0,0,1,0;0,0,0,0)$;
(8) $\phi_{\mathcal{T}}(\theta_{\mathcal{T}}(\Phi_{\mathcal{T}}([L_d]))) = (0,0,0,0,0,0,0,1;0,0,0,0)$;
(9) $\phi_{\mathcal{T}}(\theta_{\mathcal{T}}(\Phi_{\mathcal{T}}([T_{out}, R_b]))) = (0,0,0,0,0,0,0,0;1,-1,0,0)$;
(10) $\phi_{\mathcal{T}}(\theta_{\mathcal{T}}(\Phi_{\mathcal{T}}([T_{out}, L_c]))) = (0,0,0,0,0,0,0,0;1,0,0,0)$;
(11) $\phi_{\mathcal{T}}(\theta_{\mathcal{T}}(\Phi_{\mathcal{T}}([T_{in}, L_b]))) = (0,1,0,1,0,1,0,0;-1,0,0,0)$;

(12) $\phi_{\mathcal{T}}(\theta_{\mathcal{T}}(\Phi_{\mathcal{T}}([T_{in}, R_c]))) = (0,1,0,1,0,1,0,0;-1,0,0,1)$;
(13) $\phi_{\mathcal{T}}(\theta_{\mathcal{T}}(\Phi_{\mathcal{T}}([L_b, T_{out}]))) = (0,0,0,1,0,0,0,0;0,0,1,0)$;
(14) $\phi_{\mathcal{T}}(\theta_{\mathcal{T}}(\Phi_{\mathcal{T}}([L_c, T_{in}]))) = (0,0,0,0,0,1,0,1;0,0,-1,0)$;
(15) $\phi_{\mathcal{T}}(\theta_{\mathcal{T}}(\Phi_{\mathcal{T}}([R_b, T_{in}]))) = (0,0,1,0,0,0,0,1;0,1,-1,0)$;
(16) $\phi_{\mathcal{T}}(\theta_{\mathcal{T}}(\Phi_{\mathcal{T}}([R_c, T_{out}]))) = (0,0,0,0,1,0,0,0;0,0,1,-1)$;
(17) $\phi_{\mathcal{T}}(\theta_{\mathcal{T}}(\Phi_{\mathcal{T}}([T_{out}, T_{in}]))) = (0,0,0,0,0,0,0,1;1,0,-1,0)$;
(18) $\phi_{\mathcal{T}}(\theta_{\mathcal{T}}(\Phi_{\mathcal{T}}([T_{in}, T_{out}]))) = (0,1,0,1,0,1,0,0;-1,0,1,0)$;
(19) $\phi_{\mathcal{T}}(\theta_{\mathcal{T}}(\Phi_{\mathcal{T}}([L_b, R_c]))) = (0,0,0,1,0,0,0,0;0,0,0,1)$;
(20) $\phi_{\mathcal{T}}(\theta_{\mathcal{T}}(\Phi_{\mathcal{T}}([R_b, L_c]))) = (0,0,1,0,0,0,0,0;0,1,0,0)$;
(21) $\phi_{\mathcal{T}}(\theta_{\mathcal{T}}(\Phi_{\mathcal{T}}([R_c, L_b]))) = (0,0,0,0,1,0,0,0;0,0,0,-1)$;
(22) $\phi_{\mathcal{T}}(\theta_{\mathcal{T}}(\Phi_{\mathcal{T}}([L_c, R_b]))) = (0,0,0,0,0,1,0,0;0,-1,0,0)$.

PROPOSITION 4.14. *The linear map* $\phi_{\mathcal{T}} : V_{\mathcal{T}} \to \mathbb{R}^8 \times \mathbb{R}^4$ *is an isomorphism. Consequently, letting* $\theta_{\mathcal{T}} : \mathbb{R}^{12} \to V_{\mathcal{T}}$ *be the isomorphism from* Section 3.1.3*, we have that the composition*

$$\phi_{\mathcal{T}} \circ \theta_{\mathcal{T}} : \mathbb{R}^{12} \xrightarrow{\sim} \mathbb{R}^8 \times \mathbb{R}^4$$

is a linear isomorphism.

Proof. Since $V_{\mathcal{T}}$ is 12-dimensional (Proposition 3.8), it suffices to show that the image of $\phi_{\mathcal{T}}$ spans $\mathbb{R}^8 \times \mathbb{R}^4$. Indeed, one checks that the above 22 images $\{\phi_{\mathcal{T}}(\theta_{\mathcal{T}}(\Phi_{\mathcal{T}}(W_j^H)))\}_{j=1,2,\ldots,22} \subset \mathbb{R}^8_+ \times \mathbb{R}^4$ span $\mathbb{R}^8 \times \mathbb{R}^4$. □

DEFINITION 4.15. The linear isomorphism $\phi_{\mathcal{T}} \circ \theta_{\mathcal{T}} : \mathbb{R}^{12} \to \mathbb{R}^8 \times \mathbb{R}^4$ of Proposition 4.14 maps the completed KTGS cone $C_{\mathcal{T}} \subset \mathbb{R}^{12}_+$ to the ***isomorphic cone***

$$C \coloneqq \phi_{\mathcal{T}}(\theta_{\mathcal{T}}(C_{\mathcal{T}})) \subset \mathbb{R}^8_+ \times \mathbb{R}^4.$$

Note that C indeed lies in $\mathbb{R}^8_+ \times \mathbb{R}^4$ because $C_{\mathcal{T}} \subset \mathbb{R}^{12}_+$ is the completion of the KTGS cone $\mathcal{C}_{\mathcal{T}} \subset \mathbb{Z}^{12}_+$, which by definition has all nonnegative (integer) rhombus numbers $\{\beta_i\}_{i=1,2,\ldots,18}$.

Observe, in particular, that the 8 corner arcs $W_1^H, W_2^H, \ldots, W_8^H$ of Figure 13 correspond via $\phi_{\mathcal{T}} \circ \theta_{\mathcal{T}} \circ \Phi_{\mathcal{T}}$ to the first 8 standard basis elements e_i of $\mathbb{R}^8 \times \mathbb{R}^4$.

4.3.2. *Sector decomposition of* $\mathbb{R}^4$ *via the isomorphism* $\phi_{\mathcal{T}} \circ \theta_{\mathcal{T}}$. Let $C \subset \mathbb{R}^8_+ \times \mathbb{R}^4$ be the cone defined in Definition 4.15, which is isomorphic, via the isomorphism $\phi_{\mathcal{T}} \circ \theta_{\mathcal{T}} : \mathbb{R}^{12} \to \mathbb{R}^8 \times \mathbb{R}^4$, to the completed KTGS cone $C_{\mathcal{T}} \subset \mathbb{R}^{12}_+$ for the triangulated square $(\square, \mathcal{T})$.

NOTATION 4.16. Put $k = 8$, $n = 4$, $m = 14$ $(= 22 - 8)$, and $p = 42$ (compare Section B.2.2).

For $j = 1, 2, \ldots, m$, define cone points $x_j \in C$ by

$$x_j = \phi_{\mathcal{T}}(\theta_{\mathcal{T}}(\Phi_{\mathcal{T}}(W^H_{k+j}))) \in C$$

where $\Phi_{\mathcal{T}}(W^H_{j'})$ is the j'-th Hilbert basis element for the triangulated square; see Figures 13 and 14. Note that the points $\{x_j\}_{i=1,2,\ldots,m} \subset C$ are displayed explicitly in Section 4.3.1.

For $i = 1, 2, \ldots, p$, define index sets $J_i \subset \{1, 2, \ldots, m\}$ of constant size n as follows. Given i, consider the topological type $\mathcal{Q}_i \subset \mathcal{W}_i \subset \mathcal{W}_{\square}$ of the completed KTGS subcone $C^i_{\mathcal{T}} \subset \mathbb{R}^{12}_+$ (Definition 4.6). By definition of the topological type $\mathcal{Q}_i$, there are four Hilbert basis webs $W^H_{k+j_1^{(i)}}, W^H_{k+j_2^{(i)}}, W^H_{k+j_3^{(i)}}, W^H_{k+j_4^{(i)}}$, where the indices $j_r^{(i)} \in \{1, 2, \ldots, m\}$, such that $\mathcal{Q}_i = \{W^H_{k+j_r^{(i)}}\}_{r=1,2,3,4}$. We then define the index set J_i by

$$J_i = \{j_1^{(i)}, j_2^{(i)}, j_3^{(i)}, j_4^{(i)}\} \subset \{1, 2, \ldots, m\}.$$

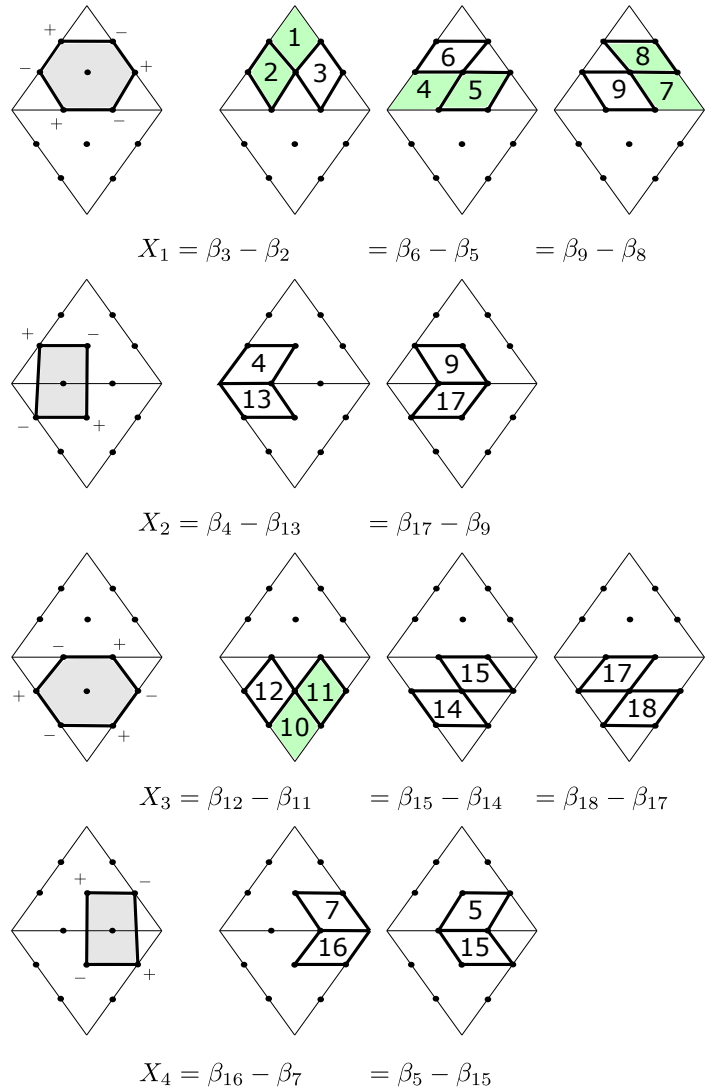

FIGURE 16. Shown are the 18 rhombus numbers $\{\beta_i\}_{i=1,2,\ldots,18}$ for the square, and the associated 4 tropical integer $\mathcal{X}$-coordinates $\{X_i\}_{i=1,2,3,4}$. The latter can be computed either as differences of rhombus numbers, or as alternating sums of the 12 positive tropical integer $\mathcal{A}$-coordinates $\{A_i\}_{i=1,2,\ldots,12}$ around the polygons displayed on the left. The rhombi colored green are those involved in the first 8 coordinates of the isomorphism $\phi_{\mathcal{T}} : V_{\mathcal{T}} \to \mathbb{R}^{12}$.

DEFINITION 4.17. Recalling Notation 4.16: for each $i = 1, 2, \ldots, 42$, define subcones $D_i \subset \mathbb{R}^4$ by (compare Section B.2.2)

$$D_i = \mathrm{span}_{\mathbb{R}_+}(\{\pi_4(x_j); j \in J_i\}) \subset \mathbb{R}^4.$$

Here, $\pi_4 : \mathbb{R}^8 \times \mathbb{R}^4 \to \mathbb{R}^4$ is the natural projection.

Just as for the subcones $C^i_{\mathcal{T}} \subset C_{\mathcal{T}}$, we call $\mathcal{Q}_i$ the ***topological type*** of the subcone $D_i \subset \mathbb{R}^4$.

REMARK 4.18. Note, by the calculations of Section 4.3.1, that the 14 vectors $\{\pi_4(x_j)\}_{j=1,2,\dots,14} \subset \mathbb{R}^4$ are nonzero and distinct.

PROPOSITION 4.19. *The subcones* $D_i \subset \mathbb{R}^4$ *are full sectors forming a sector decomposition* $\{D_i\}_{i=1,2,\dots,42}$ *of* $\mathbb{R}^4$ (*Definition* B.10).

Proof. Let us begin by giving some examples of how to describe the subcones D_i. Specifically, we will describe those 9 subcones $D_{i_j} \subset \mathbb{R}^4$ corresponding to the topological types $\mathcal{Q}_{i_j} \subset \mathcal{W}_{i_j} \subset \mathcal{W}_\square$, which in particular are subsets of the (j) web families $\mathcal{W}_{i_j}$ displayed in Figure 15; see Notation 4.2 and Remark 4.3.

REMARK 4.20. In each of the 9 examples just below, note that the ordering of the rows of the matrix, chosen to match Figure 15, does not affect the description of the subcone $D_i \subset \mathbb{R}^4$.

EXAMPLE ($i_1 = 29$). For $\mathcal{Q}_{29}$, let us write the four vectors $\pi_4(\phi_{\mathcal{T}} \circ \theta_{\mathcal{T}} \circ \Phi_{\mathcal{T}}(\mathcal{Q}_{29})) \subset \mathbb{R}^4$ in rows to form a 4×4 matrix $M_{29} = \begin{pmatrix} 0&0&1&0 \\ 0&1&0&0 \\ 0&0&0&1 \\ 1&0&0&0 \end{pmatrix}$. Then for real numbers $x, y, z, t \geqslant 0$, we get

$$\begin{pmatrix} x & y & z & t \end{pmatrix} M_{29} = \begin{pmatrix} t & y & x & z \end{pmatrix}.$$

Thus $D_{29} = \{(X_1, X_2, X_3, X_4) \in \mathbb{R}_+ \times \mathbb{R}_+ \times \mathbb{R}_+ \times \mathbb{R}_+\}$.

EXAMPLE ($i_2 = 30$). Similarly, for $\mathcal{Q}_{30}$, writing the four vectors $\pi_4(\phi_{\mathcal{T}} \circ \theta_{\mathcal{T}} \circ \Phi_{\mathcal{T}}(\mathcal{Q}_{30}))$ in rows, we get a 4×4 matrix $M_{30} = \begin{pmatrix} 0&1&-1&0 \\ 0&1&0&0 \\ 0&0&0&1 \\ 1&0&0&0 \end{pmatrix}$. Then for $x, y, z, t \geqslant 0$, we get

$$\begin{pmatrix} x & y & z & t \end{pmatrix} M_{30} = \begin{pmatrix} t & x+y & -x & z \end{pmatrix}.$$

Thus $D_{30} = \{(X_1, X_2, X_3, X_4) \in \mathbb{R}_+ \times \mathbb{R}_+ \times \mathbb{R}_- \times \mathbb{R}_+; X_2 + X_3 \geqslant 0\}$.

EXAMPLE ($i_3 = 42$). For $\mathcal{Q}_{42}$, writing the four vectors $\pi_4(\phi_{\mathcal{T}} \circ \theta_{\mathcal{T}} \circ \Phi_{\mathcal{T}}(\mathcal{Q}_{42}))$ in rows, we get a 4×4 matrix $M_{42} = \begin{pmatrix} 0&1&-1&0 \\ 1&0&-1&0 \\ 0&0&-1&0 \\ 0&0&0&-1 \end{pmatrix}$. Then for $x, y, z, t \geqslant 0$, we get

$$\begin{pmatrix} x & y & z & t \end{pmatrix} M_{42} = \begin{pmatrix} y & x & -x-y-z & -t \end{pmatrix}.$$

Thus $D_{42} = \{(X_1, X_2, X_3, X_4) \in \mathbb{R}_+ \times \mathbb{R}_+ \times \mathbb{R}_- \times \mathbb{R}_-; X_1 + X_2 + X_3 \leqslant 0\}$.

EXAMPLE ($i_4 = 17$). For $\mathcal{Q}_{17}$, writing the four vectors $\pi_4(\phi_{\mathcal{T}} \circ \theta_{\mathcal{T}} \circ \Phi_{\mathcal{T}}(\mathcal{Q}_{17}))$ in rows, we get a 4×4 matrix $M_{17} = \begin{pmatrix} 1&-1&0&0 \\ 1&0&0&0 \\ 0&0&0&-1 \\ 0&0&1&-1 \end{pmatrix}$. Then for $x, y, z, t \geqslant 0$, we get

$$\begin{pmatrix} x & y & z & t \end{pmatrix} M_{17} = \begin{pmatrix} x+y & -x & t & -z-t \end{pmatrix}.$$

Thus $D_{17} = \{(X_1, X_2, X_3, X_4) \in \mathbb{R}_+ \times \mathbb{R}_- \times \mathbb{R}_+ \times \mathbb{R}_-; X_1 + X_2 \geqslant 0 \text{ and } X_3 + X_4 \leqslant 0\}$.

EXAMPLE ($i_5 = 5$). For $\mathcal{Q}_5$, writing the four vectors $\pi_4(\phi_{\mathcal{T}} \circ \theta_{\mathcal{T}} \circ \Phi_{\mathcal{T}}(\mathcal{Q}_5))$ in rows, we get a 4×4 matrix $M_5 = \begin{pmatrix} -1&0&1&0 \\ -1&0&0&0 \\ 0&0&1&-1 \\ 0&1&0&0 \end{pmatrix}$. Then for $x, y, z, t \geqslant 0$, we get

$$\begin{pmatrix} x & y & z & t \end{pmatrix} M_5 = \begin{pmatrix} -x-y & t & x+z & -z \end{pmatrix}.$$

Thus $D_5 = \{(X_1, X_2, X_3, X_4) \in \mathbb{R}_- \times \mathbb{R}_+ \times \mathbb{R}_+ \times \mathbb{R}_-; -X_1 \geqslant X_3 + X_4 \geqslant 0\}$.

Example ($i_6 = 6$). For $\mathcal{Q}_6$, writing the four vectors $\pi_4(\phi_{\mathcal{T}} \circ \theta_{\mathcal{T}} \circ \Phi_{\mathcal{T}}(\mathcal{Q}_6))$ in rows, we get a 4×4 matrix $M_6 = \begin{pmatrix} 0 & 0 & 1 & 0 \\ -1 & 0 & 1 & 0 \\ -1 & 0 & 0 & 1 \\ 0 & 1 & 0 & 0 \end{pmatrix}$. Then for $x, y, z, t \geqslant 0$, we get

$$\begin{pmatrix} x & y & z & t \end{pmatrix} M_6 = \begin{pmatrix} -y - z & t & x + y & z \end{pmatrix}.$$

Thus $D_6 = \{(X_1, X_2, X_3, X_4) \in \mathbb{R}_- \times \mathbb{R}_+ \times \mathbb{R}_+ \times \mathbb{R}_+; -X_3 \leqslant X_1 + X_4 \leqslant 0\}$.

Example ($i_7 = 2$). For $\mathcal{Q}_2$, writing the four vectors $\pi_4(\phi_{\mathcal{T}} \circ \theta_{\mathcal{T}} \circ \Phi_{\mathcal{T}}(\mathcal{Q}_2))$ in rows, we get a 4×4 matrix $M_2 = \begin{pmatrix} 1 & 0 & 0 & 0 \\ 0 & 0 & 1 & -1 \\ 0 & 0 & 0 & -1 \\ 0 & 1 & 0 & 0 \end{pmatrix}$. Then for $x, y, z, t \geqslant 0$, we get

$$\begin{pmatrix} x & y & z & t \end{pmatrix} M_2 = \begin{pmatrix} x & t & y & -y - z \end{pmatrix}.$$

Thus $D_2 = \{(X_1, X_2, X_3, X_4) \in \mathbb{R}_+ \times \mathbb{R}_+ \times \mathbb{R}_+ \times \mathbb{R}_-; X_3 + X_4 \leqslant 0\}$.

Example ($i_8 = 1$). For $\mathcal{Q}_1$, writing the four vectors $\pi_4(\phi_{\mathcal{T}} \circ \theta_{\mathcal{T}} \circ \Phi_{\mathcal{T}}(\mathcal{Q}_1))$ in rows, we get a 4×4 matrix $M_1 = \begin{pmatrix} -1 & 0 & 0 & 0 \\ 0 & 0 & 1 & -1 \\ 0 & 0 & 0 & -1 \\ 0 & 1 & 0 & 0 \end{pmatrix}$. Then for $x, y, z, t \geqslant 0$, we get

$$\begin{pmatrix} x & y & z & t \end{pmatrix} M_1 = \begin{pmatrix} -x & t & y & -y - z \end{pmatrix}.$$

Thus $D_1 = \{(X_1, X_2, X_3, X_4) \in \mathbb{R}_- \times \mathbb{R}_+ \times \mathbb{R}_+ \times \mathbb{R}_-; X_3 + X_4 \leqslant 0\}$.

Example ($i_9 = 33$). For $\mathcal{Q}_{33}$, writing the four vectors $\pi_4(\phi_{\mathcal{T}} \circ \theta_{\mathcal{T}} \circ \Phi_{\mathcal{T}}(\mathcal{Q}_{33}))$ in rows, we get a 4×4 matrix $M_{33} = \begin{pmatrix} 1 & -1 & 0 & 0 \\ 1 & 0 & 0 & 0 \\ 0 & 0 & 1 & 0 \\ 0 & 0 & 1 & -1 \end{pmatrix}$. Then for $x, y, z, t \geqslant 0$, we get

$$\begin{pmatrix} x & y & z & t \end{pmatrix} M_{33} = \begin{pmatrix} x + y & -x & z + t & -t \end{pmatrix}.$$

Thus $D_{33} = \{(X_1, X_2, X_3, X_4) \in \mathbb{R}_+ \times \mathbb{R}_- \times \mathbb{R}_+ \times \mathbb{R}_-; X_1 + X_2 \geqslant 0 \text{ and } X_3 + X_4 \geqslant 0\}$.

In the same way as the 9 examples just demonstrated, we compute directly by hand the subcones $D_i \subset \mathbb{R}^4$ for $i = 1, 2, \ldots, 42$ as follows:

(1) $D_1 = \{(X_1, X_2, X_3, X_4) \in \mathbb{R}_- \times \mathbb{R}_+ \times \mathbb{R}_+ \times \mathbb{R}_-; X_3 + X_4 \leqslant 0\}$;
(2) $D_2 = \{(X_1, X_2, X_3, X_4) \in \mathbb{R}_+ \times \mathbb{R}_+ \times \mathbb{R}_+ \times \mathbb{R}_-; X_3 + X_4 \leqslant 0\}$;
(3) $D_3 = \{(X_1, X_2, X_3, X_4) \in \mathbb{R}_- \times \mathbb{R}_+ \times \mathbb{R}_- \times \mathbb{R}_-; X_2 + X_3 \geqslant 0\}$;
(4) $D_4 = \{(X_1, X_2, X_3, X_4) \in \mathbb{R}_+ \times \mathbb{R}_+ \times \mathbb{R}_- \times \mathbb{R}_-; X_2 + X_3 \geqslant 0\}$;
(5) $D_5 = \{(X_1, X_2, X_3, X_4) \in \mathbb{R}_- \times \mathbb{R}_+ \times \mathbb{R}_+ \times \mathbb{R}_-; -X_1 \geqslant X_3 + X_4 \geqslant 0\}$;
(6) $D_6 = \{(X_1, X_2, X_3, X_4) \in \mathbb{R}_- \times \mathbb{R}_+ \times \mathbb{R}_+ \times \mathbb{R}_+; -X_3 \leqslant X_1 + X_4 \leqslant 0\}$;
(7) $D_7 = \{(X_1, X_2, X_3, X_4) \in \mathbb{R}_- \times \mathbb{R}_- \times \mathbb{R}_+ \times \mathbb{R}_-; -X_1 \geqslant X_3 + X_4 \geqslant 0\}$;
(8) $D_8 = \{(X_1, X_2, X_3, X_4) \in \mathbb{R}_- \times \mathbb{R}_- \times \mathbb{R}_+ \times \mathbb{R}_+; -X_3 \leqslant X_1 + X_4 \leqslant 0\}$;
(9) $D_9 = \{(X_1, X_2, X_3, X_4) \in \mathbb{R}_+ \times \mathbb{R}_- \times \mathbb{R}_- \times \mathbb{R}_+; X_1 + X_2 \leqslant 0\}$;
(10) $D_{10} = \{(X_1, X_2, X_3, X_4) \in \mathbb{R}_- \times \mathbb{R}_- \times \mathbb{R}_- \times \mathbb{R}_+; X_1 + X_4 \geqslant 0\}$;
(11) $D_{11} = \{(X_1, X_2, X_3, X_4) \in \mathbb{R}_+ \times \mathbb{R}_- \times \mathbb{R}_+ \times \mathbb{R}_+; X_1 + X_2 \leqslant 0\}$;
(12) $D_{12} = \{(X_1, X_2, X_3, X_4) \in \mathbb{R}_- \times \mathbb{R}_- \times \mathbb{R}_+ \times \mathbb{R}_+; X_1 + X_4 \geqslant 0\}$;
(13) $D_{13} = \{(X_1, X_2, X_3, X_4) \in \mathbb{R}_+ \times \mathbb{R}_- \times \mathbb{R}_- \times \mathbb{R}_+; -X_3 \geqslant X_1 + X_2 \geqslant 0\}$;
(14) $D_{14} = \{(X_1, X_2, X_3, X_4) \in \mathbb{R}_+ \times \mathbb{R}_+ \times \mathbb{R}_- \times \mathbb{R}_+; -X_1 \leqslant X_2 + X_3 \leqslant 0\}$;
(15) $D_{15} = \{(X_1, X_2, X_3, X_4) \in \mathbb{R}_+ \times \mathbb{R}_- \times \mathbb{R}_- \times \mathbb{R}_-; -X_3 \geqslant X_1 + X_2 \geqslant 0\}$;

(16) $D_{16} = \{(X_1, X_2, X_3, X_4) \in \mathbb{R}_+ \times \mathbb{R}_+ \times \mathbb{R}_- \times \mathbb{R}_-; -X_1 \leqslant X_2 + X_3 \leqslant 0\}$;
(17) $D_{17} = \{(X_1, X_2, X_3, X_4) \in \mathbb{R}_+ \times \mathbb{R}_- \times \mathbb{R}_+ \times \mathbb{R}_-; X_1 + X_2 \geqslant 0, X_3 + X_4 \leqslant 0\}$;
(18) $D_{18} = \{(X_1, X_2, X_3, X_4) \in \mathbb{R}_- \times \mathbb{R}_+ \times \mathbb{R}_- \times \mathbb{R}_-; X_2 + X_3 \leqslant 0\}$;
(19) $D_{19} = \{(X_1, X_2, X_3, X_4) \in \mathbb{R}_- \times \mathbb{R}_- \times \mathbb{R}_- \times \mathbb{R}_+; X_1 + X_4 \leqslant 0\}$;
(20) $D_{20} = \{(X_1, X_2, X_3, X_4) \in \mathbb{R}_+ \times \mathbb{R}_- \times \mathbb{R}_+ \times \mathbb{R}_-; X_1 + X_2 \leqslant 0, X_3 + X_4 \geqslant 0\}$;
(21) $D_{21} = \{(X_1, X_2, X_3, X_4) \in \mathbb{R}_+ \times \mathbb{R}_- \times \mathbb{R}_+ \times \mathbb{R}_-; X_1 + X_2 \leqslant 0, X_3 + X_4 \leqslant 0\}$;
(22) $D_{22} = \{(X_1, X_2, X_3, X_4) \in \mathbb{R}_+ \times \mathbb{R}_- \times \mathbb{R}_- \times \mathbb{R}_-; X_1 + X_2 \leqslant 0\}$;
(23) $D_{23} = \{(X_1, X_2, X_3, X_4) \in \mathbb{R}_- \times \mathbb{R}_- \times \mathbb{R}_+ \times \mathbb{R}_-; X_3 + X_4 \leqslant 0\}$;
(24) $D_{24} = \{(X_1, X_2, X_3, X_4) \in \mathbb{R}_- \times \mathbb{R}_- \times \mathbb{R}_- \times \mathbb{R}_-\}$;
(25) $D_{25} = \{(X_1, X_2, X_3, X_4) \in \mathbb{R}_+ \times \mathbb{R}_- \times \mathbb{R}_+ \times \mathbb{R}_+; X_1 + X_2 \geqslant 0\}$;
(26) $D_{26} = \{(X_1, X_2, X_3, X_4) \in \mathbb{R}_- \times \mathbb{R}_+ \times \mathbb{R}_- \times \mathbb{R}_+; X_1 + X_4 \geqslant 0, X_2 + X_3 \leqslant 0\}$;
(27) $D_{27} = \{(X_1, X_2, X_3, X_4) \in \mathbb{R}_- \times \mathbb{R}_+ \times \mathbb{R}_- \times \mathbb{R}_+; X_1 + X_4 \leqslant 0, X_2 + X_3 \geqslant 0\}$;
(28) $D_{28} = \{(X_1, X_2, X_3, X_4) \in \mathbb{R}_+ \times \mathbb{R}_+ \times \mathbb{R}_+ \times \mathbb{R}_-; X_3 + X_4 \geqslant 0\}$;
(29) $D_{29} = \{(X_1, X_2, X_3, X_4) \in \mathbb{R}_+ \times \mathbb{R}_+ \times \mathbb{R}_+ \times \mathbb{R}_+\}$;
(30) $D_{30} = \{(X_1, X_2, X_3, X_4) \in \mathbb{R}_+ \times \mathbb{R}_+ \times \mathbb{R}_- \times \mathbb{R}_+; X_2 + X_3 \geqslant 0\}$;
(31) $D_{31} = \{(X_1, X_2, X_3, X_4) \in \mathbb{R}_- \times \mathbb{R}_+ \times \mathbb{R}_+ \times \mathbb{R}_+; X_1 + X_4 \geqslant 0\}$;
(32) $D_{32} = \{(X_1, X_2, X_3, X_4) \in \mathbb{R}_- \times \mathbb{R}_+ \times \mathbb{R}_- \times \mathbb{R}_+; X_1 + X_4 \geqslant 0, X_2 + X_3 \geqslant 0\}$;
(33) $D_{33} = \{(X_1, X_2, X_3, X_4) \in \mathbb{R}_+ \times \mathbb{R}_- \times \mathbb{R}_+ \times \mathbb{R}_-; X_1 + X_2 \geqslant 0, X_3 + X_4 \geqslant 0\}$;
(34) $D_{34} = \{(X_1, X_2, X_3, X_4) \in \mathbb{R}_- \times \mathbb{R}_+ \times \mathbb{R}_- \times \mathbb{R}_+; X_1 + X_4 \leqslant 0, X_2 + X_3 \leqslant 0\}$;
(35) $D_{35} = \{(X_1, X_2, X_3, X_4) \in \mathbb{R}_- \times \mathbb{R}_+ \times \mathbb{R}_+ \times \mathbb{R}_+; X_1 + X_3 + X_4 \leqslant 0\}$;
(36) $D_{36} = \{(X_1, X_2, X_3, X_4) \in \mathbb{R}_- \times \mathbb{R}_+ \times \mathbb{R}_+ \times \mathbb{R}_-; X_1 + X_3 + X_4 \geqslant 0\}$;
(37) $D_{37} = \{(X_1, X_2, X_3, X_4) \in \mathbb{R}_- \times \mathbb{R}_- \times \mathbb{R}_+ \times \mathbb{R}_+; X_1 + X_3 + X_4 \leqslant 0\}$;
(38) $D_{38} = \{(X_1, X_2, X_3, X_4) \in \mathbb{R}_- \times \mathbb{R}_- \times \mathbb{R}_+ \times \mathbb{R}_-; X_1 + X_3 + X_4 \geqslant 0\}$;
(39) $D_{39} = \{(X_1, X_2, X_3, X_4) \in \mathbb{R}_+ \times \mathbb{R}_- \times \mathbb{R}_- \times \mathbb{R}_+; X_1 + X_2 + X_3 \geqslant 0\}$;
(40) $D_{40} = \{(X_1, X_2, X_3, X_4) \in \mathbb{R}_+ \times \mathbb{R}_+ \times \mathbb{R}_- \times \mathbb{R}_+; X_1 + X_2 + X_3 \leqslant 0\}$;
(41) $D_{41} = \{(X_1, X_2, X_3, X_4) \in \mathbb{R}_+ \times \mathbb{R}_- \times \mathbb{R}_- \times \mathbb{R}_-; X_1 + X_2 + X_3 \geqslant 0\}$;
(42) $D_{42} = \{(X_1, X_2, X_3, X_4) \in \mathbb{R}_+ \times \mathbb{R}_+ \times \mathbb{R}_- \times \mathbb{R}_-; X_1 + X_2 + X_3 \leqslant 0\}$.

In particular, each subcone $D_i \subset \mathbb{R}^4$ has dimension 4, since its explicit description via inequalities shows that it has nonempty interior in $\mathbb{R}^4$. Equivalently, one can check directly by hand that the corresponding 4×4 matrix, such as in the 9 examples above, has rank 4.

Since, by Definition 4.17, the subcones $D_i \subset \mathbb{R}^4$ are generated by 4 elements, we gather that each D_i is a full subsector of $\mathbb{R}^4$.

One checks directly by hand that the 16 orthants $\mathbb{R}_\pm \times \mathbb{R}_\pm \times \mathbb{R}_\pm \times \mathbb{R}_\pm \subset \mathbb{R}^4$ decompose as:

(1) $\mathbb{R}_- \times \mathbb{R}_- \times \mathbb{R}_- \times \mathbb{R}_- = D_{24}$;
(2) $\mathbb{R}_+ \times \mathbb{R}_+ \times \mathbb{R}_+ \times \mathbb{R}_+ = D_{29}$;
(3) $\mathbb{R}_+ \times \mathbb{R}_+ \times \mathbb{R}_+ \times \mathbb{R}_- = D_2 \cup D_{28}$;
(4) $\mathbb{R}_- \times \mathbb{R}_+ \times \mathbb{R}_- \times \mathbb{R}_- = D_3 \cup D_{18}$;
(5) $\mathbb{R}_- \times \mathbb{R}_+ \times \mathbb{R}_+ \times \mathbb{R}_+ = D_6 \cup D_{31} \cup D_{35}$;
(6) $\mathbb{R}_- \times \mathbb{R}_- \times \mathbb{R}_+ \times \mathbb{R}_- = D_7 \cup D_{23} \cup D_{38}$;
(7) $\mathbb{R}_- \times \mathbb{R}_- \times \mathbb{R}_- \times \mathbb{R}_+ = D_{10} \cup D_{19}$;
(8) $\mathbb{R}_+ \times \mathbb{R}_- \times \mathbb{R}_+ \times \mathbb{R}_+ = D_{11} \cup D_{25}$;
(9) $\mathbb{R}_+ \times \mathbb{R}_+ \times \mathbb{R}_- \times \mathbb{R}_+ = D_{14} \cup D_{30} \cup D_{40}$;
(10) $\mathbb{R}_+ \times \mathbb{R}_- \times \mathbb{R}_- \times \mathbb{R}_- = D_{15} \cup D_{22} \cup D_{41}$;
(11) $\mathbb{R}_- \times \mathbb{R}_+ \times \mathbb{R}_+ \times \mathbb{R}_- = D_1 \cup D_5 \cup D_{36}$;
(12) $\mathbb{R}_+ \times \mathbb{R}_+ \times \mathbb{R}_- \times \mathbb{R}_- = D_4 \cup D_{16} \cup D_{42}$;
(13) $\mathbb{R}_- \times \mathbb{R}_- \times \mathbb{R}_+ \times \mathbb{R}_+ = D_8 \cup D_{12} \cup D_{37}$;
(14) $\mathbb{R}_+ \times \mathbb{R}_- \times \mathbb{R}_- \times \mathbb{R}_+ = D_9 \cup D_{13} \cup D_{39}$;
(15) $\mathbb{R}_+ \times \mathbb{R}_- \times \mathbb{R}_+ \times \mathbb{R}_- = D_{17} \cup D_{20} \cup D_{21} \cup D_{33}$;
(16) $\mathbb{R}_- \times \mathbb{R}_+ \times \mathbb{R}_- \times \mathbb{R}_+ = D_{26} \cup D_{27} \cup D_{32} \cup D_{34}$.

It follows that $\mathbb{R}^4 = \cup_{i=1}^{42} D_i$. It remains to show that $D_i \cap D_\ell$ has empty interior for all pairwise-distinct i, ℓ. Since this is true if D_i and D_ℓ lie in different orthants, we only need to check those pairs D_i, D_ℓ lying in the same orthant.

This is done directly by hand; however, the cases fall into only four types. First, for orthants 1,2: There is nothing to check. Second, for orthants 3, 4, 7, 8: In 3, say, the inequalities $X_3 + X_4 \leqslant 0$ and $X_3 + X_4 \geqslant 0$ have codimension 1 intersection even when defined on all of $\mathbb{R}^4$, so they do as well when restricted to the orthant. The other cases go the same. Third, for orthants 15, 16: This is similar to the second type. Lastly, for orthants 5, 6, 9, 10, 11, 12, 13, 14: In 5, say, the sectors D_6 and D_{31} similarly have codimension 1 intersection, as do the sectors D_6 and D_{35}. This is also true for $D_{31}(X_1 + X_4 \geqslant 0)$ and $D_{35}(X_1 + X_3 + X_4 \leqslant 0)$ so long as $D_{31} \cap D_{35}$ implies $X_3 = 0$, which it does, since it implies $X_3 \leqslant -X_1 - X_4 \leqslant 0$ whereas we are restricted to the orthant $\mathbb{R}_- \times \mathbb{R}_+ \times \mathbb{R}_+ \times \mathbb{R}_+$. The other cases go the same. □

We now analyze the walls (Definition B.10) in the sector decomposition $\{D_i\}_{i=1,2,\ldots,42}$ of $\mathbb{R}^4$. Recall (Definition 4.17) that $\mathcal{Q}_i$ is called the topological type of the sector D_i.

Proposition 4.21. *The third item of Theorem* 4.8 *holds word-for-word, except with* $C^i_{\mathcal{T}}$ *replaced by* D_i*, and replacing* (k) *by* (l).

In particular, $D_i \cap D_\ell$ *is a wall if and only if the intersection* $J_i \cap J_\ell$ *of their corresponding index sets has* 3 *elements* (*see the beginning of this sub-subsection,* Section 4.3.2). *In this case,*

$$D_i \cap D_\ell = \mathrm{span}_{\mathbb{R}_+}(\{\pi_4(x_j); j \in J_i \cap J_\ell\}) \subset \mathbb{R}^4. \tag{l}$$

Proof. Any wall $D_i \cap D_\ell$ must, by definition, be 3 dimensional. This restricts which indices $\{i, \ell\}$ can yield walls. Through a direct by hand check, using the explicit description by inequalities of the sector decomposition $\{D_i\}_i$ as in the proof of Proposition 4.19, one verifies that a necessary condition for $D_i \cap D_\ell$ to be a wall is for D_i and D_ℓ to be connected by an edge in the graph $\mathcal{G}$ depicted in Figure 3. We show this is also a sufficient condition.

More precisely, the goal is to show, for any two sectors D_i and D_ℓ connected by an edge in $\mathcal{G}$, that $J_i \cap J_\ell$ has 3 elements and (l) holds. In particular, $D_i \cap D_\ell$ is a cone of dimension 3. Note the inclusion $\supset$ in (l) holds automatically; see Definition 4.17.

We checked this directly by hand. There are two types of calculations, depending on whether the sectors are in different orthants or the same orthant.

As an example where the sectors are in different orthants: We demonstrate this for D_{29} and D_{30}, which were computed in detail in the proof of Proposition 4.19. There, one sees that three rows of the corresponding 4×4 matrix M_{29} appear as rows in the matrix M_{30} (recall also Remark 4.20). This means that $J_i \cap J_\ell$ has 3 elements; see Remark 4.18. Note that the row in M_{29} that is not in M_{30} corresponds to the variable x, and the row in M_{30} that is not in M_{29} corresponds to the variable x'. The inclusion $\subset$ in (l) is true since

$$(t, y, x, z) = (t', x' + y', -x', z') \in \mathbb{R}^4 \ (x, y, z, t, x', y', z', t' \geqslant 0)$$

implies $x = x' = 0$. The other different-orthant cases are similar.

As an example where the sectors are in the same orthant: We demonstrate this for D_5 and D_1, which were also computed in detail in the proof of Proposition 4.19. There, one sees that three rows of the corresponding 4×4 matrix M_5 appear as rows in the matrix M_1 (recall also Remark 4.20). This means that $J_i \cap J_\ell$ has 3 elements; see Remark 4.18. The row in M_5 not in M_1 corresponds to the variable x, and the row in M_1 not in M_5 corresponds to the variable z'. The inclusion $\subset$ in (l) is true

since

$$(-x-y,t,x+z,-z)=(-x',t',y',-y'-z')\in\mathbb{R}^4\ (x,y,z,t,x',y',z',t'\geqslant 0)$$

implies, by adding the third and fourth entries, that $x=-z'$ hence $x=z'=0$. The other same-orthant cases are similar.

We gather $D_i\cap D_\ell$ is a wall if and only if D_i and D_ℓ are connected by an edge of the graph $\mathcal{G}$, in which case $J_i\cap J_\ell$ has 3 elements. In particular, since $\mathcal{G}$ is 4-valent, the last paragraph of the third item of Theorem 4.8 holds (again, with D_i in place of $C^i_{\mathcal{T}}$).

To finish justifying the second paragraph of Proposition 4.21 (equivalently, the first paragraph of the third item of Theorem 4.8, appropriately substituted), we need to show that if $J_i\cap J_\ell$ has 3 elements (equivalently, $\mathcal{Q}_i\cap\mathcal{Q}_\ell$ has 3 elements), then $D_i\cap D_\ell$ is a wall.

So far, we have exhibited, for each i, 4 topological types $\mathcal{Q}_\ell$ such that $\mathcal{Q}_i\cap\mathcal{Q}_\ell$ has 3 elements, all corresponding to walls $D_i\cap D_\ell$. We thus need to show there are no more indices ℓ such that $\mathcal{Q}_i\cap\mathcal{Q}_\ell$ has 3 elements. For this, it suffices to establish the second paragraph of the third item of Theorem 4.8, which is a purely topological statement about webs in good position on the triangulated square; compare Observation 1.13 and Proposition 4.1. We checked this directly by hand; compare Example 4.9. □

4.3.3. *Finishing.* We are now prepared to prove the theorem.

Proof of Theorem 4.8. Let $C\subset\mathbb{R}^8_+\times\mathbb{R}^4$ be the cone isomorphic to the completed KTGS cone $C_{\mathcal{T}}\subset\mathbb{R}^{12}_+$ via the linear isomorphism $\phi_{\mathcal{T}}\circ\theta_{\mathcal{T}}:\mathbb{R}^{12}\to\mathbb{R}^8\times\mathbb{R}^4$; see Definition 4.15.

Recall also Notation 4.16 from the discussion at the beginning of Section 4.3.2, which should help with comparing the general lemmas of Section B.2.2 to the current application.

By the explicit calculation of the Hilbert basis elements $\phi_{\mathcal{T}}\circ\theta_{\mathcal{T}}\circ\Phi_{\mathcal{T}}(W_i^H)\in C$ for $i=1,2,\dots,22$ in Section 4.3.1, together with Proposition 4.19, we see that $C\subset\mathbb{R}^8_+\times\mathbb{R}^4$ satisfies the hypotheses of Lemma B.12. Indeed, $D_i\subset\pi_4(C)$ by definition, for each i. Therefore, C is 12 dimensional, so the isomorphic completed KTGS cone $C_{\mathcal{T}}$ is 12 dimensional as well. This establishes the first item of Theorem 4.8.

Let us prove that $C_{\mathcal{T}}=\cup_{i=1}^{42}C^i_{\mathcal{T}}\subset\mathbb{R}^{12}_+$; see Definition 4.6. This follows by Theorem 1.14, Proposition 4.1, and Lemma B.17. Indeed, by Theorem 1.14, every point in the KTGS positive integer cone $\mathcal{C}_{\mathcal{T}}\subset\mathbb{Z}^{12}_+$ is equal to $\Phi_{\mathcal{T}}(W)$ for some reduced web $W\in\mathcal{W}_\square$ in the square. By Proposition 4.1, the web W is an element of one of the 42 web families: $W\in\mathcal{W}_i\subset\mathcal{W}_\square$. By Observation 4.7, we have that $\Phi_{\mathcal{T}}(W)\in\mathcal{C}^i_{\mathcal{T}}$. We gather that $\mathcal{C}_{\mathcal{T}}=\cup_{i=1}^{42}\mathcal{C}^i_{\mathcal{T}}\subset\mathbb{Z}^{12}_+$. Also, the submonoids $\mathcal{C}^i_{\mathcal{T}}\subset\mathcal{C}_{\mathcal{T}}$ are finitely generated by Definition 4.6. We conclude by Lemma B.17 that we have the equality $C_{\mathcal{T}}=\cup_{i=1}^{42}C^i_{\mathcal{T}}\subset\mathbb{R}^{12}_+$ of completions, as desired.

We return to the isomorphic cone $C\subset\mathbb{R}^8_+\times\mathbb{R}^4$. Let $\{x_j\}_{j=1,2,\dots,14}$ and $\{J_i\}_{i=1,2,\dots,42}$ be defined as in the beginning of Section 4.3.2. For $i=1,2,\dots,42$, let the subcones $C_i\subset C$ be defined as in the statement of Lemma B.13. Equivalently, the subcone $C_i=\phi_{\mathcal{T}}\circ\theta_{\mathcal{T}}(C^i_{\mathcal{T}})\subset\mathbb{R}^8_+\times\mathbb{R}^4$ is the isomorphic counterpart to the subcone $C^i_{\mathcal{T}}\subset C_{\mathcal{T}}\subset\mathbb{R}^{12}_+$. It follows by the previous paragraph that $C=\cup_{i=1}^{42}C_i\subset\mathbb{R}^8_+\times\mathbb{R}^4$ in the isomorphic cone C. By this, together with another application of Proposition 4.19, we see that the hypotheses of Lemma B.13 are satisfied. Therefore, by Lemma B.13, we obtain the second item of Theorem 4.8, except with $C_{\mathcal{T}}$ and $C^i_{\mathcal{T}}$ replaced by C and C_i, respectively. Since this property is preserved by linear isomorphisms, we conclude the second item of Theorem 4.8 as stated.

Lastly, by Proposition 4.21, in particular (l), the hypothesis of Lemma B.14 is satisfied. Therefore, by Lemma B.14, the set {walls of $\{C_i\}_i$ in C} is in one-to-one correspondence with the set {walls of $\{D_i\}_i$ in $\mathbb{R}^4$} in the obvious way by the projection π_4. Moreover, a given wall $C_i \cap C_\ell$ can be computed by (m) in Lemma B.14. We conclude by the remainder of Proposition 4.21 that the first and third paragraphs of the third item of Theorem 4.8 are valid, except with $C_{\mathcal{T}}$, $C^i_{\mathcal{T}}$, and (k) replaced by C, C_i, and (m), respectively. Since the inverse of the linear isomorphism $\phi_{\mathcal{T}} \circ \theta_{\mathcal{T}}$ preserves these properties, and maps (m) to (k) (see the beginning of Section 4.3.2), we conclude the first and third paragraphs of the second item of Theorem 4.8 as stated. The second paragraph is a purely topological statement about webs in the square, and was already established during the proof of Proposition 4.21. □

The following consequence is immediate from the proof of Theorem 4.8.

Corollary 4.22. *The function*

$$\pi_4 \circ \phi_{\mathcal{T}} \circ \theta_{\mathcal{T}} : C_{\mathcal{T}} \twoheadrightarrow \mathbb{R}^4$$

is a surjection from the completed KTGS cone $C_{\mathcal{T}} \subset \mathbb{R}^{12}_+$ (in fact, from a '4 dimensional' proper subset of $C_{\mathcal{T}}$) onto $\mathbb{R}^4$. □

Recall the notion of a cornerless web $W = W_c$ in the square; see Definition 2.9. Let $\mathcal{W}^c_\square \subset \mathcal{W}_\square$ denote the set of cornerless webs up to equivalence. Note for each $i = 1, 2, \ldots, 42$ that $\mathcal{Q}_i \subset \mathcal{W}_i \cap \mathcal{W}^c_\square$.

Consider also the function $\pi_4 \circ \phi_{\mathcal{T}} \circ \theta_{\mathcal{T}} \circ \Phi_{\mathcal{T}} : \mathcal{W}_\square \to \mathbb{Z}^4 \subset \mathbb{R}^4$ defined on $\mathcal{W}_\square$. See for example the nine computations at the beginning of the proof of Proposition 4.19.

Another consequence of the proof of Theorem 4.8 is:

Corollary 4.23. *The restricted function*

$$\pi_4 \circ \phi_{\mathcal{T}} \circ \theta_{\mathcal{T}} \circ \Phi_{\mathcal{T}} : \mathcal{W}^c_\square \twoheadrightarrow \mathbb{Z}^4$$

restricted to the cornerless webs $\mathcal{W}^c_\square \subset \mathcal{W}_\square$ is a surjection onto the integer lattice $\mathbb{Z}^4 \subset \mathbb{R}^4$.

In particular, the function $\pi_4 \circ \phi_{\mathcal{T}} \circ \theta_{\mathcal{T}}$ from Corollary 4.22 maps (a '4 dimensional' proper subset of) the KTGS cone $\mathcal{C}_{\mathcal{T}} \subset \mathbb{Z}^{12}_+$ surjectively onto $\mathbb{Z}^4$.

Proof. We know that $\mathbb{R}^4 = \cup_{i=1}^{42} D_i$ and $D_i = \pi_4 \circ \phi_{\mathcal{T}} \circ \theta_{\mathcal{T}}(C^i_{\mathcal{T}})$ where $C^i_{\mathcal{T}} \supset \mathcal{C}^i_{\mathcal{T}}$ (Definition 4.6). We also know that the cone points $\Phi_{\mathcal{T}}(W^H_j)$ in $\mathcal{C}^i_{\mathcal{T}}$ for $j = 1, 2, \ldots, 8$, corresponding to the 8 corner arcs in the square, are sent by $\phi_{\mathcal{T}} \circ \theta_{\mathcal{T}}$ to the first 8 standard basis elements e_j of $\mathbb{R}^8_+ \times \mathbb{R}^4$. We gather $\pi_4 \circ \phi_{\mathcal{T}} \circ \theta_{\mathcal{T}}$ is still a surjection onto D_i when restricted to the subset

$$C'^i_{\mathcal{T}} \coloneqq \mathrm{span}_{\mathbb{R}_+}(\{\Phi_{\mathcal{T}}(W^H); W^H \in \mathcal{Q}_i\}) \subset C^i_{\mathcal{T}} \subset \mathbb{R}^{12}_+.$$

Note also that (similar to Observation 4.7)

$$\Phi_{\mathcal{T}}(\mathcal{W}_i \cap \mathcal{W}^c_\square) = \mathrm{span}_{\mathbb{Z}_+}(\{\Phi_{\mathcal{T}}(W^H); W^H \in \mathcal{Q}_i\}) \subset C'^i_{\mathcal{T}}.$$

It thus suffices to show: for any $c \in C'^i_{\mathcal{T}}$, if $\pi_4 \circ \phi_{\mathcal{T}} \circ \theta_{\mathcal{T}}(c) \in \mathbb{Z}^4 \cap D_i$, then $c \in \Phi_{\mathcal{T}}(\mathcal{W}_i \cap \mathcal{W}^c_\square)$.

Once again, we work in the isomorphic cone $C_i = \phi_{\mathcal{T}} \circ \theta_{\mathcal{T}}(C^i_{\mathcal{T}}) \subset \mathbb{R}^8_+ \times \mathbb{R}^4$, which projects to D_i by π_4. Put (see the beginning of Section 4.3.2)

$$C'_i \coloneqq \phi_{\mathcal{T}} \circ \theta_{\mathcal{T}}(C'^i_{\mathcal{T}}) = \mathrm{span}_{\mathbb{R}_+}(\{x_j; j \in J_i\}) \subset C_i \subset \mathbb{R}^8_+ \times \mathbb{R}^4$$

and note also that

$$\phi_{\mathcal{T}} \circ \theta_{\mathcal{T}} \circ \Phi_{\mathcal{T}}(\mathcal{W}_i \cap \mathcal{W}^c_\square) = \mathrm{span}_{\mathbb{Z}_+}(\{x_j; j \in J_i\}) \subset C'_i.$$

The above property is then equivalent to showing: for any $c \in C_i'$ such that $\pi_4(c) \in \mathbb{Z}^4 \cap D_i$, we have $c \in \phi_{\mathcal{T}} \circ \theta_{\mathcal{T}} \circ \Phi_{\mathcal{T}}(\mathcal{W}_i \cap \mathcal{W}_{\square}^c)$; that is, if such a $c \in C_i'$ is written $c = xx_{1^{(i)}} + yx_{2^{(i)}} + zx_{3^{(i)}} + tx_{4^{(i)}}$ for $x, y, z, t \geqslant 0$ (see the beginning of Section 4.3.2), we want to show $x, y, z, t \in \mathbb{Z}$.

This is accomplished through a direct by hand check, taking advantage of the explicit description of the sectors D_i provided in Section 4.3.2. As before, although there are 42 cases, these fall into only five types, each represented among the 9 examples demonstrated in the proof of Proposition 4.19: Type 1 corresponds to i_1; Type 2 corresponds to i_2, i_7, i_8; Type 3 corresponds to i_3; Type 4 corresponds to i_4, i_9; and Type 5 corresponds to i_5, i_6. We will only demonstrate the most nontrivial case, Type 5 (for i_5, say); the other cases are similar.

So consider $i_5 = 5$, and assume $\pi_4(c) = x\pi_4(x_{1^{(5)}}) + y\pi_4(x_{2^{(5)}}) + z\pi_4(x_{3^{(5)}}) + t\pi_4(x_{4^{(5)}}) \in D_i$ is, in addition, in $\mathbb{Z}^4$ for some $x, y, z, t \geqslant 0$. Note the vector $\pi_4(x_{j^{(5)}})$ is the j-th row of the matrix displayed in the i_5 example in the proof of Proposition 4.19. From this example, we gather that $\pi_4(c) = (-x - y, t, x + z, -z) \in \mathbb{Z}^4$. So $t, z \in \mathbb{Z}$; implying by $x + z \in \mathbb{Z}$ that $x \in \mathbb{Z}$; implying by $-x - y \in \mathbb{Z}$ that $y \in \mathbb{Z}$, as desired. □

Remark 4.24. We expect that the restricted function from Corollary 4.23 is also an injection. We suspect that there may be a proof of this result via a conjectural generalization of (k) to higher codimension intersections.

Conceptual Remark 4.25. Recall Remark 3.9.

We view the real cone $C_{\mathcal{T}} \subset \mathbb{R}^{12}_+$ as the isomorphic $\mathcal{T}$-chart $C_{\mathcal{T}} \cong -\mathcal{A}^+_{\mathrm{SL}_3,\square}(\mathbb{R}^t)_{\mathcal{T}}$.

On the other hand, via the isomorphism $\theta_{\mathcal{T}} : \mathbb{R}^{12} \to V_{\mathcal{T}} \subset \mathbb{R}^{18}$ we may view the real cone $\theta_{\mathcal{T}}(C_{\mathcal{T}}) \subset V_{\mathcal{T}}$ as the isomorphic $\mathcal{T}$-chart $\theta_{\mathcal{T}}(C_{\mathcal{T}}) \cong -\mathcal{A}^+_{\mathrm{PGL}_3,\square}(\mathbb{R}^t)_{\mathcal{T}}$.

Recall, in addition to the 12 dimensional $\mathcal{A}$-moduli spaces $\mathcal{A}_{\mathrm{SL}_3,\square}$ and $\mathcal{A}_{\mathrm{PGL}_3,\square}$, Fock–Goncharov [10] and Goncharov–Shen [19, 21] defined the $\mathcal{X}$- and $\mathcal{P}$-moduli spaces $\mathcal{X}_{\mathrm{PGL}_3,\square}$ and $\mathcal{P}_{\mathrm{PGL}_3,\square}$, which are 4- and 12-dimensional, respectively. In addition, there are canonical maps $p : \mathcal{A}_{\mathrm{SL}_3,\square} \to \mathcal{X}_{\mathrm{PGL}_3,\square}$ and $\overline{p} : \mathcal{A}_{\mathrm{SL}_3,\square} \to \mathcal{P}_{\mathrm{PGL}_3,\square}$ (the notation $\overline{p}$ may be nonstandard). The tropical points $\mathcal{X}_{\mathrm{PGL}_3,\square}(\mathbb{R}^t)$ and $\mathcal{P}_{\mathrm{PGL}_3,\square}(\mathbb{R}^t)$ of these spaces are also defined, inducing tropicalizations $p^t : \mathcal{A}_{\mathrm{SL}_3,\square}(\mathbb{R}^t) \to \mathcal{X}_{\mathrm{PGL}_3,\square}(\mathbb{R}^t)$ and $\overline{p}^t : \mathcal{A}_{\mathrm{SL}_3,\square}(\mathbb{R}^t) \to \mathcal{P}_{\mathrm{PGL}_3,\square}(\mathbb{R}^t)$ of the canonical maps.

In terms of $\mathcal{T}$-charts, we view $\mathcal{X}_{\mathrm{PGL}_3,\square}(\mathbb{R}^t)_{\mathcal{T}} \cong \mathbb{R}^4$ and $\mathcal{P}_{\mathrm{PGL}_3,\square}(\mathbb{R}^t)_{\mathcal{T}} \cong \mathbb{R}^8 \times \mathbb{R}^4$. We think of the projection $\pi_4 \circ (\phi_{\mathcal{T}} \circ \theta_{\mathcal{T}}) : \mathbb{R}^{12} \to \mathbb{R}^8 \times \mathbb{R}^4 \to \mathbb{R}^4$ as the canonical map p^t written in coordinates. We think of the isomorphism $\phi_{\mathcal{T}} \circ \theta_{\mathcal{T}} : \mathbb{R}^{12} \to \mathbb{R}^8 \times \mathbb{R}^4$ as a coordinate version of the canonical map $\overline{p}^t$.

We interpret Corollary 4.22 as saying that, when expressed in coordinates, the canonical map $p^t (\approx \pi_4 \circ \phi_{\mathcal{T}} \circ \theta_{\mathcal{T}})$ also projects the subset $-\mathcal{A}^+_{\mathrm{SL}_3,\square}(\mathbb{R}^t)_{\mathcal{T}} \subset \mathcal{A}_{\mathrm{SL}_3,\square}(\mathbb{R}^t)_{\mathcal{T}} (\approx C_{\mathcal{T}} \subset \mathbb{R}^{12})$ of positive points onto $\mathcal{X}_{\mathrm{PGL}_3,\square}(\mathbb{R}^t)_{\mathcal{T}} (\approx \mathbb{R}^4)$.

In addition, since the positive integer cone $\mathcal{C}_{\mathcal{T}} \subset \mathbb{Z}^{12}_+$ is in bijection with the set of reduced webs $\mathcal{W}_{\square}$ via the web tropical coordinate map $\Phi_{\mathcal{T}}$, and since $\mathcal{C}_{\mathcal{T}} \cong -3\mathcal{A}^+_{\mathrm{PGL}_3,\square}(\mathbb{Z}^t)_{\mathcal{T}}$ by Remark 1.6, we can interpret Corollary 4.23 as saying that, in coordinates, the canonical map $p^t (\approx \pi_4 \circ \phi_{\mathcal{T}} \circ \theta_{\mathcal{T}})$ projects a proper subset of $-3\mathcal{A}^+_{\mathrm{PGL}_3,\square}(\mathbb{Z}^t)_{\mathcal{T}} \subset \mathcal{A}_{\mathrm{SL}_3,\square}(\mathbb{Z}^t)_{\mathcal{T}} (\approx \mathcal{C}_{\mathcal{T}} \subset \mathbb{Z}^{12})$ onto $\mathcal{X}_{\mathrm{PGL}_3,\square}(\mathbb{Z}^t)_{\mathcal{T}} (\approx \mathbb{Z}^4)$.

Appendix A. Background on Fock–Goncharov–Shen theory

We briefly summarize some of the related concepts from Fock–Goncharov–Shen theory [10, 19]. Details can be found in the other references, for example, [24, Section 4]. (This appendix assumes the terminology of Section 1.1.)

Remark A.1. Although not strictly required for the main theorems of the article, the material of this appendix is intended to emphasize the important conceptual concepts guiding the rest of the paper. See, in particular, the Conceptual Remarks 1.6, 2.14, 3.9, 4.25.

A.1. SL_3-decorated local systems. Let E be a 3-dimensional vector space equipped with a volume form Ω. Let $\mathcal{A}$ denote the collection of decorated (complete) flags in E.

Let $\widehat{S}$ be a marked surface. Fix a base point x_0 in $\widehat{S}$, henceforth suppressed in the notation. For each puncture $p_i \in m_p$ let α_i be an oriented peripheral closed curve around the puncture. An SL_3-decorated local system on $\widehat{S}$ determines a pair (ρ, ξ) consisting of:

(I) a surface group representation $\rho \in \mathrm{Hom}(\pi_1(\widehat{S}), \mathrm{SL}_3)$ with unipotent monodromy along each peripheral curve α_i;

(II) a flag map $\xi : m_b \cup m_p \to \mathcal{A}$ such that each peripheral monodromy $\rho(\alpha_i)$ fixes the decorated flag $\xi(p_i) \in \mathcal{A}$. (More precisely, the flag map ξ should be defined equivariantly at the level of the universal cover $\widetilde{S}$.)

A point of the Fock–Goncharov moduli space $\mathcal{A}_{\mathrm{SL}_3,\widehat{S}}$ determines an SL_3-decorated local system up to suitable equivalence.

Let $V_{\mathcal{T}}$ (resp. $V_{\mathcal{T}_3}$) be the set of vertices of an ideal triangulation $\mathcal{T}$ (resp. ideal 3-triangulation $\mathcal{T}_3$) of $\widehat{S}$. Note that $V_{\mathcal{T}} = m_b \cup m_p \subset V_{\mathcal{T}_3}$. Put

$$I_3 \coloneqq \{V \in V_{\mathcal{T}_3} - V_{\mathcal{T}}; V \text{ lies on an edge of } \mathcal{T}\} \text{ and } J_3 \coloneqq V_{\mathcal{T}_3} - (V_{\mathcal{T}} \cup I_3).$$

We denote a vertex $V \in I_3 \cup J_3$ on a triangle (a, b, c) oriented counterclockwise by $v^{i,j,k}_{a,b,c}$ where the three nonnegative integers i, j, k summing to 3 are the least number of edges of $\mathcal{T}_3$ from V to $\overline{bc}$, from V to $\overline{ac}$, and from V to $\overline{ab}$, respectively, where $\overline{bc}$, $\overline{ac}$, $\overline{ab}$ denote the unoriented edges of $\mathcal{T}$ (see Figure 17).

Consider a vertex $V \in I_3 \cup J_3$ contained in a counterclockwise oriented ideal triangle $\Delta = (a, b, c)$. For an SL_3-decorated local system (ρ, ξ) in $\mathcal{A}_{\mathrm{SL}_3,\widehat{S}}$ let

$$(a_1, a_2, a_3), (b_1, b_2, b_3), (c_1, c_2, c_3) \in E^3$$

be bases adapted to the decorated flags $\xi(a)$, $\xi(b)$, $\xi(c) \in \mathcal{A}$ with respect to the volume form Ω. The Fock–Goncharov $\mathcal{A}$-coordinate at $V = v^{i,j,k}_{a,b,c} \in I_3 \cup J_3$ is

$$A_V(\rho, \xi) \coloneqq A_V \coloneqq A^{i,j,k}_{a,b,c} \coloneqq \Omega(a^i \wedge b^j \wedge c^k)$$

where $a^1 = a_1$, $a^2 = a_1 \wedge a_2$, etc. This is independent of the choice of bases. (Also put $A^{3,0,0}_{a,b,c} = \Omega(a^3) = \Omega(a_1 \wedge a_2 \wedge a_3) = 1$ and, similarly, $A^{0,3,0}_{a,b,c} = A^{0,0,3}_{a,b,c} = 1$.)

Given the quiver defined with respect to the orientation of the surface as in Figure 17, let

$$\varepsilon_{VW} = |\{\text{arrows from } V \text{ to } W\}| - |\{\text{arrows from } W \text{ to } V\}|.$$

For any $V \in I_3 \cup J_3$, $V \notin \partial\widehat{S}$, the Fock–Goncharov $\mathcal{X}$-coordinate at V is

$$X_V(\rho, \xi) \coloneqq X_V \coloneqq \prod_{W \in I_3 \cup J_3} A_W^{\varepsilon_{VW}}.$$

Remark A.2. By [10], the moduli space $\mathcal{A}_{\mathrm{SL}_3,\widehat{S}}$ has a cluster algebraic structure [15] described by quivers on the surface, such as that in Figure 17. In particular, each $\mathcal{A}$-coordinate transition map between different triangulations $\mathcal{T}$ and $\mathcal{T}'$ is positive rational.

Let $D = \{(2,1,0),(1,2,0),(1,1,1)\}$. Suppose the, now pointed, ideal triangle $\Delta = (a;b,c)$ is counterclockwise oriented, as in Figure 18. For $(i,j,k) \in D$, the monomials

$$\alpha^{i,j,k}_{a;b,c} \coloneqq A^{i-1,j,k+1}_{a,b,c} A^{i+1,j-1,k}_{a,b,c} / A^{i,j,k}_{a,b,c} A^{i,j-1,k+1}_{a,b,c}$$

correspond to the three rhombi in Figure 18. Define

$$P(\Delta) \coloneqq P(a;b,c) \coloneqq \alpha^{2,1,0}_{a;b,c} + \alpha^{1,2,0}_{a;b,c} + \alpha^{1,1,1}_{a;b,c}.$$

Let Θ be the collection of counterclockwise oriented pointed ideal triangles of $\mathcal{T}$. The Goncharov–Shen potential is

$$P = \sum_{\Delta \in \Theta} P(\Delta).$$

Note for a given ideal triangulation $\mathcal{T}$, the Goncharov–Shen potential is a positive Laurent polynomial in the $\mathcal{A}$-coordinates for $\mathcal{A}_{\mathrm{SL}_3,\widehat{S}}$.

Remark A.3. The Goncharov–Shen potential is mapping class group equivariant and defines a rational positive function on the moduli space $\mathcal{A}_{\mathrm{SL}_3,\widehat{S}}$. In [19], the Goncharov–Shen potentials are related to the mirror Landau-Ginzburg potentials. In [24, Section 4], the Goncharov–Shen potentials are related to generalized horocycle lengths.

The points $\mathcal{A}_{\mathrm{SL}_3,\widehat{S}}(\mathbb{P})$ are defined over any semifield $\mathbb{P}$. The tropical semifield $\mathbb{R}^t = (\mathbb{R}, \otimes, \oplus)$ is defined by $x \otimes y = x + y$ and $x \oplus y = \max\{x,y\}$. The isomorphism $x \to -x$ sends $(\mathbb{R}^t, +, \max)$ to $(\mathbb{R}^t, +, \min)$. In this appendix, we use $(\mathbb{R}^t, +, \min)$. The tropical semifields $\mathbb{Z}^t$ and $(1/3)\mathbb{Z}^t$ are similarly defined. To each ideal triangulation $\mathcal{T}$ there is associated a $\mathcal{T}$-chart $\mathcal{A}_{\mathrm{SL}_3,\widehat{S}}(\mathbb{P})_{\mathcal{T}}$. We have $\mathcal{A}_{\mathrm{SL}_3,\widehat{S}}(\mathbb{R}^t)_{\mathcal{T}} \cong \mathbb{R}^N$ and $\mathcal{A}_{\mathrm{SL}_3,\widehat{S}}(\mathbb{Z}^t)_{\mathcal{T}} \cong \mathbb{Z}^N$ and $\mathcal{A}_{\mathrm{SL}_3,\widehat{S}}((1/3)\mathbb{Z}^t)_{\mathcal{T}} \cong ((1/3)\mathbb{Z})^N$ where N is the number of $\mathcal{A}$-coordinates.

A positive Laurent polynomial f has tropicalization

$$f^t(x_1, \cdots, x_k) = \lim_{C \to -\infty} \log f(e^{Cx_1}, \cdots, e^{Cx_k})/C.$$

The tropical $\mathcal{A}$-coordinates are denoted A^t_V for $V \in I_3 \cup J_3$. (Note $(A^{3,0,0}_{a,b,c})^t = 0$ since $A^{3,0,0}_{a,b,c} = 1$.) So

$$(\alpha^{i,j,k}_{a;b,c})^t = (A^{i-1,j,k+1}_{a,b,c})^t + (A^{i+1,j-1,k}_{a,b,c})^t - (A^{i,j,k}_{a,b,c})^t - (A^{i,j-1,k+1}_{a,b,c})^t$$

and the tropicalized Goncharov–Shen potential is

$$P^t = \min\{(\alpha^{i,j,k}_{a;b,c})^t\}_{\text{all } \alpha^{i,j,k}_{a;b,c} \text{ of } P}$$

where the minimum is taken over all rhombi in all pointed ideal triangles of $\mathcal{T}$.

The condition $P^t \geqslant 0$ on $\mathcal{A}_{\mathrm{SL}_3,\widehat{S}}(\mathbb{R}^t)$ determines the space $\mathcal{A}^+_{\mathrm{SL}_3,\widehat{S}}(\mathbb{R}^t)$ of positive real tropical points as well as its $\mathcal{T}$-chart $\mathcal{A}^+_{\mathrm{SL}_3,\widehat{S}}(\mathbb{R}^t)_{\mathcal{T}}$. The spaces $\mathcal{A}^+_{\mathrm{SL}_3,\widehat{S}}(\mathbb{Z}^t)$ and $\mathcal{A}^+_{\mathrm{SL}_3,\widehat{S}}((1/3)\mathbb{Z}^t)$ as well as their $\mathcal{T}$-charts $\mathcal{A}^+_{\mathrm{SL}_3,\widehat{S}}(\mathbb{Z}^t)_{\mathcal{T}}$ and $\mathcal{A}^+_{\mathrm{SL}_3,\widehat{S}}((1/3)\mathbb{Z}^t)_{\mathcal{T}}$ are similarly defined.

A.2. PGL_3-decorated local systems. The moduli space $\mathcal{A}_{\mathrm{PGL}_3,\widehat{S}}$ is defined analogously to $\mathcal{A}_{\mathrm{SL}_3,\widehat{S}}$. Although the $\mathcal{A}$-coordinates $A^{i,j,k}_{a,b,c}$ are no longer defined for $\mathcal{A}_{\mathrm{PGL}_3,\widehat{S}}$ (as they depend on the choices of scale), the rhombus numbers $\alpha^{i,j,k}_{a;b,c}$, and so the Goncharov–Shen potential P, are defined (the choices of scale cancel out in the ratio defining $\alpha^{i,j,k}_{a;b,c}$). So, the tropical points $\mathcal{A}_{\mathrm{PGL}_3,\widehat{S}}(\mathbb{P})$ and their positive parts $\mathcal{A}^+_{\mathrm{PGL}_3,\widehat{S}}(\mathbb{P})$ with respect to the tropicalized Goncharov–Shen potential P^t are defined

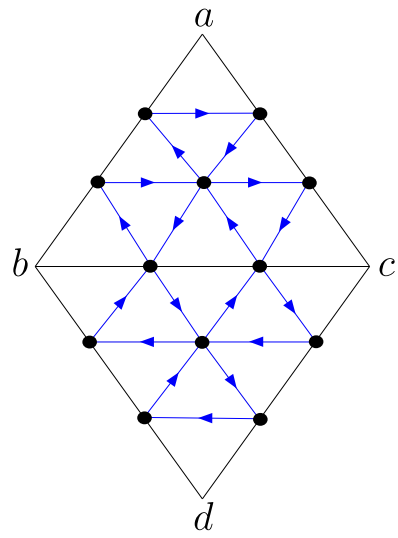

FIGURE 17. 3-triangulation with quiver.

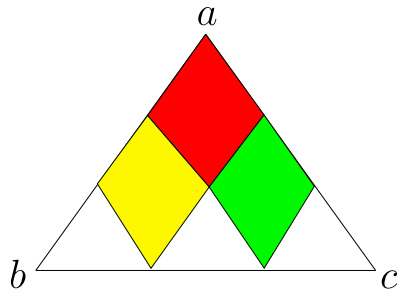

FIGURE 18. Red rhombus for $\alpha^{2,1,0}_{a;b,c}$, yellow rhombus for $\alpha^{1,2,0}_{a;b,c}$, and green rhombus for $\alpha^{1,1,1}_{a;b,c}$ in a pointed ideal triangle.

as well. We refer to the space $\mathcal{A}_{\mathrm{PGL}_3,\widehat{S}}(\mathbb{Z}^t)$ as the space of lamination-tropical points, and we refer to the space $\mathcal{A}^+_{\mathrm{PGL}_3,\widehat{S}}(\mathbb{Z}^t)$ as the space of web-tropical points.

The $\mathcal{T}$-chart $\mathcal{A}_{\mathrm{PGL}_3,\widehat{S}}(\mathbb{Z}^t)_{\mathcal{T}}$ is determined by imposing the condition $(\alpha^{i,j,k}_{a;b,c})^t \in \mathbb{Z}$ for all $(\alpha^{i,j,k}_{a;b,c})^t$ of P^t on $\mathcal{A}_{\mathrm{SL}_3,\widehat{S}}((1/3)\mathbb{Z}^t)_{\mathcal{T}} \cong ((1/3)\mathbb{Z})^N$, and the $\mathcal{T}$-chart $\mathcal{A}^+_{\mathrm{PGL}_3,\widehat{S}}(\mathbb{Z}^t)_{\mathcal{T}}$ is determined by imposing the condition $(\alpha^{i,j,k}_{a;b,c})^t \in \mathbb{Z}_+$ for all $(\alpha^{i,j,k}_{a;b,c})^t$ on $\mathcal{A}_{\mathrm{SL}_3,\widehat{S}}((1/3)\mathbb{Z}^t)_{\mathcal{T}} \cong ((1/3)\mathbb{Z})^N$.

In summary, we have the following relations among $\mathcal{T}$-charts:

$$\mathbb{Z}^N \cong \mathcal{A}_{\mathrm{SL}_3,\widehat{S}}(\mathbb{Z}^t)_{\mathcal{T}} \subset \mathcal{A}_{\mathrm{PGL}_3,\widehat{S}}(\mathbb{Z}^t)_{\mathcal{T}} \subset \mathcal{A}_{\mathrm{SL}_3,\widehat{S}}((1/3)\mathbb{Z}^t)_{\mathcal{T}} \cong ((1/3)\mathbb{Z})^N,$$
$$\mathcal{A}^+_{\mathrm{SL}_3,\widehat{S}}(\mathbb{Z}^t)_{\mathcal{T}} \subset \mathcal{A}^+_{\mathrm{PGL}_3,\widehat{S}}(\mathbb{Z}^t)_{\mathcal{T}} \subset \mathcal{A}^+_{\mathrm{SL}_3,\widehat{S}}((1/3)\mathbb{Z}^t)_{\mathcal{T}},$$
$$\mathcal{A}_{\mathrm{PGL}_3,\widehat{S}}(\mathbb{R}^t)_{\mathcal{T}} = \mathcal{A}_{\mathrm{SL}_3,\widehat{S}}(\mathbb{R}^t)_{\mathcal{T}} \cong \mathbb{R}^N,\ \mathcal{A}^+_{\mathrm{PGL}_3,\widehat{S}}(\mathbb{R}^t)_{\mathcal{T}} = \mathcal{A}^+_{\mathrm{SL}_3,\widehat{S}}(\mathbb{R}^t)_{\mathcal{T}}.$$

REMARK A.4.

(I) By [9, Remark 6.5], we equally well could have imposed the conditions defining $\mathcal{A}_{\mathrm{PGL}_3,\widehat{S}}(\mathbb{Z}^t)_{\mathcal{T}}$ and $\mathcal{A}^+_{\mathrm{PGL}_3,\widehat{S}}(\mathbb{Z}^t)_{\mathcal{T}}$ on $\mathcal{A}_{\mathrm{SL}_3,\widehat{S}}(\mathbb{R}^t)_{\mathcal{T}} \cong \mathbb{R}^N$ rather than on

$\mathcal{A}_{\mathrm{SL}_3,\widehat{S}}((1/3)\mathbb{Z}^t)_{\mathcal{T}} \cong ((1/3)\mathbb{Z})^N$. That is, all real solutions are, in fact, one third integer solutions. Moreover, in the case of $\mathcal{A}^+_{\mathrm{PGL}_3,\widehat{S}}(\mathbb{Z}^t)_{\mathcal{T}}$, these one third integer solutions are nonpositive (this is because the tropicalized rhombus numbers $(\alpha^{i,j,k}_{a;b,c})^t$ are defined with the opposite sign compared to those appearing in [9]). (Note that less confusing conventions should be possible without significant effort.)

(II) The space $\mathcal{A}_{\mathrm{PGL}_3,\widehat{S}}(\mathbb{Z}^t)$ of lamination-tropical points is called the space of 'balanced points' in [27].

(III) By [19], when $\widehat{S}$ is a disk with three marked points on its boundary, the positive integer tropical points are identified with the Knutson-Tao hive [29].

Appendix B. Cones

The proofs of the results of this appendix are elementary, and are omitted. (They are, however, provided in the arXiv version [8] of this article.)

Remark B.1. Some of our terminology might be non-standard, adapted for the purposes of this paper. For example, using the terminology of [36], a 'polyhedral cone' is what we call a cone; a 'simplicial polyhedral cone' is what we call a sector; and, a 'k-dimensional pure simplicial polyhedral fan' determines what we call a sector decomposition of a cone.

B.1. Positive integer cones and Hilbert bases. Recall that $\mathbb{Z}_+$ denotes the set of nonnegative integers.

Definition B.2. A subset $\mathcal{M} \subset \mathbb{Z}^k$ (or $\subset \mathbb{R}^k$) is a ***submonoid*** if $\mathcal{M}$ is closed under addition and contains 0.

Definition B.3. Let $\mathcal{M} \subset \mathbb{Z}^k$ (or $\subset \mathbb{R}^k$) be a submonoid. An element $x \in \mathcal{M}$ is ***irreducible*** if x is nonzero, and x cannot be written as the sum of two nonzero elements of $\mathcal{M}$.

We denote by $\mathcal{H} \subset \mathcal{M}$ the set of irreducible elements of $\mathcal{M}$.

A subset $\mathcal{D} \subset \mathcal{M}$ is:

(I) $\mathbb{Z}_+$***-spanning*** if every $x \in \mathcal{M}$ is of the form $x = \lambda_1 x_1 + \lambda_2 x_2 + \cdots + \lambda_m x_m$ for some $x_i \in \mathcal{D}$ and $\lambda_i \in \mathbb{Z}_+$, in which case we write $x \in \mathrm{span}_{\mathbb{Z}_+}(\mathcal{D})$;

(II) a ***minimum*** $\mathbb{Z}_+$-spanning set if, in addition, for every $\mathbb{Z}_+$-spanning set $\mathcal{D}' \subset \mathcal{M}$ we have $\mathcal{D} \subset \mathcal{D}'$.

Note that a minimum $\mathbb{Z}_+$-spanning set is unique if it exists.

Definition B.4. A ***positive integer cone*** $\mathcal{C}$ is a submonoid of $\mathbb{Z}^k_+$.

Proposition B.5. *The subset $\mathcal{H} \subset \mathcal{C} \subset \mathbb{Z}^k_+$ of irreducible elements of a positive integer cone $\mathcal{C} \subset \mathbb{Z}^k_+$ is the unique minimum $\mathbb{Z}_+$-spanning subset of $\mathcal{C}$.* □

Remark B.6. Note that the $\mathbb{Z}_+$-spanning property of $\mathcal{H}$ in Proposition B.5 is not true if we had only assumed that $\mathcal{C} = \mathcal{M}$ is a submonoid of $\mathbb{Z}^k$. For example, the monoid $\mathcal{M} = \mathbb{Z}^k$ has no irreducible elements. However, it is also not essential that the submonoid be contained in a single orthant; note Remark B.8 as well.

Definition B.7. Let $\mathcal{H} \subset \mathcal{C} \subset \mathbb{Z}^k_+$ be as in Proposition B.5. If $\mathcal{H}$ is a finite set, then it is called the ***Hilbert basis*** of the positive integer cone $\mathcal{C} \subset \mathbb{Z}^k_+$.

Remark B.8. Hilbert bases [23, 42] appear in linear algebra and linear programming, and are defined in more generality than what we have defined here.

B.2. Cones over the real numbers. Recall that $\mathbb{R}_+$ (resp. $\mathbb{R}_-$) denotes the set of nonnegative (nonpositive) real numbers.

B.2.1. *Cones and sector decompositions.*

Definition B.9.

(I) A ***(real) cone*** $C \subset \mathbb{R}^k$ is a subset of $\mathbb{R}^k$ such that $C = \{\sum_{i=1}^m \lambda_i c_i; \lambda_i \in \mathbb{R}_+\}$ for some finite set $\{c_i\}_{i=1,2,\dots,m} \subset \mathbb{R}^k$, called a ***generating set*** of C. We also write $C = \mathrm{span}_{\mathbb{R}_+}(c_1, c_2, \dots, c_m)$.

(II) The minimum number of elements of a generating set is called the ***rank*** of the cone C.

(III) The subspace $\widetilde{C} \subset \mathbb{R}^k$ defined by $\widetilde{C} = \{\sum_i \widetilde{\lambda}_i c_i; \widetilde{\lambda}_i \in \mathbb{R}\}$ is independent of the choice of generating set $\{c_i\}_i$, and its dimension is called the ***dimension*** of the cone C. Note $\dim(C) \leqslant \mathrm{rank}(C) < \infty$.

(IV) A cone C is a ***sector*** if $\dim(C) = \mathrm{rank}(C)$.

(V) A cone $C \subset \mathbb{R}^k$ is ***full*** if $\dim(C) = k$.

Definition B.10.

(I) A ***sector decomposition*** of a full cone $C \subset \mathbb{R}^k$ is a finite collection $\{C_i\}_{i=1,2,\dots,p}$ of subcones $C_i \subset C$ satisfying:
  (i) each C_i is a full sector;
  (ii) $C = C_1 \cup C_2 \cup \cdots \cup C_p$ is the union of the sectors C_i;
  (iii) for each distinct $i, j \in \{1, 2, \dots, m\}$, the intersection $C_i \cap C_j \subset \mathbb{R}^k$ has empty interior, that is, does not contain an open subset of $\mathbb{R}^k$.

(II) If C and C' are two full cones in $\mathbb{R}^k$, then the intersection $C \cap C'$ is a ***wall*** if $C \cap C'$ is a cone of dimension $k-1$.

Observation B.11. *If $\{C_i\}_{i=1,2,\dots,p}$ is a sector decomposition of a full cone $C \subset \mathbb{R}^k$, and if $W = C_i \cap C_\ell$ is a wall, then there is no other pair of sectors giving this wall: $W = C_{i'} \cap C_{\ell'}$ if and only if $\{i, \ell\} = \{i', \ell'\}$.* □

B.2.2. *Some technical statements about cones of the form $C \subset \mathbb{R}^k_+ \times \mathbb{R}^n$.*

Lemma B.12. *Let $C \subset \mathbb{R}^k_+ \times \mathbb{R}^n$ be a cone satisfying the following properties:*

(I) *$e_i \in C$ for $i = 1, 2, \dots, k$, where e_i is the i-th standard basis element of $\mathbb{R}^k \times \mathbb{R}^n$;*

(II) *$\pi_n(C) = \mathbb{R}^n$, where $\pi_n : \mathbb{R}^k \times \mathbb{R}^n \to \mathbb{R}^n$ is the natural projection.*

Then, $\dim(C) = k + n$. Namely, C is full. □

Lemma B.13. *Consider a full cone $C \subset \mathbb{R}^k_+ \times \mathbb{R}^n$ as in Lemma B.12. Let $\{x_j\}_{j=1,2,\dots,m}$ be a finite subset of C with $m \geqslant n$, and let $\{J_i\}_{i=1,2,\dots,p}$ for some p be a collection of index sets $J_i = \{j_1^{(i)}, j_2^{(i)}, \dots, j_n^{(i)}\} \subset \{1, 2, \dots, m\}$ of constant size n ($|J_i| = n$).*

Assume in addition:

(I) *$C = \cup_{i=1}^p C_i$ is the union of the subcones*

$$C_i = \mathrm{span}_{\mathbb{R}_+}(\{e_1, e_2, \dots, e_k\} \cup \{x_j; j \in J_i\}) \subset C \subset \mathbb{R}^k_+ \times \mathbb{R}^n \ (i = 1, 2, \dots, p);$$

(II) *the subcones*

$$D_i = \mathrm{span}_{\mathbb{R}_+}(\{\pi_n(x_j); j \in J_i\}) \subset \mathbb{R}^n \ (i = 1, 2, \dots, p)$$

are full sectors forming a sector decomposition $\{D_i\}_{i=1,2,\dots,p}$ of $\mathbb{R}^n$ (Definition B.10).

Then, the subcones $C_i \subset C$ *are full sectors forming a sector decomposition* $\{C_i\}_{i=1,2,\dots,p}$ *of* C.

Moreover, $\pi_n(C_i \cap C_\ell) = D_i \cap D_\ell$ *for all* i, ℓ. *In particular, the sector* C_i *projects via* π_n *to the sector* D_i. □

Lemma B.14. *Let the full cone* $C \subset \mathbb{R}^k_+ \times \mathbb{R}^n$, *the sector decomposition* $\{D_i\}_{i=1,2,\dots,p}$ *of* $\mathbb{R}^n$, *and the sector decomposition* $\{C_i\}_{i=1,2,\dots,p}$ *of* C *be as in Lemma* B.13.

Assume in addition:

(I) *for each* i, ℓ *such that* $D_i \cap D_\ell$ *is a wall in* $\mathbb{R}^n$ (*Definition* B.10), *we have more specifically that the intersection* $J_i \cap J_\ell \subset \{1, 2, \dots, m\}$ *of index sets has* $n-1$ *elements, and*

$$D_i \cap D_\ell = \mathrm{span}_{\mathbb{R}_+}(\{\pi_n(x_j); j \in J_i \cap J_\ell\}) \subset \mathbb{R}^n.$$

Then, for any i, ℓ, *we have that* $C_i \cap C_\ell \subset \mathbb{R}^k_+ \times \mathbb{R}^n$ *is a wall in* C *if and only if* $D_i \cap D_\ell \subset \mathbb{R}^n$ *is a wall in* $\mathbb{R}^n$. *In particular, if this is the case for a given* i, ℓ, *then*

(m) $$C_i \cap C_\ell = \mathrm{span}_{\mathbb{R}_+}(\{e_1, e_2, \dots, e_k\} \cup \{x_j; j \in J_i \cap J_\ell\}) \subset \mathbb{R}^k_+ \times \mathbb{R}^n.$$

This yields a 1*-to-*1 *correspondence* {*walls of* $\{D_i\}_i$ *in* $\mathbb{R}^n$} $\leftrightarrow$ {*walls of* $\{C_i\}_i$ *in* C}. □

B.2.3. *Cone completions.*

Definition B.15. Let $\mathcal{M} \subset \mathbb{R}^k$ be a submonoid (Definition B.2) having a finite $\mathbb{Z}_+$-spanning set $\{c_i\}_{i=1,2,\dots,m}$ (we say $\mathcal{M}$ is ***finitely generated***). Then, its ***completion*** $\overline{\mathcal{M}} \subset \mathbb{R}^k$ is the corresponding real cone with the same generating set $\{c_i\}_i$ (this is independent of the choice of generating set).

By Proposition B.5, we immediately have:

Observation B.16. *Let* $\mathcal{C} \subset \mathbb{Z}^k_+$ *be a positive integer cone* (*Definition* B.4) *admitting a Hilbert basis* $\mathcal{H} \subset \mathcal{C}$ (*Definition* B.7). *Then, the rank of its completion* $\overline{\mathcal{C}} \subset \mathbb{R}^k_+$ *is less than or equal to the number of elements of the Hilbert basis* $\mathcal{H}$. □

Lemma B.17. *Let* $\mathcal{M} \subset \mathbb{R}^k$ *be a monoid. Assume there are finitely generated submonoids* $\mathcal{M}_1, \mathcal{M}_2, \dots, \mathcal{M}_p \subset \mathcal{M}$ *such that* $\mathcal{M} = \cup_{i=1}^p \mathcal{M}_i$ (*in particular,* $\mathcal{M}$ *is finitely generated*). *Then,* $\overline{\mathcal{M}} = \cup_{i=1}^p \overline{\mathcal{M}}_i$. □

Appendix C. Flip examples in the square

In Section 2, we proved the naturality of the web tropical coordinates without having to see what the new good position of a web in the square looks like after flipping the diagonal, which is topologically subtle. In this section, we give some examples of seeing the good position after the flip. This gives us another way to check the formulas of Theorem 2.4; see also Remark 2.1 at the beginning of Section 2.

The 9 symmetry classes of web families (see Figure 15 and Remark 4.3) fall into roughly three types. Let us study the flip a bit more intensively for one example of each type.

Let $W = W_c \in \mathcal{W}_\square$ be a cornerless web in the square and belonging to the family $\mathcal{W}_{i_j} \subset \mathcal{W}_\square$, where the value of i_j depends on which of the 9 cases we are considering ($j = 1, 2, \dots, 9$); see Notation 4.2.

Recall that $\mathcal{T}$ (resp. $\mathcal{T}'$) is the triangulation shown in the left hand side (resp. right hand side) of Figure 2. Consider the web tropical coordinate maps $\Phi_\mathcal{T} : \mathcal{W}_\square \to \mathcal{C}_\mathcal{T}$ and $\Phi_{\mathcal{T}'} : \mathcal{W}_\square \to \mathcal{C}_{\mathcal{T}'}$ (see Section 1). Denote $c = \Phi_\mathcal{T}(W) \in \mathcal{C}_\mathcal{T} \subset \mathbb{Z}^{12}_+$ by

$$c = (c_j)_{j=1,2,\dots,12} = (x_1, x_2, x_3, x_4, x_5, x_6, x_7, x_8, y_1, y_2, y_3, y_4)$$

and $c' = \Phi_{\mathcal{T}'} \circ \Phi_{\mathcal{T}}^{-1}(c) \in \mathcal{C}_{\mathcal{T}'} \subset \mathbb{Z}_+^{12}$ by

$$c' = (c'_j)_{j=1,2,\ldots,12} = (x'_1, x'_2, x'_3, x'_4, x'_5, x'_6, x'_7, x'_8, z_1, z_2, z_3, z_4)$$

(compare Definition 2.3 and Figure 2). We know right away that $x_i = x'_i$ for $i = 1, 2, \ldots, 8$.

Our goal is to check that (c), (d), (e), (f) are satisfied, by presenting the explicit good position of the family $\mathcal{W}_{i_j}$ after the flip, allowing us to calculate the coordinates directly. We do this in the three example cases $j = 1, 3, 7$.

Recall in particular $x, y, z, t \in \mathbb{Z}_+$ in Figure 15.

Example (family (1)). The simplest cases are given by schematics (1) and (2) of Figure 15. We verify case (1) here. The other case is similar. We compute the c_j's and c'_j's via Figure 9; see also Section 1.3.2.

Notice in this case it is obvious that the web on the right hand side of Figure 19 is in good position with respect to the flipped triangulation.

Left hand side of Figure 19, coordinates c_j(for $j = 1, 2, \ldots, 12$):

(1) $2x + y + 2z + 2t$;
(2) $x + 2y + z + t$;
(3) $2x$;
(4) x;
(5) $2x + 2y + z + 2t$;
(6) $x + y + 2z + t$;
(7) $2t$;
(8) t;
(9) $2x + y + 2z + 3t$;
(10) $x + 2y + z + 2t$;
(11) $3x + 2y + z + 2t$;
(12) $2x + y + 2z + t$.

Right hand side of Figure 19, coordinates c'_j(for $j = 9, \ldots, 12$):

(9′) $x + y + 2z + 2t$;
(10′) $3x + 2y + z + t$;
(11′) $2x + 2y + z + t$;
(12′) $x + y + 2z + 3t$.

The following computations verify (c), (d), (e), (f) in this case.

$$\begin{aligned}(\text{c}):\ &\max\{(x + 2y + z + t) + (3x + 2y + z + 2t), (2x + y + 2z + 3t) + 2x\} - (x + 2y + z + 2t)\\ &= \max\{4x + 4y + 2z + 3t, 4x + y + 2z + 3t\} - (x + 2y + z + 2t) = 3x + 2y + z + t.\end{aligned}$$

$$\begin{aligned}(\text{d}):\ &\max\{(2x + y + 2z + 3t) + (x + y + 2z + t), 2t + (3x + 2y + z + 2t)\} - (2x + y + 2z + t)\\ &= \max\{3x + 2y + 4z + 4t, 3x + 2y + z + 4t\} - (2x + y + 2z + t) = x + y + 2z + 3t.\end{aligned}$$

$$\begin{aligned}(\text{e}):\ &\max\{(2x + y + 2z + 2t) + (x + y + 2z + 3t), t + (3x + 2y + z + t)\} - (2x + y + 2z + 3t)\\ &= \max\{3x + 2y + 4z + 5t, 3x + 2y + z + 2t\} - (2x + y + 2z + 3t) = x + y + 2z + 2t.\end{aligned}$$

$$\begin{aligned}(\text{f}):\ &\max\{(3x + 2y + z + t) + (2x + 2y + z + 2t), (x + y + 2z + 3t) + x\} - (3x + 2y + z + 2t)\\ &= \max\{5x + 4y + 2z + 3t, 2x + y + 2z + 3t\} - (3x + 2y + z + 2t) = 2x + 2y + z + t.\end{aligned}$$

Example (family (3)). The next simplest cases are given by schematics (3), (4), (5), (6), and (9) of Figure 15. We verify case (3) here. The other four cases are similar. We compute the c_j's and c'_j's via Figure 9; see also Section 1.3.2.

Unlike in the previous example, it is less obvious that the schematic appearing on the right hand side of Figure 20 faithfully displays how the good position looks after the flip. That this is indeed the case is a bit subtle topologically, however can be

verified by an explicit procedure that draws the desired flipped bigon on top of the starting web as represented by the left hand side of Figure 20. We demonstrate this bigon drawing procedure in Figure 24.

The schematic diagram of the web in good position restricted to the flipped bigon in the right hand side of Figure 20 is shown in the left hand side of Figure 21. It is an enjoyable exercise to check that this bigon schematic agrees with the web example schematically shown in Figure 24.

Another guiding example showing the web in good position after the flip (without using schematics), is provided in the right hand side of Figure 21.

Left hand side of Figure 20, coordinates c_j(for $j = 1, 2, \ldots, 12$):

(1) $x + 2y$;
(2) $2x + y$;
(3) $x + y + z + t$;
(4) $2x + 2y + 2z + 2t$;
(5) $x + y + z$;
(6) $2x + 2y + 2z$;
(7) $2y + z + 2t$;
(8) $y + 2z + t$;
(9) $x + 3y + 2z + t$;
(10) $2x + 2y + 2z + t$;
(11) $3x + 3y + 3z + 2t$;
(12) $x + y + z + 2t$.

Right hand side of Figure 20, coordinates c'_j(for $j = 9, \ldots, 12$):

(9′) $2x + 3y + z + t$;
(10′) $3x + 2y + z + t$;
(11′) $x + 3y + 2z + 2t$;
(12′) $2x + 4y + 3z + 2t$.

The following computations verify (c), (d), (e), (f) in this case.

$$\begin{gathered}\text{(c)}\colon \max\{(2x+y)+(3x+3y+3z+2t),(x+3y+2z+t)+(x+y+z+t)\}\\ -(2x+2y+2z+t)\\ =\max\{5x+4y+3z+2t,2x+4y+3z+2t\}-(2x+2y+2z+t)=3x+2y+z+t.\end{gathered}$$

$$\begin{gathered}\text{(d)}\colon \max\{(x+3y+2z+t)+(2x+2y+2z),(2y+z+2t)+(3x+3y+3z+2t)\}\\ -(x+y+z+2t)\\ =\max\{3x+5y+4z+t,3x+5y+4z+4t\}-(x+y+z+2t)=2x+4y+3z+2t.\end{gathered}$$

$$\begin{gathered}\text{(e)}\colon \max\{(x+2y)+(2x+4y+3z+2t),(y+2z+t)+(3x+2y+z+t)\}\\ -(x+3y+2z+t)\\ =\max\{3x+6y+3z+2t,3x+3y+3z+2t\}-(x+3y+2z+t)=2x+3y+z+t.\end{gathered}$$

$$\begin{gathered}\text{(f)}\colon \max\{(3x+2y+z+t)+(x+y+z),(2x+4y+3z+2t)+(2x+2y+2z+2t)\}\\ -(3x+3y+3z+2t)\\ =\max\{4x+3y+2z+t,4x+6y+5z+4t\}-(3x+3y+3z+2t)=x+3y+2z+2t.\end{gathered}$$

Example (family (7)). The last group of cases are given by schematics (7) and (8) of Figure 15. We verify case (7) here. The other case is similar. We compute the c_j's and c'_j's via Figure 9; see also Section 1.3.2.

Note that, unlike for the previous two examples, in this case there are two possibilities: $z \geqslant t$ and $z \leqslant t$. In Figure 22, we display the case when $z \geqslant t$ (the $z \leqslant t$ case is similar).

As for the previous example, it is not immediately obvious that the schematic appearing on the right hand side of Figure 22 displays the correct good position. We again verify this by explicitly drawing the flipped bigon, as shown in Figure 25.

The schematic diagram of the web in good position restricted to the flipped bigon in the right hand side of Figure 22 is shown in the left hand side of Figure 23. It is an enjoyable exercise to check that this bigon schematic agrees with the web example schematically shown in Figure 25.

Another guiding example showing the web in good position after the flip (without using schematics), is provided in the right hand side of Figure 23.

We demonstrate the calculation when $z \geqslant t$ (the case $z \leqslant t$ is similar).

Left hand side of Figure 22, coordinates c_j(for $j = 1, 2, \ldots, 12$):

(1) $2x + t$;
(2) $x + 2t$;
(3) $2y + z$;
(4) $y + 2z$;
(5) $2x + 2y + 2t$;
(6) $x + y + t$;
(7) $2x + 2y + 2z$;
(8) $x + y + z$;
(9) $3x + y + z + t$;
(10) $2x + y + z + 2t$;
(11) $2x + 3y + 2z + 2t$;
(12) $x + 2y + 2z + t$.

Right hand side of Figure 22, coordinates c'_j(for $j = 9, \ldots, 12$):

(9′) $2x + 2y + z + t$;
(10′) $x + 2y + z + 2t$;
(11′) $x + y + 2z - t$;
(12′) $3x + 3y + 2z + t$.

The following computations verify (c), (d), (e), (f) in this case. Note that the last equation uses the assumption $z \geqslant t$.

$$\begin{aligned}(\text{c}):\max\{(x+2t)+(2x+3y+2z+2t),(3x+y+z+t)+(2y+z)\}-(2x+y+z+2t)\\ =\max\{3x+3y+2z+4t,3x+3y+2z+t\}-(2x+y+z+2t)=x+2y+z+2t.\end{aligned}$$

$$\begin{aligned}(\text{d}):\max\{(3x+y+z+t)+(x+y+t),(2x+2y+2z)+(2x+3y+2z+2t)\}\\ -(x+2y+2z+t)\\ =\max\{4x+2y+z+2t,4x+5y+4z+2t\}-(x+2y+2z+t)=3x+3y+2z+t.\end{aligned}$$

$$\begin{aligned}(\text{e}):\max\{(2x+t)+(3x+3y+2z+t),(x+y+z)+(x+2y+z+2t)\}-(3x+y+z+t)\\ =\max\{5x+3y+2z+2t,2x+3y+2z+2t\}-(3x+y+z+t)=2x+2y+z+t.\end{aligned}$$

$$\begin{aligned}(\text{f}):\max\{(x+2y+z+2t)+(2x+2y+2t),(3x+3y+2z+t)+(y+2z)\}\\ -(2x+3y+2z+2t)\\ =\max\{3x+4y+z+4t,3x+4y+4z+t\}-(2x+3y+2z+2t)\\ =(3x+4y+4z+t)-(2x+3y+2z+2t)=x+y+2z-t.\end{aligned}$$

Acknowledgements. We are profoundly grateful to Dylan Allegretti, Francis Bonahon, Charlie Frohman, Sasha Goncharov, Linhui Shen, Daping Weng, Tommaso Cremaschi, and Subhadip Dey for many very helpful conversations and for generously offering their time as this project developed.

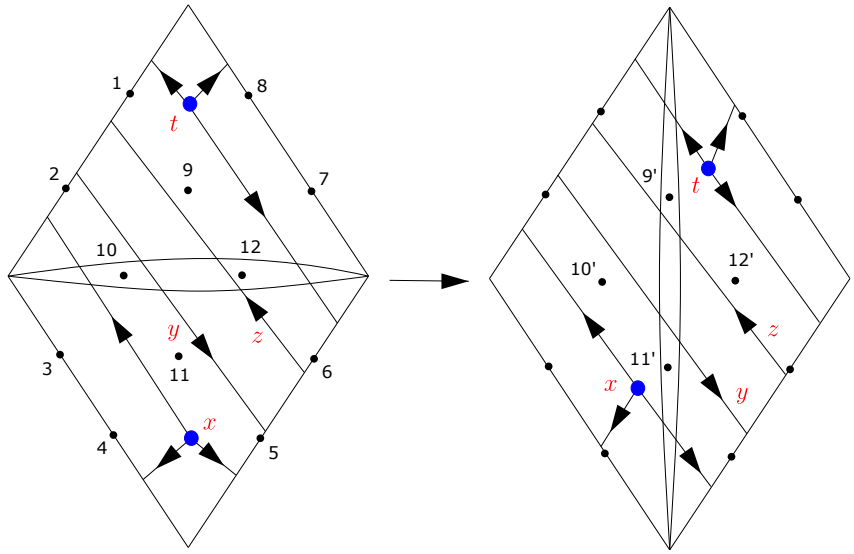

FIGURE 19. Family (1).

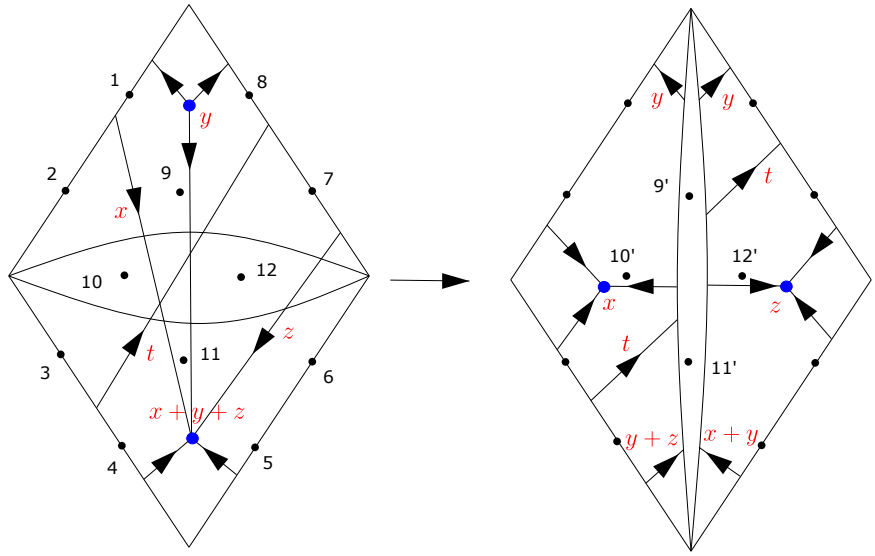

FIGURE 20. Family (3).

Much of this work was completed during very enjoyable visits to Tsinghua University in Beijing, supported by a GEAR graduate internship grant, and the University of Southern California in Los Angeles. We would like to take this opportunity to extend our enormous gratitude to these institutions for their warm hospitality.

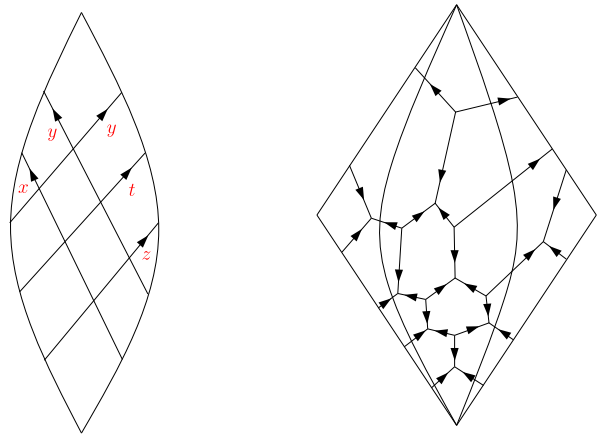

FIGURE 21. Family (3). Left: Bigon schematic after the flip. Right: An example of the web in good position after the flip: $x = y = z = t = 1$.

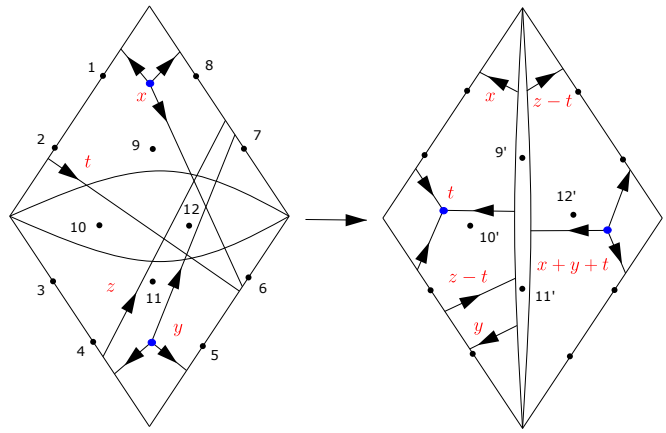

FIGURE 22. Family (7), shown when $z \geqslant t$.

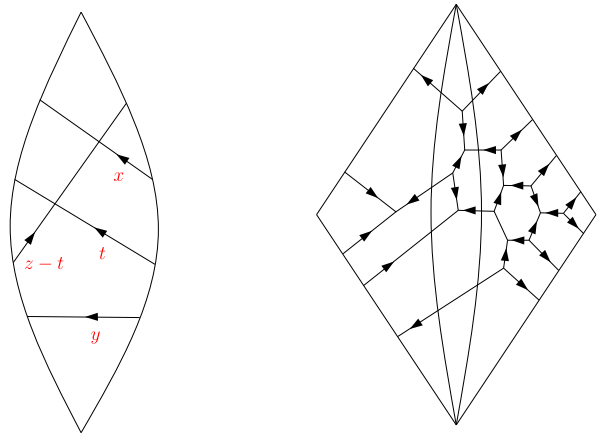

FIGURE 23. Family (7), $z \geqslant t$. Left: Bigon schematic after the flip. Right: An example of the web in good position after the flip: $x = y = t = 1$ and $z = 2$.

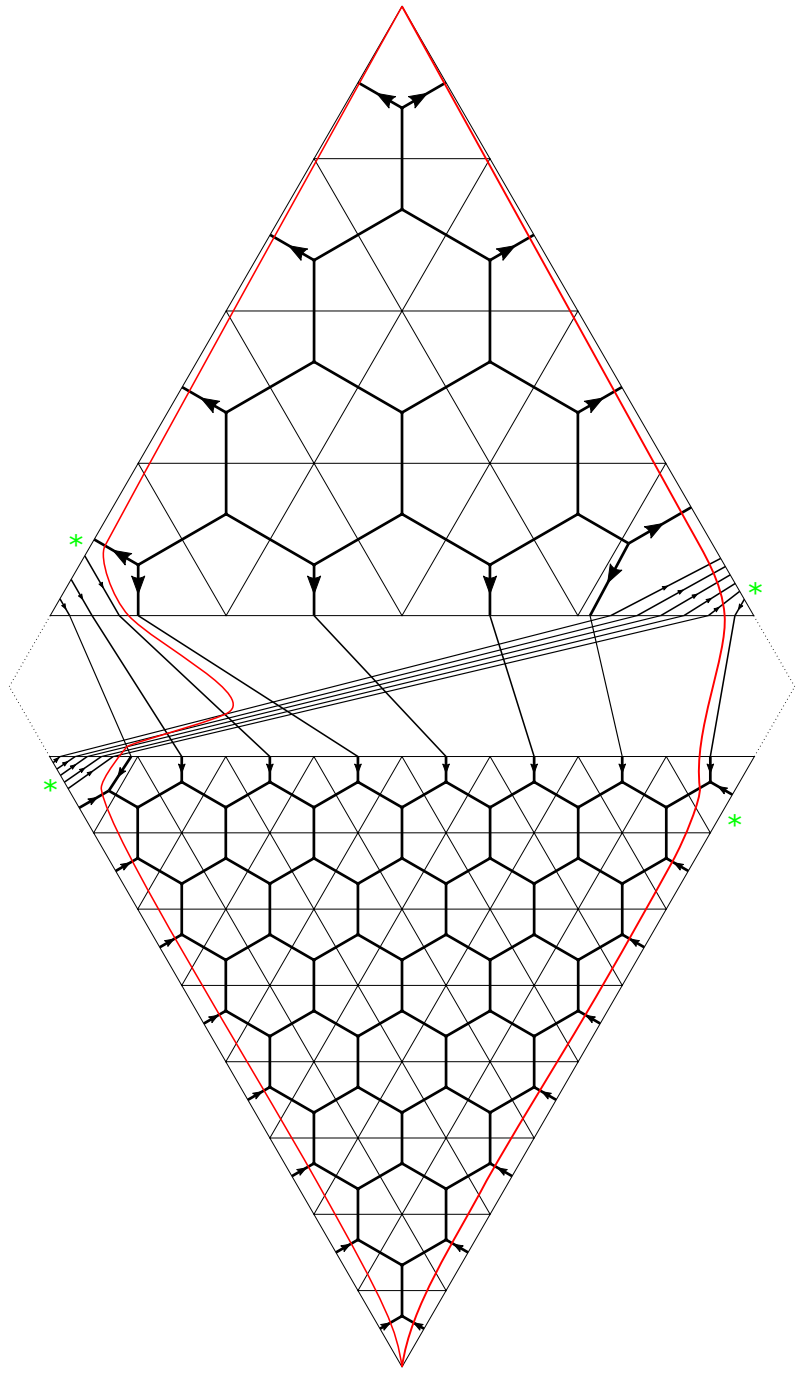

FIGURE 24. Family (3). Bigon drawing procedure in the example $x = 3, y = 4, z = 1, t = 5$. The web represented by the schematic is in good position with respect to the red bigon. The green asterisks separate the honeycombs from the corner arcs in the flipped triangulation. Compare Figures 20 and 21.

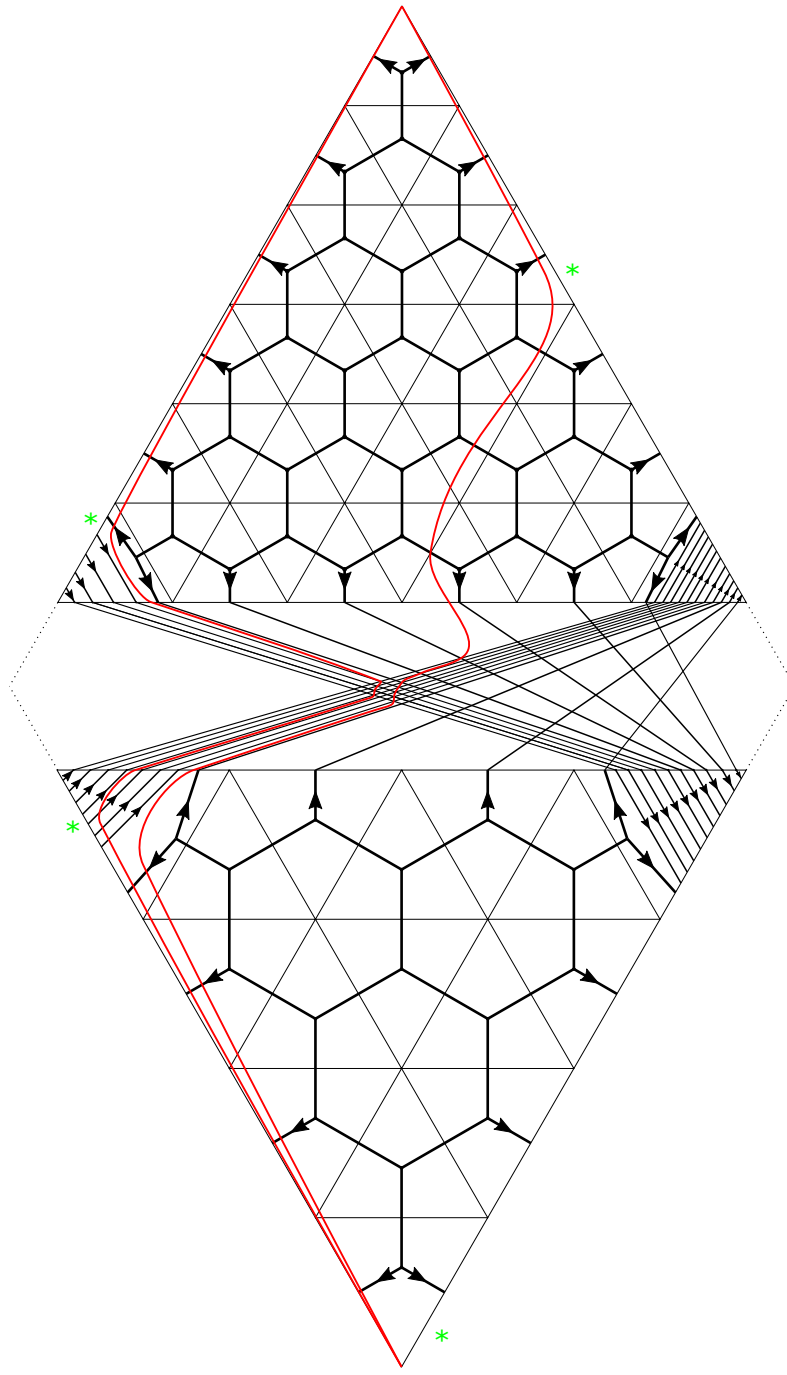

FIGURE 25. Family (7). Bigon drawing procedure in the example $x = 6, y = 4, z = 7, t = 4$. The web represented by the schematic is in good position with respect to the red bigon. The green asterisks separate the honeycombs from the corner arcs in the flipped triangulation. Compare Figures 22 and 23.

References

[1] N. Abdiel and C. Frohman, *The localized skein algebra is Frobenius*, Algebr. Geom. Topol. **17** (2017), no. 6, 3341–3373.

[2] T. Akhmejanov, *Non-elliptic webs and convex sets in the affine building*, Doc. Math. **25** (2020), 2413–2443.

[3] D. G. L. Allegretti and H. K. Kim, *A duality map for quantum cluster varieties from surfaces*, Adv. Math. **306** (2017), 1164–1208.

[4] D. Bullock, *Rings of* $\mathrm{SL}_2(\mathbf{C})$*-characters and the Kauffman bracket skein module*, Comment. Math. Helv. **72** (1997), no. 4, 521–542.

[5] S. Cautis, J. Kamnitzer, and S. Morrison, *Webs and quantum skew Howe duality*, Math. Ann. **360** (2014), no. 1-2, 351–390.

[6] D. C. Douglas, *Points of quantum* SL_n *coming from quantum snakes*, Algebr. Geom. Topol. **24** (2024), 2537–2570.

[7] D. C. Douglas, *Quantum traces for* $\mathrm{SL}_n(\mathbb{C})$*: the case* $n = 3$, J. Pure Appl. Algebra **228** (2024), article no. 107652 (50 pages).

[8] D. C. Douglas and Z. Sun, *Tropical Fock-Goncharov coordinates for* SL_3*-webs on surfaces II: naturality*, 2020, `https://arxiv.org/abs/2012.14202`.

[9] D. C. Douglas and Z. Sun, *Tropical Fock-Goncharov coordinates for* SL_3*-webs on surfaces I: construction*, Forum Math. Sigma **12** (2024), article no. e5 (55 pages).

[10] V. V. Fock and A. B. Goncharov, *Moduli spaces of local systems and higher Teichmüller theory*, Publ. Math. Inst. Hautes Études Sci. **103** (2006), 1–211.

[11] V. V. Fock and A. B. Goncharov, *Dual Teichmüller and lamination spaces*, in Handbook of Teichmüller theory. Vol. I, IRMA Lect. Math. Theor. Phys., vol. 11, Eur. Math. Soc., Zürich, 2007, pp. 647–684.

[12] V. V. Fock and A. B. Goncharov, *Moduli spaces of convex projective structures on surfaces*, Adv. Math. **208** (2007), no. 1, 249–273.

[13] V. V. Fock and A. B. Goncharov, *Cluster ensembles, quantization and the dilogarithm*, Ann. Sci. Éc. Norm. Supér. (4) **42** (2009), no. 6, 865–930.

[14] S. Fomin, L. Williams, and A. Zelevinsky, *Introduction to cluster algebras. Chapters 4–5*, 2017, `https://arxiv.org/abs/1707.07190`.

[15] S. Fomin and A. Zelevinsky, *Cluster algebras. I. Foundations*, J. Amer. Math. Soc. **15** (2002), no. 2, 497–529.

[16] B. Fontaine, J. Kamnitzer, and G. Kuperberg, *Buildings, spiders, and geometric Satake*, Compos. Math. **149** (2013), no. 11, 1871–1912.

[17] C. Frohman and A. S. Sikora, $SU(3)$*-skein algebras and webs on surfaces*, Math. Z. **300** (2022), no. 1, 33–56.

[18] D. Gaiotto, G. W. Moore, and A. Neitzke, *Spectral networks*, Ann. Henri Poincaré **14** (2013), no. 7, 1643–1731.

[19] A. B. Goncharov and L. Shen, *Geometry of canonical bases and mirror symmetry*, Invent. Math. **202** (2015), no. 2, 487–633.

[20] A. B. Goncharov and L. Shen, *Donaldson-Thomas transformations of moduli spaces of G-local systems*, Adv. Math. **327** (2018), 225–348.

[21] A. B. Goncharov and L. Shen, *Quantum geometry of moduli spaces of local systems and representation theory*, 2019, `https://arxiv.org/abs/1904.10491`.

[22] M. Gross, P. Hacking, S. Keel, and M. Kontsevich, *Canonical bases for cluster algebras*, J. Amer. Math. Soc. **31** (2018), no. 2, 497–608.

[23] D. Hilbert, *Ueber die Theorie der algebraischen Formen*, Math. Ann. **36** (1890), no. 4, 473–534.

[24] Y. Huang and Z. Sun, *McShane identities for higher Teichmüller theory and the Goncharov–Shen potential*, Mem. Amer. Math. Soc. **286** (2023), v+116.

[25] T. Ishibashi and S. Kano, *Unbounded* $\mathfrak{sl}_3$*-laminations and their shear coordinates*, 2022, `https://arxiv.org/abs/2204.08947`.

[26] D. Jordan, I. Le, G. Schrader, and A. Shapiro, *Quantum decorated character stacks*, 2021, `https://arxiv.org/abs/2102.12283`.

[27] H. K. Kim, SL_3*-laminations as bases for* PGL_3 *cluster varieties for surfaces*, 2020, `https://arxiv.org/abs/2011.14765`.

[28] H. K. Kim, *Naturality of* SL_3 *quantum trace maps for surfaces*, 2021, `https://arxiv.org/abs/2104.06286`.

[29] A. Knutson and T. Tao, *The honeycomb model of* $\mathrm{GL}_n(\mathbf{C})$ *tensor products. I. Proof of the saturation conjecture*, J. Amer. Math. Soc. **12** (1999), no. 4, 1055–1090.

[30] M. Kontsevich and Y. Soibelman, *Stability structures, motivic Donaldson-Thomas invariants and cluster transformations*, 2008, `https://arxiv.org/abs/0811.2435`.

[31] G. Kuperberg, *Spiders for rank* 2 *Lie algebras*, Comm. Math. Phys. **180** (1996), no. 1, 109–151.
[32] I. Le, *Higher laminations and affine buildings*, Geom. Topol. **20** (2016), no. 3, 1673–1735.
[33] I. Le, *An approach to higher Teichmüller spaces for general groups*, Int. Math. Res. Not. IMRN **2019** (2019), 4899–4949.
[34] I. Le, *Cluster structures on higher Teichmuller spaces for classical groups*, Forum Math. Sigma **7** (2019), article no. e13 (165 pages).
[35] I. Le, *Intersection pairings for higher laminations*, Algebr. Comb. **4** (2021), no. 5, 823–841.
[36] D. Maclagan and B. Sturmfels, *Introduction to tropical geometry*, Graduate Studies in Mathematics, vol. 161, American Mathematical Society, Providence, RI, 2015.
[37] G. Muller, *Skein and cluster algebras of marked surfaces*, Quantum Topol. **7** (2016), no. 3, 435–503.
[38] D. Mumford, J. Fogarty, and F. Kirwan, *Geometric invariant theory*, third ed., Ergebnisse der Mathematik und ihrer Grenzgebiete (2), vol. 34, Springer-Verlag, Berlin, 1994.
[39] R. C. Penner, *The decorated Teichmüller space of punctured surfaces*, Comm. Math. Phys. **113** (1987), no. 2, 299–339.
[40] J. H. Przytycki, *Skein modules of* 3*-manifolds*, Bull. Polish Acad. Sci. Math. **39** (1991), no. 1-2, 91–100.
[41] J. H. Przytycki and A. S. Sikora, *On skein algebras and* $\mathrm{Sl}_2(\mathbf{C})$*-character varieties*, Topology **39** (2000), no. 1, 115–148.
[42] A. Schrijver, *On total dual integrality*, Linear Algebra Appl. **38** (1981), 27–32.
[43] L. Shen, Z. Sun, and D. Weng, *Intersections of Dual* SL_3*-Webs*, 2023, https://arxiv.org/abs/2311.15466.
[44] A. S. Sikora, SL_n*-character varieties as spaces of graphs*, Trans. Amer. Math. Soc. **353** (2001), no. 7, 2773–2804.
[45] A. S. Sikora, *Skein theory for* $\mathrm{SU}(n)$*-quantum invariants*, Algebr. Geom. Topol. **5** (2005), 865–897.
[46] A. S. Sikora and B. W. Westbury, *Confluence theory for graphs*, Algebr. Geom. Topol. **7** (2007), 439–478.
[47] Z. Sun, A. Wienhard, and T. Zhang, *Flows on the* $\mathrm{PGL}(V)$*-Hitchin component*, Geom. Funct. Anal. **30** (2020), no. 2, 588–692.
[48] W. P. Thurston, *Three-dimensional geometry and topology. Vol. 1*, Princeton Mathematical Series, vol. 35, Princeton University Press, Princeton, NJ, 1997.
[49] V. G. Turaev, *Algebras of loops on surfaces, algebras of knots, and quantization*, in Braid group, knot theory and statistical mechanics, Adv. Ser. Math. Phys., vol. 9, World Sci. Publ., Teaneck, NJ, 1989, pp. 59–95.
[50] A. Wienhard, *An invitation to higher Teichmüller theory*, Proceedings of the International Congress of Mathematicians—Rio de Janeiro 2018. Vol. II. Invited lectures, World Sci. Publ., Hackensack, NJ, 2018, pp. 1013–1039.
[51] E. Witten, *Quantum field theory and the Jones polynomial*, Comm. Math. Phys. **121** (1989), no. 3, 351–399.
[52] D. Xie, *Higher laminations, webs and N=2 line operators*, 2013, https://arxiv.org/abs/1304.2390.

Daniel C. Douglas, Virginia Tech, Department of Mathematics, 225 Stanger Street, Blacksburg, VA 24061 (USA)
E-mail : dcdouglas@vt.edu

Zhe Sun, University of Science and Technology of China, School of Mathematical Sciences, 96 Jinzhai Road, Hefei 230026 (China)
E-mail : sunz@ustc.edu.cn